

## ABSTRACT

HAO, ZISU. Understanding and Predicting Temperatures in Municipal Solid Waste Landfills (Under the direction of Dr. Morton A. Barlaz and Dr. Joel J. Ducoste).

Landfilling is generally the most cost-effective approach for municipal solid waste disposal. However, there have been several reports of municipal solid waste (MSW) landfills that experienced temperatures in excess of 80–100 °C. Elevated temperatures have caused damage to landfill infrastructures and pose environmental risks. Although aerobic and anaerobic reactions have been recognized as heat generation sources within landfills, the causes of excessive heat accumulation in elevated temperature landfills remain unclear. The objective of this study was to develop a mathematical model to predict heat generation, accumulation and propagation from biotic and abiotic reactions that occur in MSW landfills.

Initially, a batch reactor model was developed to identify an appropriate mathematical approach for the representation of heat generation sources including aerobic and anaerobic biological reactions, anaerobic metal corrosion, acid-base reactions, ash hydration and carbonation, and pyrolysis. In the batch reactor model, the landfill temperature and reactant concentrations do not vary spatially within the landfill which represents an important limitation in representing landfills. The predicted maximum temperature associated with biological reactions ranged from 62 to 69 °C for cases with and without heat loss, respectively. Inclusion of ash hydration and carbonation, and Al corrosion (1.7% Al and 100% corroded area) resulted in temperature rises of 14 and 26 °C in 10 years, respectively.

A transient three-dimensional finite element model (FEM-3DM) was developed to describe spatially dependent heat transfer in landfills. The FEM-3DM incorporates gas-liquid-heat reactive transfer in a landfill with biotic and abiotic reactions and spatially-dependent heat transfer processes (e.g. conduction and condensation). Model simulations showed a convex temperature

profile in the landfill body and the maximum temperature occurs at a depth of 50 m for an 80 m landfill. The simulation results also showed that the 80 m landfill reached higher maximum temperatures than the 40 m landfill. The model was useful in exploring the impact of three disposal scenarios involving ash; segregation of ash in the center of the landfill, segregation in a corner, and mixed with the MSW. The fraction of the waste predicted to exceed 65 °C was 0, 0.08, and 0.11 for the base case (MSW only), ash-in-corner, and ash-in-center scenarios, respectively. Thus, the impacted waste volume associated with the corner and center scenarios are sufficiently close that operational considerations will likely dictate ash placement. Simulations predicted that the disposal of 10 to 20% ash can result in 49 to 81% of the waste mass exceeding 65 °C, which suggests that a segregation strategy has merit so to minimize the volume of MSW that experiences an elevated temperature (65 °C). By hydrating the waste prior to burial, about 40% of the total energy can be eliminated prior to burial; this results in a reduction of the maximum temperature of ~40 °C. Multiple site-specific considerations will dictate whether the ash is hydrated by the waste generator or at a landfill. Similarly, the presence of Al had a significant impact on waste temperatures. Finally, the model can be applied to develop optimal management and engineering strategies to prevent excess heat accumulation.

© Copyright 2020 Zisu Hao  
All Rights Reserved

Understanding and Predicting Temperatures in Municipal Solid Waste Landfills

by  
Zisu Hao

A dissertation submitted to the Graduate Faculty of  
North Carolina State university  
in partial fulfillment of the  
requirements for the Degree of  
Doctor of Philosophy

Civil Engineering

Raleigh, North Carolina  
2020

APPROVED BY:

---

Dr. Morton A. Barlaz  
Committee Co-Chair

---

Dr. Joel J. Ducoste  
Committee Co-Chair

---

Dr. Fanxing Li

---

Dr. Yuntian Zhu

## **BIOGRAPHY**

Zisu Hao grew up in Kaifeng, China. In 2007, Mr. Hao received a Bachelor of Science in Chemical and Engineering in the Department of Chemical Engineering at Beijing University of Chemical Technology (BUCT), Beijing, China. From 2007 to 2014 Mr. Hao worked as a graduate researcher under the direction of Dr. Zihao Wang and Dr. Weidong Zhang in the State Key Laboratory of Chemical Resource Engineering at BUCT, where he received a Doctoral Degree in Chemical Engineering. In Fall 2014 he began graduate studies in the Department of Civil, Construction, and Environmental Engineering at North Carolina State University, and worked as a graduate researcher from 2014 to 2015 on the quantification of grease interceptor effluent fatty acids under the direction of Dr. Ducoste. Beginning in 2015, Mr. Hao started research on the topic of landfill modeling and served as a teaching assistant in 2019. His graduate course work has focused on computational fluid dynamics and solid waste management, under the direction of Dr. Barlaz and Dr. Ducoste. His dissertation focuses on modeling to understand heat accumulation, transfer, and propagation in municipal solid waste landfills.

## **DEDICATION**

This dissertation is dedicated to my wife, Qian, who has been a constant source of inspiration, motivation, encouragement, and support throughout my life.

## ACKNOWLEDGMENTS

I would like to express my deepest appreciation to Dr. Barlaz. His wealth of knowledge, guidance, encouragement, and support allowed me to reach higher levels of achievement in my research career than I would have been capable of otherwise. By his example, he has shown me what an outstanding researcher/professor/person should be.

I am extremely grateful for having Dr. Ducoste as my secondary mentor throughout my graduate career at NC State. His patience, enthusiasm, and motivation have deeply inspired me. I am very grateful to him for offering me the chance to broaden my horizons in multiple research fields.

I would also like to thank my other committee members, Dr. Fanxing Li and Dr. Yuntian Zhu for generously offering their time, guidance, and brilliant comments and suggestions, thanks to you.

My sincere thanks also go to Dr. Mohammad Pour-Ghaz for providing me insightful comments during our group meetings, to Dr. Mei Sun for helping me with model parameterization, to Dr. Castellano and Mr. Jake Rhoads for helping me build experimental setups, and to Drs. Detlef Knappe, Francis de los Reyes, and Jack Edwards for their wonderful lectures.

I would like to thank graduate students/friends for all the fun we have had in the last several years: Dr. Florentino De La Cruz, Asmita Narode, Sierra Schupp, Qiwen Cheng, Juan Fausto Ortiz, Arpit Sardana, Joe Weaver, Yi Chun Lai, Amanda Karam, Amie McElroy, Zachary Hopkins, Chuhui Zhang, Samrin Kusum, Divya Malyala, Diyuan Wang, and Yixuan Wang.

I would like to express my special thanks to my lovely family, my wife Qian, my daughter Mira, my son Maxen, my parents and parents-in-law gave me the everlasting confidence, support and encouragement to complete my degree and to pursue my dreams. You are amazing.

## TABLE OF CONTENTS

LIST OF TABLES .....	vii
LIST OF FIGURES .....	viii
Chapter 1. Introduction and Research Objectives.....	1
Chapter 2. Literature Review .....	7
2.1 Current research related to ETLFs .....	7
2.2 Landfill models with heat and/or mass transfer .....	9
2.3 References.....	15
Chapter 3. Heat Generation and Accumulation in Municipal Solid Waste Landfills (Env. Sci. & Technol. 2017, 51, 12434–12442).....	19
3.1 Abstract .....	19
3.2 Introduction.....	19
3.3 Model development .....	21
3.4 Model parameterization and input assumptions .....	32
3.5 Results and discussion .....	33
3.6 Incorporation of pyrolysis.....	41
3.7 Implications and future work.....	45
3.8 Supporting information.....	45
3.9 References.....	66
Chapter 4. Finite Element Modeling of Landfills to Inform Heat Generation, Transport and Accumulation.....	72
4.1 Abstract .....	72
4.2 Introduction.....	72
4.3 Modeling Approach .....	75
4.4 Results and Discussion .....	86

4.5 Comparison of Model Simulations to Field Data .....	100
4.6 Summary and Implications .....	102
4.7 Supplemental Data .....	104
4.8 References .....	122
Chapter 5. Conclusions and Recommendations.....	126

## LIST OF TABLES

Table 1-1. The enthalpies of main biotic and abiotic reactions in landfills .....	4
Table 2-1. Current research related to ETLFs. ....	7
Table 2-2. Summary of landfill modelling research .....	10
Table 2-3. Heat generation/source terms in modelling literature .....	14
Table 3-1. Default model parameters used to describe landfill characteristics .....	33
Table 3-2. Impact of gas condensation on waste temperature <sup>a</sup> .....	40
Table 3-S1. Previous models on heat generation in landfills.....	46
Table 3-S2. Constants of the density function (Eqn. 3-S3) of water vapor (Wagner and Pruß, 2002) .....	51
Table 3-S3. Heat capacities of gases and water (approximate values at 20 °C and 1.01×10 <sup>5</sup> Pa).....	52
Table 3-S4. Characteristics of MSW as discarded.....	53
Table 3-S5. Chemical constituents that undergo hydration and carbonation in municipal solid waste incinerator (MSWI) bottom ash samples <sup>a</sup> .....	55
Table 3-S6. Average thicknesses of metals from containers and other sources .....	56
Table 3-S7. Chemical composition of biodegradable waste components <sup>a</sup> .....	57
Table 3-S8. Biodegradable and reactive constituents in MSW considered in model.....	58
Table 3-S9. Nomenclature .....	59
Table 4-1. Cumulative normalized landfill volume (CNLV) with temperatures greater than 65 °C and 80 °C in Year 20.....	99
Table 4-S1. Default model parameters used to describe landfill characteristics .....	108
Table 4-S2. Physical parameters of MSW, leachate, and landfill gas (adopted from Hao et al., 2017; Tian and Benson, unpublished data, 2019).....	109

## LIST OF FIGURES

Figure 3-1. Schematic of the Landfill Batch Reactor Model.....	22
Figure 3-2. Heat accumulation associated with MSW biodegradation in the presence and absence of O <sub>2</sub> . Solid lines represent cases without heat removal. Dashed lines consider heat removal process (Conv = convection, Evap = evaporation, heat loss = evaporation + convection + infiltration), 2x DecayRate = decay rate ( $k_m$ ) doubled for each biodegradable component listed in Table 3-S4.....	36
Figure 3-3. Impact of ash hydration and carbonation on landfill temperature. The solid and dashed black lines represent the base cases given in Figure 3-2. The blue and green lines represent the presence of 10% ash (Table 3-S5) and 90% MSW. The ashhyd line considers hydration only. The ashcrb lines consider hydration and carbonation as hydration is an essential reaction for carbonation at landfill temperatures. The plot simulates the sensitivity to 20% ash. The ash hydration and carbonation rates are 0.5 and 0.1 yr <sup>-1</sup> , respectively. ....	37
Figure 3-4. Impacts of Al corrosion on landfill temperature using the corrosion rates given in Table 3-1. The solid and dashed black lines represent the base cases given in Figure 3-2. The lines for 50% and 25% simulate partial corrosion across the surface area. ....	39
Figure 3-5. Simulation results with pyrolysis incorporated into the batch reactor model. The solid and dashed black lines represent the base case given in Figure 3-2. The red and blue lines consider different initiation temperatures for pyrolysis with (dashed) and without (solid) heat loss. ....	44
Figure 3-S1. Inhibition function described in Eqn. 3-11. ....	60
Figure 3-S2. Impact of ash carbonation on landfill temperature with varying carbonation rates. The solid and dashed black lines represent the base cases given in Figure 3-2. The blue and green lines represent the presence of 10% ash (Table 3-S5) and 90% MSW. The ashcrb simulation includes hydration and carbonation. For the ashcrb case, the ash hydration and carbonation rates are 0.5 and 0.1yr <sup>-1</sup> , respectively. These rates were decreased by 50% for the ashcrb 0.5x Rates case.....	61

Figure 3-S3. Impact of Al corrosion on landfill temperature with temporally varying corrosion rates. The corrosion rate for the first 6 months was assumed to be ten times higher than the default rates given in Table 3-1. Thereafter, the default rates were used. The % represents the fraction of the total surface area available for corrosion. The solid and dashed black lines represent the base cases as given in Figure 3-2 and represent only biological reactions .....62

Figure 3-S4. Impact of Fe corrosion on landfill temperature with varying corrosion rates. The solid and dashed black lines represent the base cases as given in Figure 3-2 and represent only biological reactions. The Fe corrosion rate is 0.0005 mm/yr (Table 3-1) unless specified as 0.005 mm/yr. The % represents the fraction of the total surface area available for corrosion. ....63

Figure 3-S5. Impact of acid-base neutralization reactions on landfill temperature. The solid and dashed black lines represent the base case given in Figure 3-2 and represents only biological reactions .....64

Figure 3-S6. Heat accumulation associated with MSW biodegradation, ash hydration and carbonation, Al and Fe corrosion, and acid-base neutralization reactions. The solid and dashed black lines represent the base case given in Figure 3-2. The red lines represent a case with 80% MSW, 20% ash, double the CH<sub>4</sub> generation rate, and the base case Al, Fe, and carboxylic acid contents. ....65

Figure 4-1. Geometry of the three-dimensional finite element model.....76

Figure 4-2. Temperature contours for a landfill receiving MSW only .....87

Figure 4-3. Temperature profiles for MSW only in the central cross section .....88

Figure 4-4. Temperature profiles and contours for MSW only with 20 and 30 °C at the top boundary .....90

Figure 4-5. Temperature profiles and evolution of volume fraction for 40 m and 80 m high landfills .....92

Figure 4-6. Temperature profiles and evolution for MSW only with doubled decay rates .....93

Figure 4-7. Temperature contours for the landfill with an ash column in the center (the disposal scenario is illustrated in part a) .....	96
Figure 4-8. Temperature profiles for a landfill with an ash column (dashed line) in the center (a and b: hydration and carbonation; c and d: carbonation only) .....	97
Figure 4-9. Temperature profiles for ash-MSW mixture with 10 % (a) and 20% (b) ash.....	98
Figure 4-10. Normalized temperature profiles for simulation results and field data (Hanson et al. 2010).....	101
Figure 4-S1. Scheme of the waste disposal strategy.....	105
Figure 4-S2. Domain and boundaries applied in the model.....	110
Figure 4-S3. Inhibition function and normalized experimental CH <sub>4</sub> potential described in Eq. 4-S1.....	111
Figure 4-S4. Discretization of the landfill domain .....	112
Figure 4-S5. Cross section for temperature evolution for the 80 m MSW only case .....	113
Figure 4-S6. Temperature profiles for MSW only with doubled MSW thermal conductivity.....	114
Figure 4-S7. Temperature contours for a landfill with an ash column in the corner (the disposal scenario is illustrated in part a).....	115
Figure 4-S8. Temperature profiles for a landfill with an ash column (dashed line) in the corner .....	116
Figure 4-S9. Isothermal contours for MSW only, ash column in the center, and ash column in the corner .....	117
Figure4-S10. Volume fraction of regions with elevated temperatures for the MSW only, ash-in-center, and ash-in-corner cases .....	118
Figure 4-S11. Temperature contours for a landfill with an ash column in the center with carbonation only (the disposal scenario is illustrated in part a).....	119
Figure 4-S12. Temperature profiles for Al-MSW mixture with 1.7 % (a) and 3.4% (b) Al .....	120

Figure 4-S13. Cumulative normalized volumes with varying temperatures for MSW only and ash-in-center cases in Year 20 .....121

## **Chapter 1. Introduction and Research Objectives**

Landfilling has been used as the most cost-effective approach to global municipal solid waste (MSW) disposal and is the dominant management alternative in both developing and developed countries (Kjeldsen et al., 2002; Southen and Rowe, 2004; Durmusoglu et al., 2005; Karak et al., 2013). MSW is highly heterogeneous with varying compositions based on cultural background and residential and commercial makeup of the generating community. Organic waste makes up the highest proportion of MSW in low- and middle-income countries, while paper, plastics, glass, metal fractions increase in the waste stream for high-income countries. Paper, food, and yard wastes are the major cellulose-containing organic matter and their anaerobic decomposition after burial in landfills produces methane and carbon dioxide, commonly referred to as landfill gas (LFG), and heat. Typically, the maximum temperatures in MSW landfills are less than 55 °C and heat generated from the related biotic reactions are balanced with heat released to the environment (Yeşiller et al., 2005; Hanson et al., 2010; Hanson et al., 2013). However, there have been several reports of MSW landfills that have been recently experiencing temperatures in excess of 80–100 °C (Calder and Stark, 2010; Luettich and Yafrate, 2016; Jafari et al., 2017).

Elevated temperatures have caused damage to gas and leachate infrastructure with softening and buckling, increases in fugitive gas emissions and odor complaints, rapid settlement, and reduced CH<sub>4</sub> content that may impact energy generation processes and LFG treatment. Elevated leachate volumes with increasing chemical oxygen demand (COD) and salt content have also been observed in elevated temperature landfills (ETLFs), and additional challenges include leachate seeps. Gas and leachate collecting pipes and geomembranes are made from polymers, which are sensitive to temperature. Stark et al. (2010) reported that elevated temperatures could

consume, burn, and remove the reinforcing material from MSW which leads to reduced slope stability. The reduction of service life and/or effectiveness of high density polyethylene (HDPE) geomembranes at elevated temperatures was documented by Jafari et al. (2014). The high temperatures in landfills generate thermal gradients, leading to the movement of water vapor from hotter areas to cooler areas and subsequent condensation (Hao et al., 2017; Southen and Rowe, 2004). Increased monitoring and management, expensive remediation, and possibly even permanent closure may be required for ETLFs.

A number of heat-generating reactions occur when MSW and other non-hazardous wastes are buried in landfills. Reactions include both aerobic and anaerobic biodegradation (Li et al., 2011; Grillo, 2014), anaerobic metal corrosion (Calder and Stark, 2010), acid-base neutralization (Rees, 1980), and ash hydration and carbonation (Speiser et al., 2000; Li et al., 2007). The enthalpies of aforementioned reactions are presented in Table 1-1. While not documented in landfills, there are reports of thermochemical (pyrolytic) reactions in biomass that may occur in landfills at elevated but undefined temperatures (Kwon and Castaldi, 2012; Ciuta et al., 2014). While the aforementioned reactions generate heat in landfills, understanding the extent to which heat accumulates is critical. In addition, due to the heterogeneity and large scale of landfills, heat generation, accumulation, and propagation in landfills are spatially dependent. Moreover, the importance of waste placement strategies and scheduling, landfill depth and the disposal of a number of non-MSW wastes as it impacts heat generation, accumulation, and propagation has not been investigated.

The overall objective of this research was to develop a mathematical model to predict heat generation, accumulation and propagation from biological and chemical reactions that occur in MSW landfills. Initially, a batch reactor model was developed to identify an appropriate

mathematical approach for the representation of heat generation sources including aerobic and anaerobic biological reactions, anaerobic metal corrosion, acid-base reactions, ash hydration and carbonation, and pyrolysis. However, in the batch reactor model, the landfill temperature and reactant concentrations do not vary spatially within the landfill which represents an important limitation in representing landfills. Therefore, a transient three-dimensional finite element model (FEM-3DM) was developed to describe spatially dependent heat transfer mechanisms in landfills. The FEM-3DM incorporates gas-liquid-heat reactive transfer in a landfill with biotic and abiotic reactions and spatially-dependent heat transfer processes (e.g. conduction and condensation).

Chapter 2 presents a literature review of modeling studies on heat and mass transfer in landfills.

Chapter 3 describes the development of a batch reactor model to quantify the importance of aerobic and anaerobic biodegradation, anaerobic metal corrosion, acid-base neutralization, and ash hydration and carbonation. The model also incorporates heat accumulation, consumption, and release from landfills. However, conduction and temperature distribution cannot be considered in a batch reactor model. This chapter has been published in *Environmental Science and Technology* (Hao et al, 2017).

Chapter 4 presents the development of a transient three-dimensional model to better represent the heterogeneity of actual landfills, to incorporate the impacts of boundary and initial conditions, and to consider spatially dependent heat transfer mechanisms to better understand heat generation, accumulation, and propagation. This chapter is formatted for submission to the *Journal of Geotechnical and Geoenvironmental Engineering*. Finally,

Chapter 5 includes the overall conclusions, implications, and recommendations.

**Table 1-1.** The enthalpies of main biotic and abiotic reactions in landfills

Reaction	Chemical formula	$\Delta H$
Aerobic methane oxidation	$CH_4 + 2O_2 \rightarrow CO_2 + 2H_2O$	$-27822 \frac{kJ}{kg O_2}$
Cellulose oxidation	$(C_6H_{10}O_5)_n + 6nO_2 \rightarrow 6nCO_2 + 5nH_2O$	$-17360 \frac{kJ}{kg cellulose}$
Anaerobic cellulose degradation	$(C_6H_{10}O_5)_n + nH_2O \rightarrow 3nCH_4 + 3nCO_2$	$-1672 \frac{kJ}{kg cellulose}$
Anaerobic protein degradation	$8C_{16}H_{24}O_5N + 66H_2O \rightarrow 75CH_4 + 53CO_2 + 8NH_3$	$-1295 \frac{kJ}{kg protein}$
Anaerobic lipid degradation	$2C_{16}H_{32}O_2 + 14H_2O \rightarrow 23CH_4 + 9CO_2$	$-1826 \frac{kJ}{kg lipids}$
Ash hydration (Ca)	$CaO + H_2O \rightarrow Ca(OH)_2$	$-1164 \frac{kJ}{kg CaO}$
Ash carbonation (Ca)	$Ca(OH)_2(s) + HCO_3^- \rightarrow CaCO_3(s) + H_2O + OH^-$	$-624 \frac{kJ}{kg Ca(OH)_2}$
Ash carbonation (Ca)	$Ca(OH)_2(s) + HCO_3^- \rightarrow CaCO_3(aq) + H_2O + OH^-$	$-792 \frac{kJ}{kg Ca(OH)_2}$
Ash carbonation (Ca)	$Ca(OH)_2(s) + CO_2 \rightarrow CaCO_3(s) + H_2O$	$-1550 \frac{kJ}{kg Ca(OH)_2}$
Ash carbonation (Ca)	$Ca(OH)_2(s) + CO_2 \rightarrow CaCO_3(aq) + H_2O$	$-1718 \frac{kJ}{kg Ca(OH)_2}$
Al anaerobic corrosion	$Al + 3H_2O \rightarrow Al(OH)_3 + \frac{3}{2}H_2$	$-15922 \frac{kJ}{kg Al}$
Fe anaerobic corrosion	$Fe + CO_2 + H_2O \rightarrow FeCO_3 + H_2$	$-1268 \frac{kJ}{kg Fe}$
H <sub>2</sub> consumption	$4H_2 + CO_2 \rightarrow CH_4 + 2H_2O$	$-20625 \frac{kJ}{kg H_2}$

## References

- Abuel-Naga, H.M. and Bouazza, A., 2012. Thermomechanical behavior of saturated geosynthetic clay liners. *Journal of Geotechnical and Geoenvironmental Engineering*, 139(4), pp.539-547.
- Calder, G.V. and Stark, T.D., 2010. Aluminum reactions and problems in municipal solid waste landfills. *Practice Periodical of Hazardous, Toxic, and Radioactive Waste Management*, 14(4), pp.258-265.
- Ciuta, S., Patuzzi, F., Baratieri, M. and Castaldi, M.J., 2014. Biomass energy behavior study during pyrolysis process by intraparticle gas sampling. *Journal of analytical and applied pyrolysis*, 108, pp.316-322.
- Durmusoglu, E., Corapcioglu, M.Y. and Tuncay, K., 2005. Landfill settlement with decomposition and gas generation. *Journal of Environmental Engineering*, 131(9), pp.1311-1321.
- Grillo, R.J., 2014. Energy recycling–landfill waste heat generation and recovery. *Current Sustainable/Renewable Energy Reports*, 1(4), pp.150-156.
- Hanson, J.L., Yeşiller, N. and Oettle, N.K., 2010. Spatial and temporal temperature distributions in municipal solid waste landfills. *Journal of Environmental Engineering*, 136(8), pp.804-814.
- Hanson, J.L., Yeşiller, N., Onnen, M.T., Liu, W.L., Oettle, N.K. and Marinos, J.A., 2013. Development of numerical model for predicting heat generation and temperatures in MSW landfills. *Waste management*, 33(10), pp.1993-2000.
- Hao, Z., Sun, M., Ducoste, J.J., Benson, C.H., Luetlich, S., Castaldi, M.J. and Barlaz, M.A., 2017. Heat Generation and Accumulation in Municipal Solid Waste Landfills. *Environmental science & technology*, 51(21), pp.12434-12442.
- Hoorweg, D. and Bhada-Tata, P., 2012. *What a waste: a global review of solid waste management* (Vol. 15, p. 116). World Bank, Washington, DC.
- Jafari, N.H., Stark, T.D. and Thalhamer, T., 2017. Spatial and temporal characteristics of elevated temperatures in municipal solid waste landfills. *Waste management*, 59, pp.286-301.
- Jafari, N.H., Stark, T.D. and Rowe, R.K., 2013. Service life of HDPE geomembranes subjected to elevated temperatures. *Journal of Hazardous, Toxic, and Radioactive Waste*, 18(1), pp.16-26.
- Karak, T., Bhagat, R.M. and Bhattacharyya, P., 2012. Municipal solid waste generation, composition, and management: the world scenario. *Critical Reviews in Environmental Science and Technology*, 42(15), pp.1509-1630.

- Kjeldsen, P., Barlaz, M.A., Rooker, A.P., Baun, A., Ledin, A. and Christensen, T.H., 2002. Present and long-term composition of MSW landfill leachate: a review. *Critical reviews in environmental science and technology*, 32(4), pp.297-336.
- Kwon, E.E. and Castaldi, M.J., 2012. Urban energy mining from municipal solid waste (MSW) via the enhanced thermo-chemical process by carbon dioxide (CO<sub>2</sub>) as a reaction medium. *Bioresource technology*, 125, pp.23-29.
- Li, X., Bertos, M.F., Hills, C.D., Carey, P.J. and Simon, S., 2007. Accelerated carbonation of municipal solid waste incineration fly ashes. *Waste management*, 27(9), pp.1200-1206.
- Li, H., Sanchez, R., Qin, S.J., Kavak, H.I., Webster, I.A., Tsotsis, T.T. and Sahimi, M., 2011. Computer simulation of gas generation and transport in landfills. V: Use of artificial neural network and the genetic algorithm for short- and long-term forecasting and planning. *Chemical engineering science*, 66(12), pp.2646-2659.
- Luetlich, S.M. and Yafrate, N., 2016. Measuring Temperatures in an Elevated Temperature Landfill. In *Geo-Chicago 2016* (pp. 162-176).
- Rees, J.F., 1980. Optimisation of methane production and refuse decomposition in landfills by temperature control. *Journal of chemical technology and biotechnology*, 30(1), pp.458-465.
- Southen, J.M. and Rowe, R.K., 2004. Investigation of the behavior of geosynthetic clay liners subjected to thermal gradients in basal liner applications. In *Advances in Geosynthetic Clay Liner Technology: 2nd Symposium*. ASTM International.
- Stark, T.D., Akhtar, K. and Hussain, M., 2010. Stability analysis for a landfill experiencing elevated temperatures. In *GeoFlorida 2010: Advances in Analysis, Modeling & Design* (pp. 3110-3119).
- Yeşiller, N., Hanson, J.L. and Liu, W.L., 2005. Heat generation in municipal solid waste landfills. *Journal of Geotechnical and Geoenvironmental Engineering*, 131(11), pp.1330-1344.

## Chapter 2. Literature Review

This chapter is organized into two major sections. The first section presents current research on ETLFs. The second section reviews selected landfill models that focus on heat and/or mass balances in MSW landfills.

### 2.1 Current research related to ETLFs

Table 2-1 presents selected published research on ETLFs, which mainly focused on the impacts of elevated temperature on the infrastructure of landfill facilities as well as case studies. A major limitation of the literature is that the heat transfer mechanisms associated with biotic and abiotic reactions have not been investigated which is the fundamental basis for understanding the mechanisms of ETLFs. Although some reactive wastes such as Al dross and ash were considered as the heat sources that led to elevate temperatures, the quantification of heat generation based on the applicable chemical reactions were not explored (Klein et al., 2003; Calder and Stark, 2010). Therefore, a quantitative approach that describes heat generation, accumulation, and release in MSW landfills is essential to better understand the causes and mechanisms of ETLFs.

**Table 2-1.** Current research related to ETLFs.

	<b>Research content</b>	<b>Summary</b>
Calder and Stark (2010)	Al reactions	Introduction of chemical reactions involving elemental Al in landfills
Stark et al. (2010)	Slope stability	Stability analyses of a MSW landfill experiencing elevated temperature due to an Al waste reaction
Martin et al. (2011)	Indicators of exothermic reactions	Introduction of techniques for determining whether an exothermic Al waste reaction and/or combustion exists in an MSW landfill
Karademir and Frost (2011)	Geomembranes	Investigation of the impacts of temperature on interface shear behavior between geotextiles and geomembranes
Abuel-Naga and Bouazza (2012)	Clay liners	Assessment of the volume change behavior of geosynthetic clay liners (GCLs) under elevated temperatures

**Table 2-1.** Current research related to ETLFs (Continued).

Hoor and Rowe (2012)	Geomembranes	Use tire chips as thermal insulation between primary and secondary liners to reduce the temperature of secondary geomembranes
Ishimori and Katsumi (2012)	Clay liners	Studies of temperature effects on the swelling capacity and hydraulic performance of geosynthetic clay liners with varying temperature
Luan et al. (2012)	Cr(VI) transfer	Evaluation of the impact of temperature on the transport of Cr(VI) through landfill liners containing granular activated carbon and activated bentonite
Barclay and Rayhani (2013)	Clay liners	Studies of temperature on hydration of geosynthetic clay liners in landfills
Coccia et al. (2013)	Geothermal heat exchangers	Characterization of the thermal resource of landfilled municipal solid waste and the implementation of geothermal heat exchange systems in landfills
Krushelnitzky and Brachman (2013)	HDPE pipe	Quantification of HDPE pipe deflections that were impacted by elevated temperatures when deeply buried
Ewais et al. (2014)	Geomembranes	Evaluation of service life of a high-density polyethylene geomembrane under simulated landfill conditions at 85 °C
Grillo (2014)	Energy Recycling	Case studies with efficiency and cost effectiveness of landfill based geothermal systems
Jafari et al. (2014)	Geomembranes	Potential effects of elevated temperatures on a HDPE geomembrane
Kwak et al. (2015)	Geosynthetic-soil interface	Investigation of the chemical and thermal effects on the cyclic shear behavior of a geosynthetic-soil interface
Luettich and Yafrate (2016)	Temperature monitoring	Development and installation of a fiber-optic distributed temperature sensing (FODTS) system in an ETLF
Jafari and Stark (2016)	Settlement	Discussion of the mechanisms for slope instability, including elevated gas pressures, perched leachate surfaces, and reduced MSW shear strength.
Várfalvi et al. (2016)	Heat generation estimation	Estimation of heat generation in a landfill during its operation
Yesiller et al. (2016)	Heat management strategies	A conceptual framework for heat management in MSW landfills with three strategies: extraction, regulation, and supplementation by adding heat to or removing heat from a landfill using external thermal energy sources.

**Table 2-1.** Current research related to ETLFs (Continued).

Jafari and Stark (2015a, 2015b) Jafari et al. (2017a, 2017b)	Case study	Characteristics of elevated temperature landfills such as elevated wellhead temperature, decreasing ratios of CH <sub>4</sub> to CO <sub>2</sub> , pressure increase, elevated concentration of H <sub>2</sub> and CO.
---	------------	--

## **2.2 Landfill models with heat and/or mass transfer**

A number of mathematical models have been developed to investigate various aspects of landfill relevant processes/conditions as summarized in Table 2-2. Processes that have been modeled include (1) transport of LFG (e.g. CO<sub>2</sub> and CH<sub>4</sub>), leachate, and solute, (2) temperatures in a landfill body with constant or seasonal boundary conditions, (3) the thermo-biological behavior, and (4) heat and gas generation. The majority of landfill energy balance models focused on heat generation from waste biodegradation and none investigated heat generation from abiotic reactions. First-order kinetics were applied to describe the rates of biological reactions. In Table 2-2, the modeled landfills were assumed to be a homogenous media to simplify the models' complexity (all models listed in Table 2-2), indicating that the models cannot simulate heat propagation from regions with elevated temperature.

**Table 2-2.** Summary of landfill modelling research

Processes Included		HB	MB	MoB	HConv	MConv	Cond	Rad	Diff	GT	BR	CR	Inf	Stress
Year	Author													
1979	Findikakis and Leckie		O	O		O			O	O	O			
1996	El-Fadel	O	O			O	O			O	O	O		
1997	Yoshida	O					O				O		O	
1997	Thomas	O	O	O		O	O		O	O				O
1997	Ferguson	O	O			O	O		O	O				
1998	Berglund	O			O		O			O			O	
1999	Ferguson	O	O			O	O		O	O				
1999	Thomas	O	O		O	O	O		O	O				
2002	Hashemi		O			O			O	O	O	O		
2002	Islam		O			O			O		O			
2002	Jang		O			O			O					
2003	Yoshida	O			O		O				O		O	
2003	Klein	O					O						O	
2004	White	O	O								O	O		
2005	Neusinger	O	O	O		O	O		O	O	O	O		
2005	Ferguson	O	O			O	O		O	O				
2005	Durmusoglu									O	O			O
2006	Hashemi		O			O			O	O	O	O		
2007	Hashemi		O			O			O	O	O	O		
2007	Hettiarachchi	O	O		O	O	O		O	O	O		O	
2009	Moqbel	O				O	O				O	O		
2010	Hashemi		O			O			O	O	O	O		
2010	Gawande		O								O	O		
2010	Gawande	O	O								O	O		
2010	Garg	O	O			O	O		O	O				
2011	Navaee-Ardeh	O			O		O				O		O	

**Table 2-2.** Summary of landfill modelling research (Continued)

2012	Megalla	O				O	O	O			O	
2013	Hanson	O					O				O	O
2013	Xi and Xiong		O			O				O		O
2013	Zambra and Moraga	O	O				O		O		O	
2014	White		O				O			O		O
2014	Hussein		O			O				O		
2015	Ng	O	O			O	O		O	O	O	O
2015	Faitli						O					
2015	Soporan	O	O	O		O	O			O		
2015	Kutsyi	O	O			O	O		O	O	O	O
2015	Xie		O				O			O		
2016	Hubert	O	O	O	O	O	O		O	O	O	O

**HB:** Heat Balance; **MB:** Mass Balance; **MoB:** Momentum Balance; **HConv:** Heat Convection; **MConv:** Mass Convection; **Cond:** Conduction; **Rad:** Radiation; **Diff:** Diffusion; **GT:** Gas transfer; **BR:** Biological Reactions; **CR:** Chemical Reactions; **Inf:** Infiltration.

Boundary temperature plays an important role in the accumulation and transfer of heat. Yoshida et al. (1997) predicted an increase of maximum temperature by 55 °C using a 1-D model by assuming that the boundary temperatures of the surface and landfill bottom were 15 °C. However, field data from four landfills (British Columbia, Michigan, New Mexico, and Alaska) fluctuated seasonally near the landfill edges and surface (Hanson et al., 2013). For the bottom boundary of a landfill, an impact on the adjacent soil temperature up to 50 m from the core of the landfill was reported by Ferguson and Palanathakumar (2015). The temperatures from the landfill core to the 50 m soil layer decreased from 37 °C to 10 °C.

Anaerobic decomposition was predicted to result in landfill temperatures above 70 °C (Yoshida et al., 1997). For a bioreactor landfill with leachate recirculation, a vertical gradient of 1 to 10 °C/m between different layers in the landfill was predicted, and the maximum temperature in the deepest layer was 55 °C (Gholamifard et al., 2008). Leachate injection was predicted to decrease temperature and when eliminated, a rapid temperature increase was predicted (Gholamifard et al., 2008). Hubert et al. (2016) reported that the simulated temperature near the bottom of a bioreactor landfill was greater than 70 °C and the temperature increased until Year 5 before decreasing from the complete degradation of organic matter.

The emphasis of these models has been on describing the depth-wise temperature distribution in landfills by incorporating biodegradation reactions only. Both field and predicted temperature profiles display maximum temperatures at central locations of the waste mass (Yoshida et al., 1997; Hanson et al., 2010; Neusinger et al., 2005), yet boundary conditions and other spatially resolved heat loss processes may affect the location of the maximum temperature location. In addition, the maximum temperature increased with the landfill height (Neusinger et al., 2005).

## Heat generation/source terms in modelling studies

The initiation of ETLFs may be attributed to heat generation and accumulation that exceeds the rate of heat loss and release. Therefore, a mathematical description of the heat generation terms is required for the accurate prediction of temperature. In the literature, several types of heat sources have been proposed. Constant heat generation and release were incorporated by Klein et al. (2003) and Nastev et al. (2001). Klein et al. (2003) found that the energy release from a bottom ash landfill was  $250 \text{ MJ/m}^3$ , resulting in a peak temperature of  $97 \text{ }^\circ\text{C}$ . Nastev et al. (2001) assumed that the heat generation rate was  $40.2 \text{ kJ/mol}$  of generated  $\text{CH}_4$  and  $\text{CO}_2$ . The maximum and minimum heat flux out of the landfill were  $0.39 \text{ W/m}^2$  and  $6.8 \times 10^{-7} \text{ W/m}^2$ .

Heat generation was also estimated based on the generating/decaying rates of indicator species (e.g.  $\text{CH}_4$ ,  $\text{O}_2$ ) and the enthalpies of associated biotic reactions. Table 2-3 displays the typical heat generation/source terms proposed in the literature. Several indicator species were used for the estimation of heat generation rates from anaerobic reactions, including carboxylic acids (El-Fadel et al., 1996),  $\text{CH}_4$  (Yoshida et al., 1997; Ng et al., 2015; Garg and Achari, 2010), cellulose (Gholamifard et al., 2008), and organic matter (Kutsyi, 2015; Hubert et al., 2016). In addition, Arrhenius-type equations were also applied by Zambra and Moraga (2013).

To consider the impact of temperature on heat generation rates, empirical functions such as step-function, exponential growth and decay function, and bi-exponential decaying functions, were proposed and parameterized based on field data at specific landfills (Yoshida et al., 1997; Gholamifard et al., 2008; Klein et al., 2003). These empirical models have been successful in simulating temperatures at specific landfills, but they cannot be extended to predict temperatures in other landfills due to their non-mechanistic characterization.

**Table 2-3.** Heat generation/source terms in modelling literature

<b>Authors</b>	<b>Heat generation term</b>
El-Fadel et al. (1996)	$Q_{Bio} = \Delta H_{AC} R_{AC}$
Yoshida et al. (1997), Ng et al. (2015), and Garg and Achari (2010)	$Q_{Bio} = \Delta H_{CH_4} R_{CH_4}$
Kutsyi (2015) and Hubert et al. (2016)	$Q_{Bio} = \Delta H_{Biom} R_{Biom}$
Gholamifard et al. (2008)	$Q_{Bio} = \Delta H_{Hyds} R_{BioSub} + \Delta H_{CH_4} R_{CH_4}$
Zambra and Moraga (2013)	$Q_{cel} = \Delta H_{cel} (1 - \varepsilon) A_{cel} \rho_{cel} c_{O_2} e^{\left(\frac{-E_{cel}}{R_0 T}\right)}$
Zambra and Moraga (2013)	$Q_{Biom} = \Delta H_{Biom} (1 - \varepsilon) \rho_{Biom} \frac{A_{grow} e^{\left(\frac{-E_{grow}}{R_0 T}\right)}}{1 + A_{inhi} e^{\left(\frac{-E_{inhi}}{R_0 T}\right)}}$
Neusinger et al. (2005)	$Q_{Bio} = \Lambda \Delta T$

### Summary of the published landfill models

A number of landfill models have been proposed and applied to describe various aspects of heat generation in landfills. However, consideration of heat generation due to biological reactions alone is not sufficient to elucidate the generation, accumulation, and propagation of heat in landfills that contain many different wastes. The major limitations of published models include: (1) no implicit coupling with multiphase, multidimensional transport of heat and liquid/gas with biotic and abiotic reactions, (2) lack of potential abiotic reactions and heat release mechanisms such as evaporation of water and moisture condensation, and (3) unable to incorporate spatially dependent mechanisms/variables including heat conduction, boundary conditions, and waste disposal strategy. In summary, the complex chemical and biological processes involved in MSW degradation along with potential abiotic reactions and their impacts on heat and mass transfer processes require new modeling approaches to predict heat generation, accumulation and propagation in landfills.

## 2.3 References

- Abuel-Naga, H.M. and Bouazza, A., 2012. Thermomechanical behavior of saturated geosynthetic clay liners. *Journal of Geotechnical and Geoenvironmental Engineering*, 139(4), pp.539-547.
- Barclay, A. and Rayhani, M.T., 2013. Effect of temperature on hydration of geosynthetic clay liners in landfills. *Waste Management & Research*, 31(3), pp.265-272.
- Berglund, C., 1998. Environmental hydraulics of sanitary landfills. *Journal of Hydraulic Research*, 36(1), pp.101-116.
- Calder, G.V. and Stark, T.D., 2010. Aluminum reactions and problems in municipal solid waste landfills. *Practice Periodical of Hazardous, Toxic, and Radioactive Waste Management*, 14(4), pp.258-265.
- Coccia, C.J., Gupta, R., Morris, J. and McCartney, J.S., 2013. Municipal solid waste landfills as geothermal heat sources. *Renewable and sustainable energy reviews*, 19, pp.463-474.
- El-Fadel, M., Findikakis, A.N. and Leckie, J.O., 1996. Numerical modelling of generation and transport of gas and heat in landfills I. Model formulation. *Waste management & research*, 14(5), pp.483-504.
- Ewais, A.M.R., Rowe, R.K., Brachman, R.W.I. and Arnepalli, D.N., 2014. Service life of a high-density polyethylene geomembrane under simulated landfill conditions at 85 °C. *Journal of Geotechnical and Geoenvironmental Engineering*, 140(11), p.04014060.
- Ferguson, W.J. and Thomas, H.R., 1997. A numerical study of the effect of thermal gradient on landfill gas migration. In *Proceedings of the Conference on Geoenvironmental Engineering-Contaminated ground: fate of pollutants and remediation*. London: Thomas Telford (pp. 181-186).
- Ferguson, W.J. and Palanathakumar, B., 2005. A fully coupled finite element model of landfill gas migration in a partially saturated soil. *CMES: Computer Modeling in Engineering*.
- Findikakis, A.N. and Leckie, J.O., 1979. Numerical simulation of gas flow in sanitary landfills. *Journal of the Environmental Engineering Division*, 105(5), pp.927-945.
- Gholamifard, S., Eymard, R. and Duquennoi, C., 2008. Modeling anaerobic bioreactor landfills in methanogenic phase: Long term and short term behaviors. *Water research*, 42(20), pp.5061-5071.
- Garg, A. and Achari, G., 2010. A comprehensive numerical model simulating gas, heat, and moisture transport in sanitary landfills and methane oxidation in final covers. *Environmental modeling & assessment*, 15(5), pp.397-410.

- Grillo, R.J., 2014. Energy recycling–landfill waste heat generation and recovery. *Current Sustainable/Renewable Energy Reports*, 1(4), pp.150-156.
- Hanson, J.L., Yeşiller, N. and Oettle, N.K., 2010. Spatial and temporal temperature distributions in municipal solid waste landfills. *Journal of Environmental Engineering*, 136(8), pp.804-814.
- Hanson, J.L., Yeşiller, N., Onnen, M.T., Liu, W.L., Oettle, N.K. and Marinos, J.A., 2013. Development of numerical model for predicting heat generation and temperatures in MSW landfills. *Waste management*, 33(10), pp.1993-2000.
- Hoor, A. and Rowe, R.K., 2012. Application of tire chips to reduce the temperature of secondary geomembranes in municipal solid waste landfills. *Waste management*, 32(5), pp.901-911.
- Hubert, J., Liu, X.F. and Collin, F., 2016. Numerical modeling of the long term behavior of Municipal Solid Waste in a bioreactor landfill. *Computers and Geotechnics*, 72, pp.152-170.
- Ishimori, H. and Katsumi, T., 2012. Temperature effects on the swelling capacity and barrier performance of geosynthetic clay liners permeated with sodium chloride solutions. *Geotextiles and Geomembranes*, 33, pp.25-33.
- Jafari, N.H. and Stark, T.D., 2015a. Spatial classification of elevated temperatures in MSW landfills. In *Geo-Chicago 2016* (pp. 285-296).
- Jafari, N.H. and Stark, T.D., 2015b. Progression of Elevated Temperatures in MSW Landfills. In *Geo-Chicago 2016* (pp. 232-243).
- Jafari, N.H. and Stark, T.D., Slope and Settlement Movements of an MSW Landfill during Elevated Temperatures. In *Geo-Chicago 2016* (pp. 275-284).
- Jafari, N.H., Stark, T.D. and Thalhamer, T., 2017a. Spatial and temporal characteristics of elevated temperatures in municipal solid waste landfills. *Waste management*, 59, pp.286-301.
- Jafari, N.H., Stark, T.D. and Thalhamer, T., 2017b. Progression of Elevated Temperatures in Municipal Solid Waste Landfills. *Journal of Geotechnical and Geoenvironmental Engineering*, 143(8), p.05017004.
- Jafari, N.H., Stark, T.D. and Rowe, R.K., 2014. Service life of HDPE geomembranes subjected to elevated temperatures. *Journal of Hazardous, Toxic, and Radioactive Waste*, 18(1), pp.16-26.
- Karademir, T. and Frost, J.D., 2011. Elevated temperature effects on geotextile-geomembrane interface strength. In *Geo-Frontiers 2011: Advances in Geotechnical Engineering* (pp. 1023-1033).

- Klein, R., Nestle, N., Niessner, R. and Baumann, T., 2003. Numerical modelling of the generation and transport of heat in a bottom ash monofill. *Journal of hazardous materials*, 100(1-3), pp.147-162.
- Krushelnitzky, R.P. and Brachman, R.W.I., 2013. Buried high-density polyethylene pipe deflections at elevated temperatures. *Geotextiles and Geomembranes*, 40, pp.69-77.
- Kutsyi, D.V., 2015. Numerical modeling of landfill gas and heat transport in the deformable MSW landfill body. Part 1. Development of the model. *Thermal Engineering*, 62(6), pp.403-407.
- Kwak, C.W., Park, I.J. and Park, J.B., 2015. Development of Modified Interface apparatus and prototype cyclic simple shear test considering chemical and thermal effects. *Geotechnical Testing Journal*, 39(1), pp.20-34.
- Luan, M., Lu, H. and Zhang, J., 2012. The Transport of Cr (VI) Through Landfill Liners at Different Temperature and pH. *Physical and Numerical Simulation of Geotechnical Engineering*, (7), pp.45-49.
- Luetlich, S.M. and Yafrate, N., 2016. Measuring Temperatures in an Elevated Temperature Landfill. In *Geo-Chicago 2016* (pp. 162-176).
- Martin, J.W., Stark, T.D., Thalhamer, T., Gerbasi, G.T. and Gortner, R.E., 2011. Reaction and combustion indicators in MSW landfills. In *Geo-Frontiers 2011: Advances in Geotechnical Engineering* (pp. 1045-1054).
- Nastev, M., Therrien, R., Lefebvre, R. and Gelinas, P., 2001. Gas production and migration in landfills and geological materials. *Journal of contaminant hydrology*, 52(1-4), pp.187-211.
- Ng, C.W.W., Feng, S. and Liu, H.W., 2015. A fully coupled model for water–gas–heat reactive transport with methane oxidation in landfill covers. *Science of the Total Environment*, 508, pp.307-319.
- Neusinger, R., Drach, V., Ebert, H.P. and Fricke, J., 2005. Computer simulations that illustrate the heat balance of landfills. *International journal of thermophysics*, 26(2), pp.519-530.
- Stark, T.D., Akhtar, K. and Hussain, M., 2010. Stability analysis for a landfill experiencing elevated temperatures. In *GeoFlorida 2010: Advances in Analysis, Modeling & Design* (pp. 3110-3119).
- Thomas, H.R. and Ferguson, W.J., 1999. A fully coupled heat and mass transfer model incorporating contaminant gas transfer in an unsaturated porous medium. *Computers and Geotechnics*, 24(1), pp.65-87.
- Várfalvi, J., Kontra, J., Takács, J. and Krajčík, M., 2016. Estimation and Measurement of Heat from Municipal Landfills. In *Applied Mechanics and Materials* (Vol. 832, pp. 103-108).

- Yeşiller, N., Hanson, J.L., Kopp, K.B. and Yee, E.H., 2016. Heat management strategies for MSW landfills. *Waste Management*, 56, pp.246-254.
- Yoshida, H. T. N.; Hozumi, H. Theoretical Study on Heat Transport Phenomena in a Sanitary Landfill. In *Proceedings Sardinia 97, Sixth International Landfill Symposium, 1997*; pp 13–17.
- Zambra, C.E. and Moraga, N.O., 2013. Heat and mass transfer in landfills: Simulation of the pile self-heating and of the soil contamination. *International Journal of Heat and Mass Transfer*, 66, pp.324-333.

## **Chapter 3. Heat Generation and Accumulation in Municipal Solid Waste Landfills (Env. Sci. & Technol. 2017, 51, 12434–12442)**

### **3.1 Abstract**

There have been reports of North American landfills that are experiencing temperatures in excess of 80 – 100 °C. However, the processes causing elevated temperatures are not well understood. The objectives of this study were to develop a model to describe the generation, consumption and release of heat from landfills, to predict landfill temperatures, and to understand the relative importance of factors that contribute to heat generation and accumulation. Modeled heat sources include energy from aerobic and anaerobic biodegradation, anaerobic metal corrosion, ash hydration and carbonation, and acid-base neutralization. Heat removal processes include landfill gas convection, infiltration, leachate collection, and evaporation. The landfill was treated as a perfectly mixed batch reactor. Model predictions indicate that both anaerobic metal corrosion and ash hydration/carbonation contribute to landfill temperatures above those estimated from biological reactions alone. Exothermic pyrolysis of refuse, which is hypothesized to be initiated due to a local accumulation of heat, was modeled empirically to illustrate its potential impact on heat generation.

### **3.2 Introduction**

Recently, there have been several reports of municipal solid waste (MSW) landfills that have been experiencing temperatures in excess of 80 – 100 °C (Calder and Stark, 2010; Luettich and Yafrate, 2016; Jafari et al., 2017). In some cases, these elevated temperatures have resulted in damage to the landfill's gas collection system, rapid settlement with subsequent implications for the integrity of the landfill cover and slope stability, elevated leachate volume and strength,

reduced methane content that may impact landfill gas treatment and energy generation processes, odorous gases, and/or challenges with regulatory compliance (Calder and Stark, 2010; Li et al., 2011). In cases where the elevated temperature extends to the bottom of the landfill, there may also be impacts on the service life of the geomembrane liner. Consequently, elevated temperature landfills (ETLFs) often require increased monitoring and management. While some ETLF owners have acknowledged receipt of reactive wastes that are a source of excessive heat, other owners are unaware of the burial of such wastes. Moreover, there is considerable uncertainty as to the mechanisms controlling heat accumulation in landfills.

Hanson et al. (2010) reported on spatial and temporal variations in temperatures at landfills in Alaska, British Columbia, Michigan, and New Mexico, and reported temperature ranges of 0.9 – 33.0, 14.4 – 49.2, 14.8 – 55.6, and 20.5 – 33.6 °C, respectively. Within these landfills, temperatures fluctuated seasonally near the landfill edges and surface, but had a stable core (Hanson et al., 2005 and 2008). In contrast to these ranges, temperatures above 100 °C have been reported at some ETLFs (Calder and Stark, 2010; Luettich and Yafrate, 2016; Jafari et al., 2017).

A number of heat-generating reactions occur when MSW and other non-hazardous wastes are buried in landfills. Reactions include both aerobic and anaerobic biodegradation (Li et al., 2011; Grillo, 2014), anaerobic metal corrosion (Calder and Stark, 2010), and acid-base neutralization (Rees, 1980). Some landfills accept ash from the combustion of coal, MSW, or other carbonaceous materials. Fly ash typically contains oxides (e.g., CaO), that undergo both hydration and carbonation reactions (Speiser et al., 2000; Li et al., 2007). While not documented in landfills, there are reports of thermochemical (pyrolytic) reactions in biomass (Kwon and Castaldi, 2012; Ciuta et al., 2014). Pyrolytic reactions may occur in landfills at elevated but

undefined temperatures. While these aforementioned reactions generate heat in landfills, understanding the extent to which heat accumulates is critical.

Several studies in which aspects of heat generation in landfills have been modeled are summarized in Table 3-S1 of the Supporting Information (SI). Unfortunately, published models do not consider abiotic reactions including metal corrosion, acid-base neutralization, ash hydration and carbonation, or pyrolysis. In addition, many models incorporate complex descriptions of biological processes (El-Fadel et al., 1996a; White et al., 2004; Grag, 2010; Fytanidis and Voudrias, 2014). While mechanistically accurate, parameterization in a landfill context is difficult and adds uncertainty. A second limitation of the aforementioned models is that they neglect other heat flows including the evaporation of water that saturates landfill gas, and moisture condensation.

The objective of this study was to develop a mathematical model to predict temperature impacts associated with a number of biological and chemical reactions that may occur in MSW landfills. Modeled heat sources include aerobic and anaerobic biological reactions, anaerobic metal corrosion, acid-base reactions, and ash hydration and carbonation. The model includes convective heat transport and removal mechanisms, including heat that is removed due to leachate collection, gas extraction, and evaporation. The governing equations for each heat source and sink are described next, followed by selected model simulations and sensitivity analyses.

### **3.3 Model development**

A model was developed to describe a single addition of MSW to a landfill, thus representing a relatively simple system for quantifying heat generation (Figure 3-1). The single addition of MSW was assumed to be a non-continuous and perfectly mixed closed unit where biotic and abiotic reactions occur. Therefore, the landfill unit was modeled as a batch reactor.

Based on the developed model, the temperature and concentrations do not vary spatially within the landfill unit, which was assumed to be surrounded by other waste with liquid and gas flux into and out of the unit volume. Water that enters with the waste as well as that from infiltration is considered. Since the system is closed and based on the single addition of MSW, gas and water movement only influence the transport of heat from the system but do not change the physical properties of the MSW. For this system, the outlet gas and liquid phases have the same temperature as the landfill unit. The model was developed to maximize flexibility with respect to user-specified input parameters in recognition of the site-specific nature of landfills as well as parameter uncertainty.

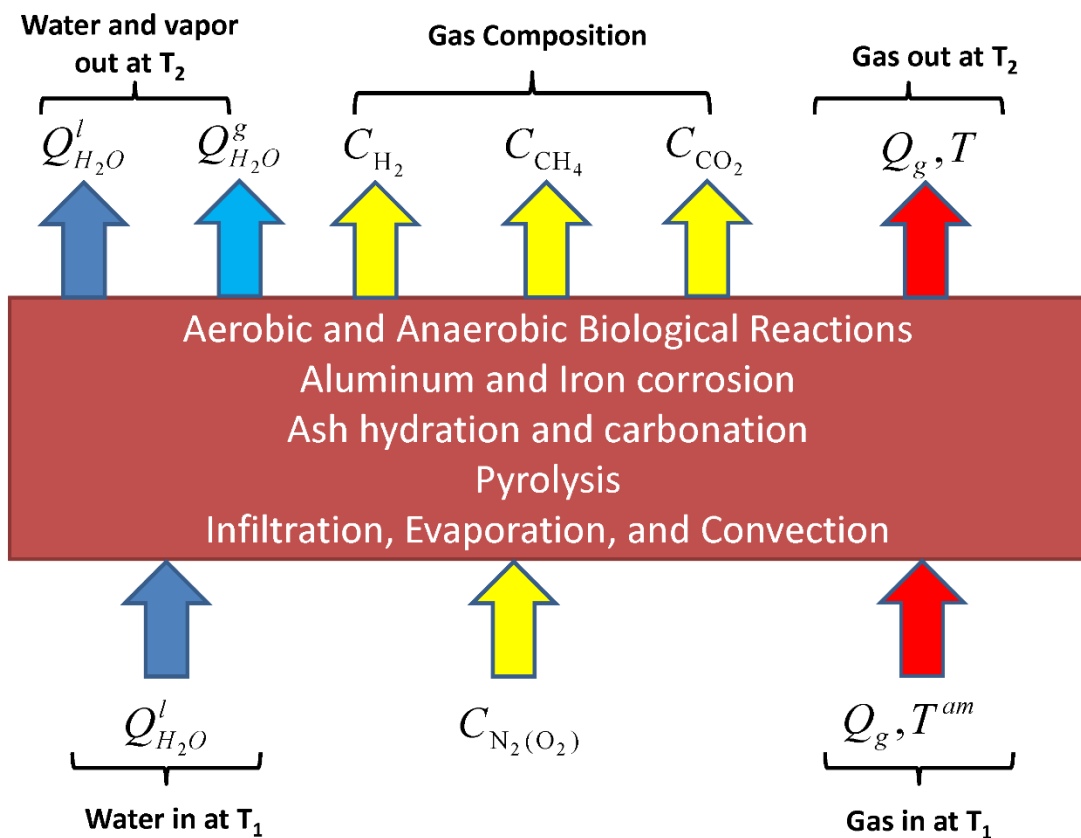


**Figure 3-1.** Schematic of the Landfill Batch Reactor Model. ( $Q$  is flow rate,  $T$  is temperature, and  $C$  is concentration)

The model employs an energy balance, where heat accumulation is equal to the net heat influx and heat generation (Eqn. 3-1).

$$\begin{aligned}
 \rho_s C_{p,s} V \frac{dT}{dt} = & \sum_{i=anaer. metal, H_2, ash} R_i (-\Delta H_i) V + S_{O_2} (-\Delta H_{aer}) \\
 & + \sum_{i=CH_4, CO_2} C_{p,i} R_i (T^{am} - T) V - \rho_{v, H_2O} L_{eva} \sum_{i=CH_4, CO_2, N_2} Q_i \\
 & + \rho_{H_2O} C_{p, H_2O} A Q_{H_2O} (T^{am} - T)
 \end{aligned} \tag{3-1}$$

where  $\rho_s$  and  $C_{p,s}$  are the weighted average density and heat capacity of the buried waste (Eqns. 3-S1 and 3-S2),  $V$  and  $A$  are the volume and surface area of the landfill,  $R_i$  is the generation rate of the indicator species,  $\Delta H_i$  is the heat (enthalpy change) of the chemical reactions,  $S_{O_2}$  is the biological  $O_2$  consumption rate,  $\Delta H_{aer}$  is the enthalpy change due to aerobic biodegradation,  $C_{p,i}$  is the heat capacity of species  $i$ ,  $T^{am}$  is the ambient temperature,  $T$  is the temperature in the landfill,  $\rho_{v, H_2O}$  is the density of saturated water vapor (Eqn. 3-S3) (Wagner and Pruß, 2002),  $L_{eva}$  is the latent heat of water evaporation ( $-2400 \frac{kJ}{kg H_2O}$ ),  $\rho_{H_2O}$  and  $C_{p, H_2O}$  are the density and heat capacity of water,  $Q_i$  is the flow rate of gaseous component  $i$ , and  $Q_{H_2O}$  is the infiltration rate.

The left side of Eqn. 3-1 represents heat accumulation in a landfill unit volume. The first term on the right side is the heat gain from chemical and anaerobic biodegradation reactions, the second term is the heat gain from aerobic biodegradation, and the third, fourth, and fifth terms are heat losses by convection, evaporation, and infiltration, respectively.

#### *Convection and infiltration*

Convection includes gas and liquid transport through the landfill. The temperature of gases and liquid entering the system are user specified. Heat removal from the transport of landfill gas,

which is comprised of CH<sub>4</sub>, CO<sub>2</sub>, and N<sub>2</sub>, represents convection due to gas transfer. Determination of gas flow rates is described in the section on biodegradation reactions.

Liquid movement is based on infiltration, assuming that water percolates vertically through the landfill until it is removed in the leachate collection system. The model does not allow liquid accumulation. Infiltration is based on an assumed rate of leachate generation [volume/(area-day)] that was adopted from industry estimates of typical leachate generation (Table 3-1). The flow of gas and liquid in the landfill leads to convective heat transfer, which is proportional to the temperature difference between the landfill and inlet fluid temperatures. The effect of infiltration on landfill temperature can therefore be considered as the convection of water. The heat capacities of the wastes, liquids, and gases are presented in Tables 3-1 and 3-S3.

#### *Evaporation and condensation*

Phase changes of water will consume or release energy. Inlet landfill gas (LFG) was assumed to be saturated with moisture at the initial gas temperature and LFG was assumed to remain saturated with increasing landfill temperatures. Thus, the evaporation of water from the waste to saturate LFG represents an energy sink. In contrast, if the temperature of refuse surrounding the landfill unit (Figure 3-1) was cooler than the refuse in the unit, then as hot LFG flows to the surrounding waste, energy would be released due to condensation. In the current batch reactor model formulation, variations in waste temperature and condensation could not be considered.

To assess the importance of condensation, a separate analysis was conducted. Assuming saturated LFG travels from BOX1 (hot) to BOX2 (cool), the temperature of BOX2 will increase from its initial temperature ( $T^{in}$ ) to the equilibrium temperature ( $T_2$ ) as a result of condensation

with subsequent energy release. The heat release ( $E_A$ ) includes the phase change of hot LFG leaving BOX1 at  $T_1$  and the decrease in water temperature from  $T_1$  to  $T_2$  (Eqn. 3-2).

$$E_A = (\rho_{H_2O(g),T_1} - \rho_{H_2O(g),T_2})V_{LFG}[L_{eva} + C_{p,H_2O}(T_1 - T_2)] \quad (3-2)$$

where  $\rho_{H_2O(g),T_1}$  and  $\rho_{H_2O(g),T_2}$  represent the density of steam at  $T_1$  and  $T_2$ , and  $V_{LFG}$  is the volume of LFG released from BOX1. Similarly, the heat absorbed by solid waste and water in BOX2 will result in a temperature change from  $T^{in}$  to  $T_2$  ( $E_B$ ) and can be written as:

$$E_B = \omega[\rho_s(1 - \varphi)C_{p,s}(T_2 - T^{in}) + \varphi\rho_{H_2O(l)}C_{p,H_2O}(T_2 - T^{in})] \quad (3-3)$$

where  $\omega$  is the volume ratio of BOX1 to BOX2,  $\rho_s$  and  $\rho_{H_2O(l)}$  are the density of waste and liquid water,  $\varphi$  is the moisture content in the waste, and  $T^{in}$  is the initial temperature of BOX2. At steady state, the heat released from hot LFG ( $E_A$ ) is equal to the heat absorbed by BOX2 ( $E_B$ ), and the temperature ( $T_2$ ) can be calculated.

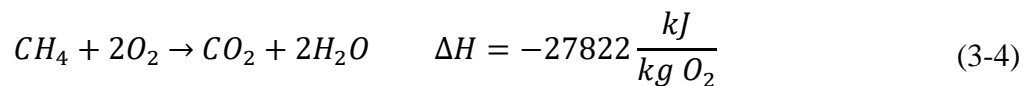
The heat released by condensation consists of the phase change of water at  $T_1$  and water cooling from  $T_1$  to  $T_2$ . The MSW in BOX2 is heated from  $T^{in}$  to  $T_2$ . Since the moisture content and density of saturated LFG are functions of temperature, the heat balance equation is coupled with Eqn. 3-3 and solved simultaneously.

### *Aerobic Biodegradation*

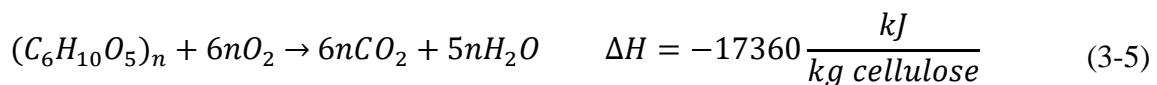
When waste is disposed in a landfill, some air is entrained at burial (Sanchez et al., 2010). This air was assumed to be rapidly consumed and the resulting temperature increase is considered when specifying the initial waste temperature. As freshly buried waste is by definition near the

landfill surface, heat loss will be high and the initial O<sub>2</sub> content was assumed to be an insignificant source of energy. Of more potential significance is the impact of air intrusion that may result from excess vacuum applied to the landfill's gas collection and control system (GCCS). Ideally, GCCS operation would not result in air intrusion; but the presence of N<sub>2</sub> in LFG suggests that some air intrusion occurs. The available O<sub>2</sub> was estimated from the LFG production rate (described below) and the user-specified N<sub>2</sub> concentration. Consequently, the volume of O<sub>2</sub> intrusion was estimated as 21/78 times the volume of N<sub>2</sub> based on the composition of air.

Several potential substrates may react with O<sub>2</sub>. For simplicity, two are considered in this analysis, methane and cellulose (Eqns. 3-4 and 3-5). If the bacteria that convert CH<sub>4</sub> to CO<sub>2</sub> in the presence of O<sub>2</sub> (methanotrophs) survive without O<sub>2</sub>, then aerobic methane oxidation (Eqn. 3-4) is likely to dominate O<sub>2</sub> consumption. While the long-term survival of methanotrophs has not been tested in landfills, they have been reported to survive for ~170 years in deep, aged lake sediments (Rothfuss et al., 1997).



In contrast, if methanotrophs do not survive, then cellulose oxidation (Eqn. 3-5) will likely govern. The effect of both substrates (CH<sub>4</sub> and cellulose) is considered in the Results.



The biological O<sub>2</sub> consumption rate was calculated using Eqn. 3-6.

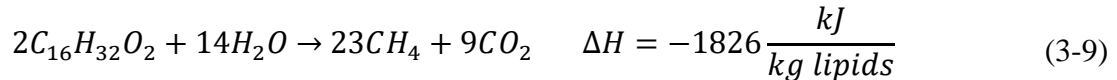
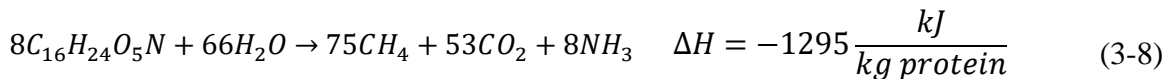
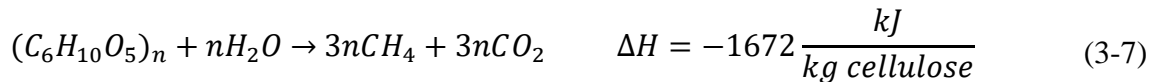
$$S_{O_2} = \frac{21}{78} \rho_{O_2} Q_{N_2} \quad (3-6)$$

where  $\rho_{O_2}$  is the density of  $O_2$ , and  $Q_{N_2}$  is the flow rate of  $N_2$ . Since aerobic reactions are much faster than anaerobic reactions,  $O_2$  was assumed to be consumed instantaneously after entering the landfill.

The  $\Delta H$  for the biological reactions in Eqns. 3-4 and 3-5 and below does not consider that some energy associated with substrate conversion is used for cell synthesis. As such, the enthalpies used in the model represent an upper limit on the amount of energy released.

#### *Anaerobic Biodegradation*

Three biodegradable components of MSW (carbohydrates, protein, lipids) were considered as substrates for  $CH_4$  generation. The stoichiometry and energetics for each substrate are presented in Eqns. 3-7 to 3-9, with carbohydrates (cellulose, hemicellulose, starch) represented as cellulose.



The rate of heat release was calculated from the rate of  $CH_4$  generation as described here. In practice, US EPA's LFG emissions model (LandGEM) is typically used to estimate  $CH_4$  generation and the default value for the  $CH_4$  generation rate constant ( $k_m$ ) in non-arid regions is  $0.04 \text{ yr}^{-1}$  (U.S. EPA, 1998 and 2005). The LandGEM modeling approach was adopted here. Using

$k_m$  for MSW, de la Cruz and Barlaz (2010) described a method to estimate waste component specific decay rates ( $k_{mi}$ ) for the major biodegradable components of MSW (food waste, grass, leaves, various types of paper). The CH<sub>4</sub> generation rate was calculated for each waste component using Eqn. 3-10 and previously reported values for  $L_0$  and  $k_{mi}$  for each waste component (Table 3-S4). The CH<sub>4</sub> generation rate was then used with the stoichiometric relationships defined in Eqns. 3-7 to 3-9 to estimate the substrate biodegradation rate and subsequent rate of heat release. With the exception of food waste, all biodegradation was attributed to carbohydrates. Food waste was divided into carbohydrate, protein and lipid fractions as described in Table 3-S4.

$$Q_{ni} = f_{CH_4}(T)k_{mi}L_{0i} \sum_{p=0}^n \sum_{q=0.0}^{0.9} \frac{M_p}{10} e^{-k_{mi}t_{p,q}} \quad (3-10)$$

where  $Q_{ni}$  is the CH<sub>4</sub> generation rate in year  $n$  of biodegradable component  $i$ ,  $f_{CH_4}(T)$  is defined in Eqn.3-11,  $k_{mi}$  is the first-order decay rate constant of biodegradable component  $i$ ,  $L_{0i}$  is the CH<sub>4</sub> generation potential of biodegradable component  $i$ ,  $M_p$  is the waste mass placement in year  $p$ ,  $q$  is an intra-annual time increment used to calculate CH<sub>4</sub> generation, and  $t$  is time. For the model described here, only one mass of MSW was disposed at one time.

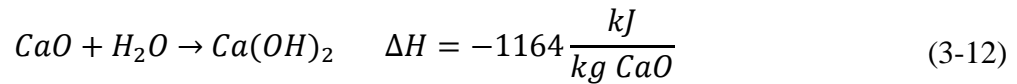
While methanogens have been reported to survive at temperatures as high as 89 °C, this is not typical (Amend and Shock, 2001). Thermophilic methanogens in anaerobic digesters and methanogenesis from acetate are reported to have an upper temperate limit of ~75 °C (Zinder et al., 1984; Nozhevnikova et al., 1999; Sosnowski et al., 2003; Nielsen et al., 2004). To account for the influence of temperature on CH<sub>4</sub> generation, an inhibition function [ $f_{CH_4}(T)$ ] was developed (Eqn. 3-11).

$$f_{CH_4}(T) = 4 \frac{T^6}{K_T^6 + T^6} \frac{K_T^7}{K_T^7 + T^7} \quad (3-11)$$

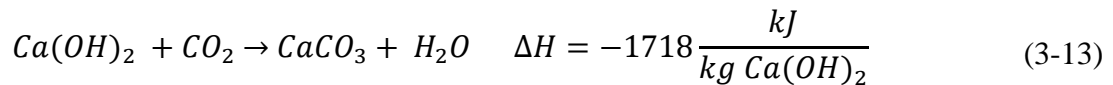
where  $T$  is temperature and  $K_T$  is a constant (37 °C). The inhibition function is 1 at 37 °C and diminishes as the temperature increases (Figure 3-S1).

#### *Ash hydration and carbonation*

Ash disposed in landfills typically contains several oxides/hydroxides including CaO/Ca(OH)<sub>2</sub>, MgO/Mg(OH)<sub>2</sub>, Na<sub>2</sub>O/NaOH, K<sub>2</sub>O/KOH, and P<sub>2</sub>O<sub>5</sub> (Speiser et al., 2000; Rendek et al., 2007; Morales-Flórez et al., 2015). The hydration of CaO is illustrated in Eqn. 3-12 and hydration of other oxides is given in Eqns. 3-S4 to 3-S7.



Ultimately, the generated hydroxides are converted to carbonates by reacting with CO<sub>2</sub>, as described by Eqn. 3-13 for Ca(OH)<sub>2</sub> and Eqns. 3-S8 to 3-S10 for other hydroxides (Li et al., 2007).



Both water and CO<sub>2</sub> were assumed to be present in excess and both hydration and carbonation are explored in the results.

The presence of oxides versus hydroxides is specific to the waste source and the manner in which the ash is handled prior to disposal. As such, the user can specify the content of the ash and

the fraction that is present as oxides and hydroxides (default values are presented in Table 3-S5). The rates of ash hydration and carbonation were assumed to follow first-order reaction models (Eqns. 3-14 and 3-15).

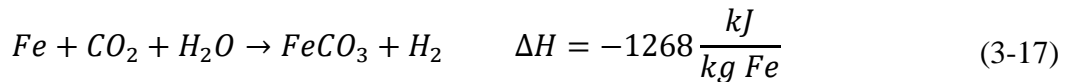
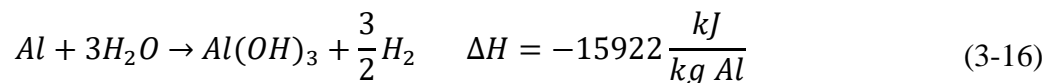
$$R_{hyd} = c_{oxide}k_{hyd} \quad (3-14)$$

$$R_{crb} = c_{hydroxide}k_{crb} \quad (3-15)$$

where  $R_{hyd}$  and  $R_{crb}$  are the rates of ash hydration and carbonation,  $c_{oxide}$  and  $c_{hydroxide}$  are the concentration of oxides and hydroxides in the ash, and  $k_{hyd}$  and  $k_{crb}$  are the reaction rate constants for hydration and carbonation, respectively.

#### *Anaerobic metal corrosion*

Landfills receive Al and Fe in elemental form from both MSW and special wastes that may include Al processing waste and auto shredder residue (Calder and Stark, 2010; Ahmed et al., 2014). Both Al and Fe have been reported to undergo corrosion reactions (Eqns. 3-16 and 3-17).



The rate and extent of corrosion will be governed by the surface area of the metal as well as the presence of protective coatings or oxides, and environmental conditions. To model heat generation from the corrosion of Al and Fe, corrosion was assumed to occur uniformly across the metal surface at a rate specified in  $\text{mm}\cdot\text{yr}^{-1}$ . To account for pitting type corrosion, which would

not impact the entire surface, sensitivity analyses were conducted with reduced effective surface areas.

The content of Al and Fe in MSW was coupled with metal sheet thickness and metal density to estimate the total surface area available for corrosion. Three categories of Al were considered (containers, foil, other) to allow for three thicknesses and three alloys, while two categories with two thicknesses were considered for Fe (containers, other). The characteristics of each metal are presented in Table 3-S6 and additional information on metal corrosion is presented in the SI.

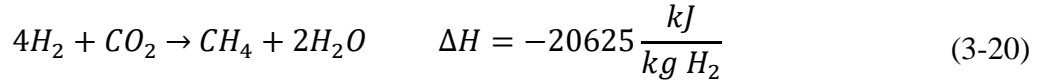
The reaction rates for anaerobic metal corrosion (Al and Fe) are described by Eqns. 3-18 and 3-19:

$$R_{Al}^i = \rho_{Al} \alpha_{Al}^j A_{Al}^i \quad (3-18)$$

$$R_{Fe}^i = \rho_{Fe} \alpha_{Fe}^j A_{Fe}^i \quad (3-19)$$

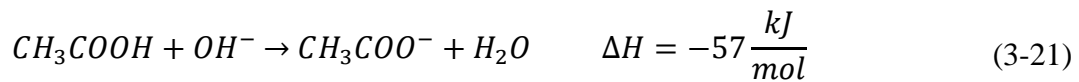
where  $R_{Al}^i$  and  $R_{Fe}^i$  are the reaction rates of metal source  $i$  ( $i=Al$  or  $Fe$  containers, Al foil, and other Al or Fe in Table 3-S6),  $\rho_{Al}$  and  $\rho_{Fe}$  are the density of Al and Fe,  $\alpha_{Al}^j$  and  $\alpha_{Fe}^j$  are the corrosion rates of metal alloy  $j$ , and  $A_{Al}^i$  and  $A_{Fe}^i$  are the surface area of metal  $i$ .

Hydrogen is a product of metal corrosion and can be converted to  $CH_4$  by hydrogenotrophic methanogens (Eqn. 3-20). Since  $CO_2$  is a major constituent in LFG, the  $H_2$  generated was assumed to be consumed instantaneously at the rate at which it is generated subject to the temperature inhibition defined in Eqn. 3-11.



#### *Neutralization (Acid-base reaction)*

Carboxylic acids are anaerobic biodegradation intermediates. When the microbial activity involved in waste decomposition is balanced, carboxylic acids do not accumulate and acid-base reactions are of little energetic consequence. However, there are scenarios in which carboxylic acids accumulate and the landfill pH may decrease to ~5. In this scenario, acidic leachate may percolate through the landfill and be neutralized by hydroxide ions generated by ash hydration and metal corrosion processes and/or the buffer capacity of the refuse. Acid-base neutralization was represented in the model with the simplifying assumption that all carboxylic acids are present as acetic acid (Eqn. 3-21). Neutralization was assumed to be instantaneous and the concentration of acetic acid is user-specified.



### **3.4 Model parameterization and input assumptions**

The parameters required to describe the physical characteristics of the landfill and the waste are presented in Table 3-1. The chemical composition of the MSW was estimated from the composition of each waste component (Table 3-S7). The biodegradable components in the waste include carbohydrates (25.4%), protein (4.4%) and lipids (8.3%), and the complete chemical composition is given in Table 3-S8. The values in Tables 3-1 and 3-S8 represent a base case and illustrative sensitivity analyses are presented with the results.

**Table 3-1.** Default model parameters used to describe landfill characteristics

<b>Parameter</b>	<b>Unit</b>	<b>Value</b>	<b>Comments and citations</b>
Initial mass	Mg	544	Daily waste mass for medium sized landfill (20% moisture)
Depth	m	30	Assumption
Infiltration rate	$\text{m}^3 \cdot \text{m}^{-2} \cdot \text{yr}^{-1}$	0.137	Value used in industry for landfills in regions receiving $\sim 100 \text{ cm rain} \cdot \text{yr}^{-1}$
Infiltration time	yr	20	Assumed time prior to placement of low conductivity final cover
Initial temperature	$^{\circ}\text{C}$	40	Assumed in consideration of some self-heating associated with initial aerobic decomposition
Ambient temperature	$^{\circ}\text{C}$	20	Assumed environmental temperature
Waste density	$\text{kg} \cdot \text{m}^{-3}$	890	Approximate industry average
Ash density	$\text{kg} \cdot \text{m}^{-3}$	1281	Approximate industry average
Waste heat capacity	$\text{kJ} \cdot \text{kg}^{-1} \cdot ^{\circ}\text{C}^{-1}$	1.32	Estimated as the sum of the heat capacity of individual components multiplied by their fractions (Yoshida and Hozumi, 1997). Default waste composition data given in Tables 3-S4 and 3-S7 and heat capacities given in Table 3-S4.
Ash heat capacity	$\text{kJ} \cdot \text{kg}^{-1} \cdot ^{\circ}\text{C}^{-1}$	0.8	Liang et al. (2008)
CH <sub>4</sub> generation rate constant ( $k_m$ )	$\text{yr}^{-1}$	component specific	Data for $k_m$ given in Table 3-S4.
CH <sub>4</sub> Production potential ( $L_0$ )	$\text{m}^3 \text{ CH}_4 \cdot \text{Mg}^{-1} \text{ waste}$	component specific	Data for $L_0$ given in Table 3-S4.
N <sub>2</sub>	%	2	Used to quantify air intrusion
Corrosion rate of Al (alloy 3004)	$\text{mm} \cdot \text{yr}^{-1}$	0.003	Eashwar et al. (1990)
Corrosion rate of Al (alloy 1100)	$\text{mm} \cdot \text{yr}^{-1}$	$2.54 \times 10^{-4}$	Ezuber et al. (2008)
Corrosion rate of coated Al (alloy 3004)	$\text{mm} \cdot \text{yr}^{-1}$	$5.17 \times 10^{-4}$	Shabani-Nooshabadi et al. (2009)
Corrosion rate of steel	$\text{mm} \cdot \text{yr}^{-1}$	$5 \times 10^{-4}$	Smart et al. (2001)

**Table 3-1.** Default model parameters used to describe landfill characteristics (Continued)

Corrosion rate of coated steel	mm·yr <sup>-1</sup>	2.54×10 <sup>-4</sup>	Smith et al. (1973)
Rate of ash hydration	yr <sup>-1</sup>	0.5	Assumption
Rate of ash carbonation	yr <sup>-1</sup>	0.1	Assumed rate is 20% of hydration rate based on literature from other environments (Morales-Flórez et al., 2015).
Acetic acid concentration	g·L <sup>-1</sup>	35	Assumption

### 3.5 Results and discussion

Relative contributions of various processes to heat accumulation and loss were evaluated through a series of systematic simulations. The base case simulation uses parameters at the default values (Tables 3-1 and 3-S8). The first set of simulations is based on biological reactions only, after which the contributions attributable to ash hydration and carbonation, metal corrosion, acid-base neutralization, and condensation are considered.

#### *Biodegradation*

Simulations of heat generation due to aerobic and anaerobic biodegradation of MSW are presented in Figure 3-2. Simulations were conducted with and without consideration of heat loss processes (evaporation, convection, cooling due to infiltration). Simulations without heat loss represent an upper bound as some heat loss is expected in landfills due to gas and leachate removal, and evaporation. The 2% N<sub>2</sub> cases translates to the availability of ~0.5% O<sub>2</sub>.

In the base case, the assumed air intrusion results in a ~1 °C increase relative to the temperature resulting from anaerobic decomposition only. When gas collection and leachate removal are the only heat removal processes, the model predicts a slight temperature decrease

relative to no heat loss. Similarly, the heat loss due to evaporation is relatively low because temperature inhibition of biological gas production reduces evaporative heat loss. In the absence of the temperature inhibition term (Eqn. 3-11), evaporative heat loss dominates (data not shown). When infiltration is added as a heat sink, the temperature decrease between years 12 and 20 reflects heat loss associated with the infiltration of cooler water and leachate removal from the system. The temperature increase after year 20 is due to the assumed placement of a final cover with the subsequent cessation of infiltration and leachate removal, and the dynamic equilibrium between heat generation from biodegradation and heat removal processes.

When the infiltration rate was increased by 50% relative to the base case, there is some additional cooling and the effect is most pronounced between years 10 and 20 at which time infiltration is constant but heat from biodegradation is decreasing. The case of evaporation plus convection is also a case of no infiltration (e.g., arid conditions) and the maximum temperature difference between no infiltration and infiltration at 150% of the base case infiltration rate is ~8 °C.

When the CH<sub>4</sub> generation rate constant is doubled, the predicted temperature is most sensitive to the rate about 5 years after waste burial at which time methane generation is not completely inhibited due to high temperature (Eqn. 3-10). The temperature increase due to the consumption of CH<sub>4</sub> as opposed to cellulose as the biodegradable substrate under aerobic conditions was less than 0.6 °C and cellulose was adopted as the substrate for aerobic biodegradation.

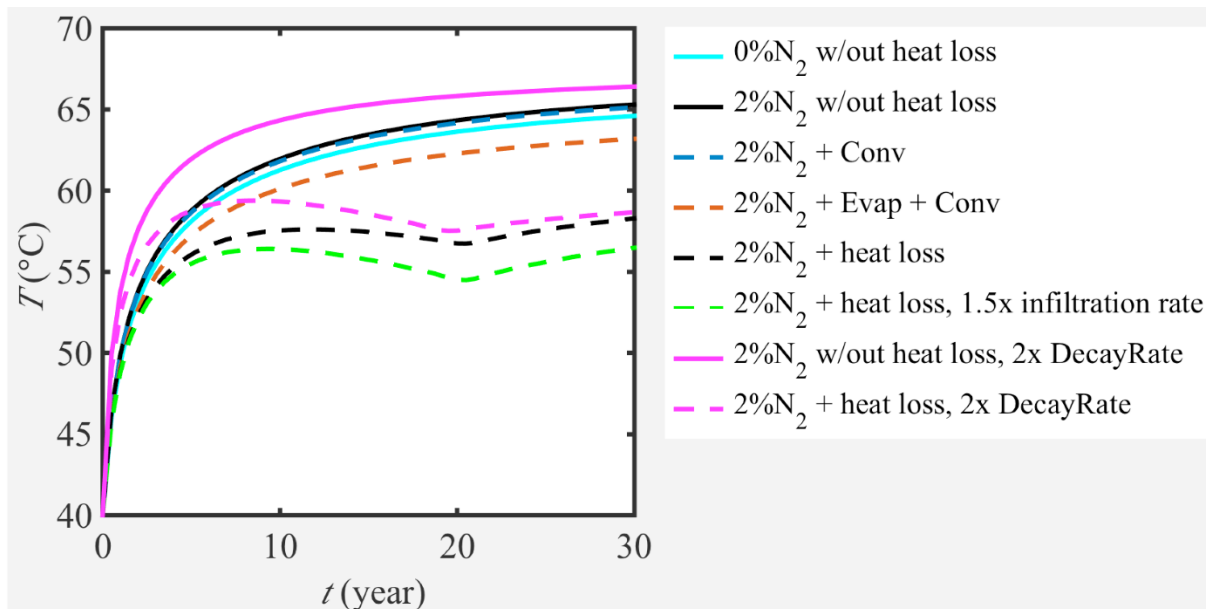


**Figure 3-2.** Heat accumulation associated with MSW biodegradation in the presence and absence of  $O_2$ . Solid lines represent cases without heat removal. Dashed lines consider heat removal process (Conv = convection, Evap = evaporation, heat loss = evaporation + convection + infiltration), 2x DecayRate = decay rate ( $k_m$ ) doubled for each biodegradable component listed in Table 3-S4.

### *Ash hydration*

Figure 3-3 displays the predicted temperature in a landfill that contains a mixture of MSW (90%) and ash (10%). The presence of ash results in additional heat accumulation due to ash hydration and carbonation. Considering ash hydration only, the model predicts a  $\sim 12$  °C temperature increase in year 10 for cases with and without heat loss. Inclusion of ash carbonation results in increases of  $\sim 28$  °C relative to the base case in year 10 for cases without and with heat loss. This trend is consistent with the greater enthalpy change associated with carbonation relative to hydration and the temperature trends also reflect the slower rate of carbonation relative to hydration. When the ash content of the buried waste is doubled, the year 10 temperature increases relative to the base case are 72 and 67 °C for cases without and with heat loss, respectively. In simulations of carbonation with heat loss, the temperature increase after year 20 is due to the

continued slow release of energy from carbonation in contrast to the rapid release of heat in hydration simulations.

The temperature is sensitive to the rate of ash carbonation which is uncertain but likely enhanced by typical LFG CO<sub>2</sub> concentrations of ~50% (Figure 3-S2). While not considered in these simulations, the heat generation associated with ash hydration and carbonation may also accelerate other reactions for which the reaction rate is temperature dependent.

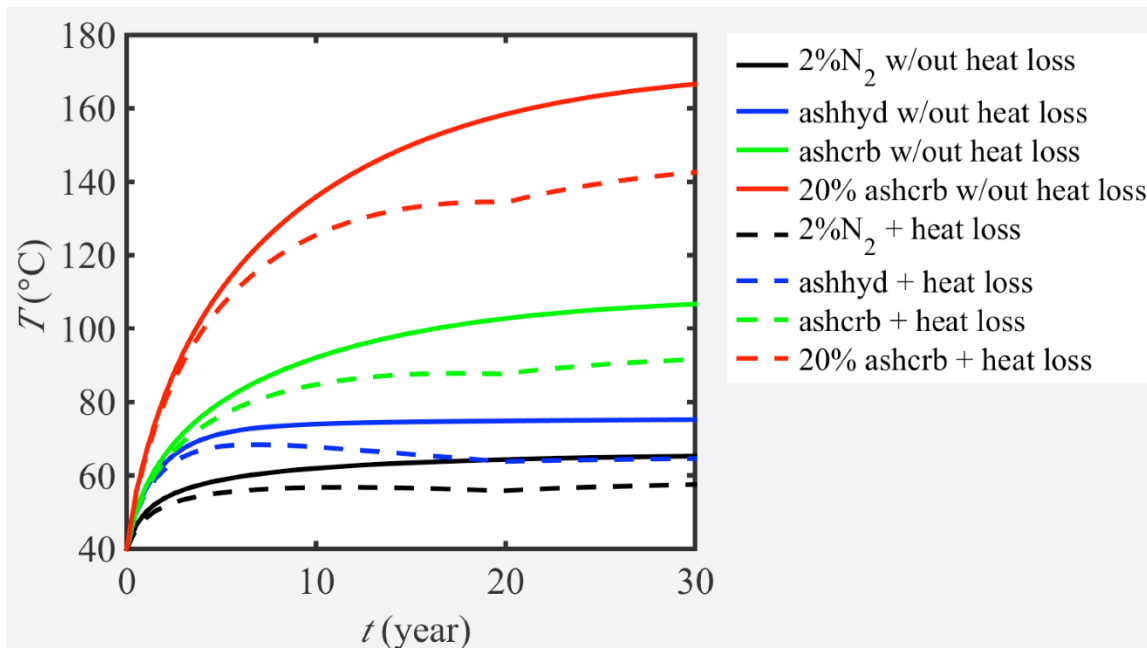


**Figure 3-3.** Impact of ash hydration and carbonation on landfill temperature. The solid and dashed black lines represent the base cases given in Figure 3-2. The blue and green lines represent the presence of 10% ash (Table 3-S5) and 90% MSW. The ashhyd line considers hydration only. The ashcrb lines consider hydration and carbonation as hydration is an essential reaction for carbonation at landfill temperatures. The plot simulates the sensitivity to 20% ash. The ash hydration and carbonation rates are 0.5 and 0.1 yr<sup>-1</sup>, respectively.

### *Metal corrosion*

Simulations of the impact of Al corrosion on temperature are presented in Figure 3-4. For the temperature profiles without heat loss, the slope decreases at years 22 and 31 are due to the consumption of Al foil and Al containers, respectively. The predicted temperatures indicate that Al corrosion may significantly impact landfill temperatures. For example, the year 10 increase in

predicted temperature is ~20 °C relative to the base case for simulations with and without heat loss, and a 100% corroded surface area (i.e., uniform corrosion). At the predicted temperatures, biological methane production is inhibited and the H<sub>2</sub> produced from Al corrosion will accumulate. Infiltration is again the dominant heat loss mechanism though not apparent from the temperature profiles.

To consider the occurrence of pitting as opposed to uniform corrosion, the affected surface area was reduced, which results in a decrease in heat accumulation. When heat removal processes are incorporated, temperatures are still elevated relative to the MSW only case. For the case of 50% corroded surface area, the temperature increases 9 °C compared to the MSW only case at year 10.

The effect of a higher corrosion rate for the first 6 months is presented in Figure 3-S3. The complete consumption of Al foil occurs 5 years earlier than the case with a constant corrosion rate, and the year 10 increase in predicted temperature is slightly higher than that predicted for a uniform corrosion rate, which is due to the greater heat release in the first 6 months after burial.

In contrast to Al corrosion, which resulted in predicted year 10 temperatures of 19 °C above the base case with heat loss considered, the increase associated with Fe corrosion is less than 1 °C at year 10 (Figures 3-4 and 3-S4). These results are consistent with the enthalpy data in Eqns. 3-16 and 3-17. However, the temperature impact of Fe is sensitive to corrosion rate (Figure 3-S4).

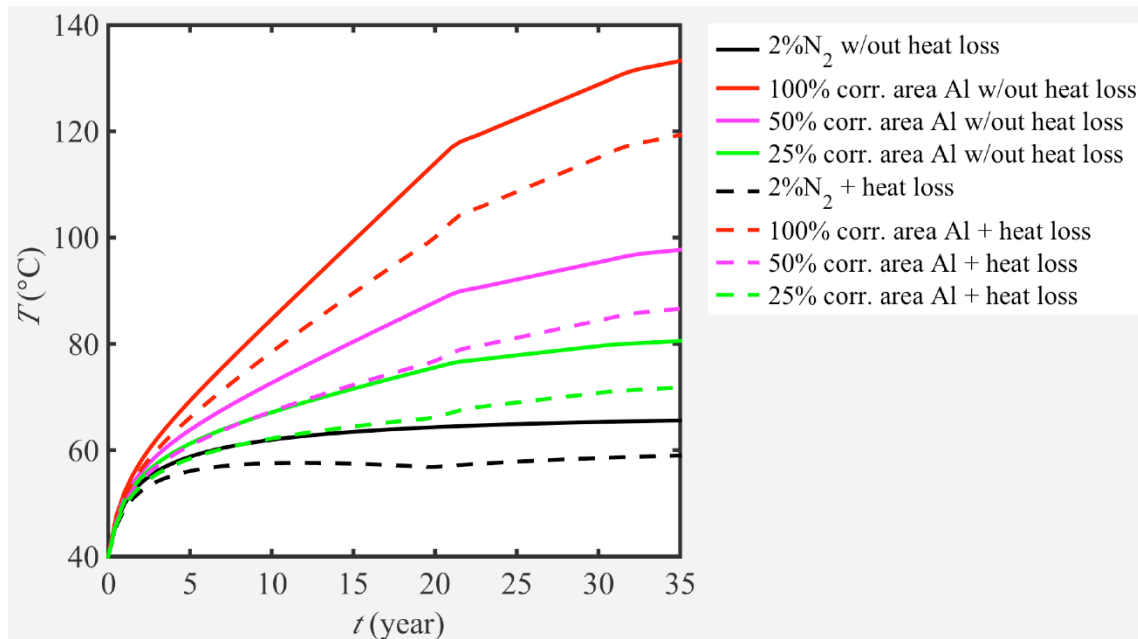


**Figure 3-4.** Impacts of Al corrosion on landfill temperature using the corrosion rates given in Table 3-1. The solid and dashed black lines represent the base cases given in Figure 3-2. The lines for 50% and 25% simulate partial corrosion across the surface area.

#### *Neutralization reaction*

To evaluate the importance of acid-base neutralization, 35 g/L of acid was assumed to be neutralized. The results are presented in Figure 3-S5 and indicate that heat generation due to neutralization is not important using the base case assumptions, as the temperature increased by only 0.7 °C in year 30.

#### *Condensation*

Condensation reactions could not be evaluated in the model. Thus, separate calculations were performed as described by Eqns. 3-2 and 3-3. There are a number of variables that affect the impact of condensation including the temperature of the gas moving from BOX1 (hot) to BOX2 (cool), the simulation time, and the relative volumes of BOX1 and BOX2. In an actual landfill, the hottest gas would interact with a directly adjacent small mass of refuse, which suggests that the mass in BOX1 should be larger than that in BOX2.

The results show that the temperature in BOX2 increases with an increase in the temperature of the gas in BOX1, simulation time, and the ratio of BOX1 to BOX2 (Table 3-2). These results suggest that condensation of LFG can result in elevated temperatures when condensation impacts a relatively small volume of refuse. Condensation may occur as LFG moves laterally and represents a mechanism for the spread of heat in ETLFs.

**Table 3-2.** Impact of gas condensation on waste temperature<sup>a</sup>

Temp of gas flowing from BOX1 $T_1$ (°C)	Simulation Time (yr)	The volume ratio of BOX1 to BOX2 ( $\omega$ )	Temp of waste in Box2 after equilibration $T_2$ (°C) <sup>a</sup>
70	0.1	1	41
	0.1	10	44
	1	1	44
	1	10	60
85	0.1	1	41
	0.1	10	49
	1	1	49
	1	10	75

<sup>a</sup>. The initial temperature of BOX2 was assumed to be 40 °C.

#### *Maximum Plausible Temperature*

The maximum (year 30) temperatures associated with biological reactions are about 65 and 58 °C, for cases without and with heat loss, respectively. In contrast, even when heat loss is considered, the presence of 1.7% Al resulted in a predicted year 10 temperature of 77 °C for a case with 100% corroded area available. To develop a higher but plausible temperature, a simulation was conducted with 80% MSW, 20% ash, waste decay rates that are double the default values, and the base case Al, Fe, and carboxylic acid contents. The predicted year 10 temperatures are 151 and 162 °C for cases with and without heat loss, respectively (Figure 3-S6). While temperatures up to ~140 °C have been reported at ETLFs (Calder and Stark, 2010; Jafari et al., 2017), most landfills that receive the types of waste considered in the model simulations do not reach

temperatures of even 77 °C as estimated for Al corrosion, suggesting that the model is overestimating temperatures in some cases.

There are several potential explanations for the overestimate. Metal corrosion has the largest contribution to heat accumulation but the concentration and corrosion rate applied in the simulations are uncertain and some corrosion may have occurred prior to burial. Second, the relative concentrations of oxides vs. hydroxides are uncertain as are the rates of hydration and carbonation.

The described model assumes a completely mixed system although landfills are heterogeneous with variable reactant concentrations and reaction rates. Localized accumulations of reactive materials (e.g., Al) may occur, resulting in areas where the temperature exceeds that predicted in a batch reactor. The potential significance of a local accumulation of a reactive waste could be even more important considering that an alkaline waste (e.g., fly ash) will accelerate the rate of anaerobic Al corrosion. To explore the significance of a localized accumulation of heat, the potential for such an accumulation to initiate self-sustaining pyrolysis is explored in the following section.

### **3.6 Incorporation of pyrolysis**

To better understand the characteristics of pyrolysis in a landfill and its potential impact on temperature, the pyrolysis process was incorporated into the model. Unfortunately, pyrolysis in a landfill has not been quantified and the present implementation is exploratory. Pyrolysis of lignocellulosic materials has been described as a first-order reaction (Eqn. 3-22) (Orfao et al., 1999).

$$R_{pyro} = c_{cel}k_{pyro} \quad (3-22)$$

where  $R_{pyro}$  is the rate of the pyrolytic reaction,  $c_{cel}$  is the cellulose concentration, and  $k_{pyro}$  is the reaction rate constant.

Mok et al. (1983) and Antal and Gronli (2003) showed that cellulose pyrolysis consists of endothermic and exothermic stages. In the endothermic stage, the combination of external heat and the presence of volatiles are required to raise the temperature to initiate an exothermic stage. In the exothermic stage, the pyrolytic reaction itself provides sufficient heat for the reaction to be self-sustaining. The products of exothermic pyrolysis include char, tar, condensable volatile species, and H<sub>2</sub>, CO, CO<sub>2</sub>, and H<sub>2</sub>O.

Three parameters were used to represent pyrolysis empirically: (1) initiation temperature ( $T_{ini}$ ), (2) reaction rate constant ( $R_{pyro}$ ), and (3) enthalpy ( $\Delta H_{pyro}$ ). An initiation function is proposed to describe exothermic pyrolysis initiation (Eqn. 3-23). Exothermic pyrolysis begins and a heat generation rate calculated when the system temperature ( $T$ ) exceeds  $T_{ini}$ .

$$f_{ini}(T) = 0.2\sqrt{2\pi}erf\left[\left(\frac{T - T_{ini}}{\sqrt{2}}\right) + 2.5\right] \quad (3-23)$$

To incorporate pyrolysis into the model, an additional source term was added to the right side of Eqn. 3-1 and is shown as the last term in Eqn. 3-24:

$$\begin{aligned}
\rho_s C_{p,s} V \frac{dT}{dt} = & \sum_{i=anaer,metal,H_2,ash} R_i (-\Delta H_i) V \\
& + \sum_{i=CH_4,CO_2} C_{p,i} R_i (T^{am} - T) V + S_{O_2} (-\Delta H_{aer}) \\
& - \rho_{v,H_2O} L_{eva} \sum_{i=CH_4,CO_2,N_2} Q_i + \rho_{H_2O} C_{p,H_2O} A Q_{H_2O} (T^{am} - T) \\
& + f_{ini}(T) R_{pyro} (-\Delta H_{pyro}) V
\end{aligned} \tag{3-24}$$

A range of enthalpy changes ( $\Delta H_{pyro}$ ) have been reported for cellulose pyrolysis ( $-2100$  to  $2510 \text{ kJ}\cdot\text{kg}^{-1}$ ) (Milosavljevic et al., 1996). As  $\Delta H_{pyro}$  for hemicellulose, starch, protein, lipids, and lignin have not been published, cellulose was used as the representative substrate.

To simulate the potential impact of pyrolysis, initiation temperatures ( $T_{ini}$ ) of  $120$  and  $180$  °C were assumed along with a  $\Delta H_{pyro}$  of  $-1000 \text{ kJ/kg}$  cellulose and a reaction rate of  $1 \text{ yr}^{-1}$ . All biological and chemical processes were simulated using the default values in Tables 3-1 and 3-S8. The simulations presented in Figure 3-5 reflect the heat released by biodegradation until the temperature exceeds the maximum temperature for anaerobic biodegradation, as well as heat release due to Al and Fe corrosion, ash hydration and carbonation, and acid-base neutralization. When the  $T_{ini}$  is  $120$  °C, the landfill temperature is predicted to exceed the pyrolysis initiation temperature in years 11 and 14 for the no heat loss and heat loss cases, respectively. Once pyrolysis occurs, the model predicts a sharp temperature increase. Thereafter, the temperature continues to increase even when heat loss is considered. This is because convective and evaporative heat losses are low, as only gas generation from biological reactions was considered, and biological reactions are inhibited. At a  $T_{ini}$  of  $180$  °C, the system does not exceed the initiation temperature, even for

the case without heat removal. In ongoing experimental work, reactors are being operated to characterize the initiation and energetics of MSW pyrolysis.

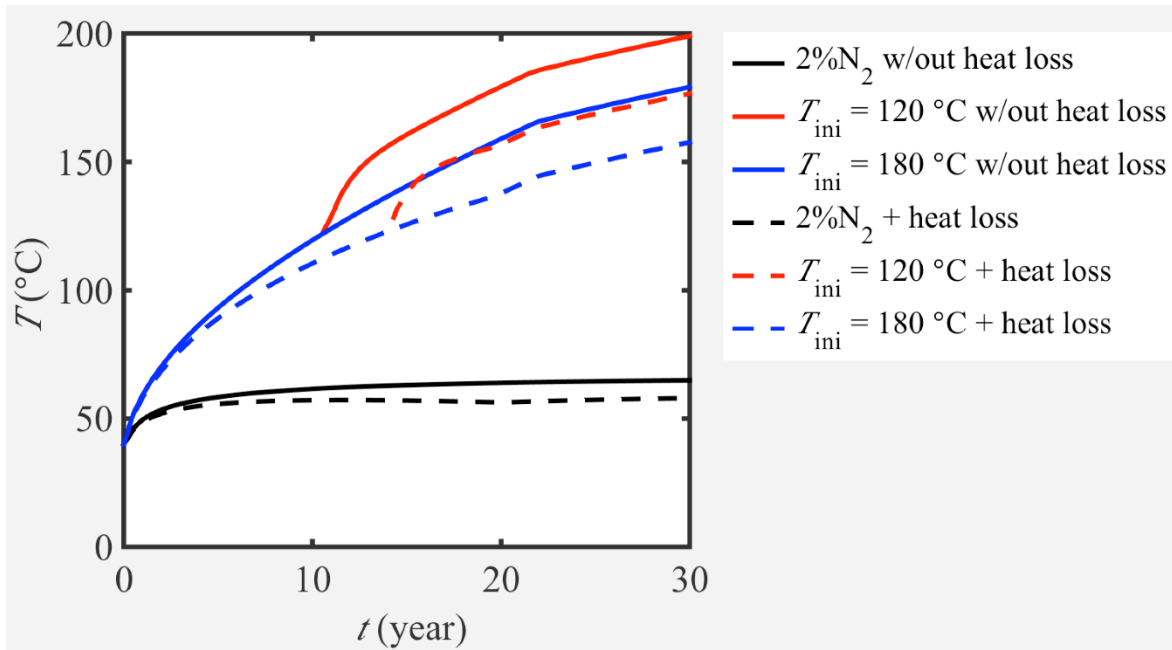


**Figure 3-5.** Simulation results with pyrolysis incorporated into the batch reactor model. The solid and dashed black lines represent the base case given in Figure 3-2. The red and blue lines consider different initiation temperatures for pyrolysis with (dashed) and without (solid) heat loss.

### **3.7 Implications and future work**

The results highlight the importance of heat removal on landfill temperatures, as predicted temperatures are considerably higher in the absence of convection and evaporation. While neither metal corrosion nor ash hydration and carbonation in MSW landfills is fully understood, the results show that these reactions have the potential to significantly increase landfill temperature.

There is uncertainty in many of the default parameter values as they were adopted from literature on systems other than landfills. In addition to parameter uncertainty, the first-order representation of ash hydration and carbonation has not been demonstrated in a landfill, further emphasizing the need for process-related research applicable to landfills. The predicted temperatures associated with metal corrosion are not realistic as some metal is routinely disposed in landfills and ETLFs are not widespread. Similarly, while exothermic pyrolysis is hypothesized to be important in ETLFs, the model adopted in this study must be considered illustrative until a better understanding of landfill pyrolysis is developed. A model that treats the landfill as series of interconnected control volumes with varying waste properties allowed in each control volume is under development to incorporate the heterogeneity of a landfill in which reactive wastes and air intrusion may be localized.

### **3.8 Supporting information**

Summary of previously published models, additional background on metal corrosion, additional modeling parameters, data on waste composition, summary of model nomenclature, illustration of the biological temperature inhibition function, simulations of Al and Fe corrosion and acid-base neutralization, and additional sensitivity analysis.

## Published models on heat generation in landfills

**Table 3-S1.** Previous models on heat generation in landfills

Reference	Description
El-Fadel et al. (1996b)	<ul style="list-style-type: none"> <li>• Described heat generation rate by incorporating a kinetic expression into a gas generation-microbial growth model</li> <li>• Assumed a proportional relationship between heat generation rate and acetic acid formation rate</li> </ul>
El-Fadel et al. (1996c)	<ul style="list-style-type: none"> <li>• Predicted methane production in consideration of biochemical and temperature feedback loops</li> <li>• Landfill temperature appears to be controlled by 1) total gas generation at specific depths; and 2) the imposed boundary condition at the landfill surface</li> </ul>
Yoshida and Hozumi (1997)	<ul style="list-style-type: none"> <li>• Developed a 1-D model to simulate the temperature distribution in a landfill</li> <li>• Incorporated heat transport and generation from biological decomposition</li> <li>• Predicted temperatures of ~70 °C caused by anaerobic biodegradation</li> <li>• Methane production was affected by temperature</li> </ul>
Gholamifard et al. (2007)	<ul style="list-style-type: none"> <li>• Developed a moisture-dependent biodegradation model</li> <li>• Simulated temperatures in a lab-scale bioreactor landfill with leachate recirculation</li> <li>• The calculation of heat generation rate was based on the methane production rate</li> <li>• Demonstrated an initial decrease in temperature with leachate injection, but was unable to predict the sharp rise in temperature thereafter</li> <li>• The additional heat generation was hypothesized to be related to aerobic biodegradation</li> </ul>
Gholamifard et al. (2008)	<ul style="list-style-type: none"> <li>• Developed a coupled biological and heat transport model</li> <li>• Predicted a vertical gradient of 1–10 °C/m between different layers</li> <li>• The maximum temperature in the deepest layer was 55 °C</li> </ul>

**Table 3-S1.** Previous models on heat generation in landfills (Continued)

---

Klein et al. (2003)	<ul style="list-style-type: none"><li>• Simulated temperature development in a bottom ash monofill</li><li>• The heat production due to exothermic reactions in the bottom ash is computed using a biexponential decaying heating rate</li><li>• The highest temperature (at the landfill center) was predicted to reach 97 °C after storage for 4 months</li></ul>
Neusinger et al. (2005)	<ul style="list-style-type: none"><li>• Simulated the thermal behavior of landfills by coupling heat and gas transfer</li><li>• Heat generation from biochemical reactions</li><li>• Heat transport in the solid matrix and heat transfer between fluids and the solid phase were not considered</li><li>• The maximum temperatures (in the center of the landfill) was ~80 °C</li></ul>
Gawande et al. (2010)	<ul style="list-style-type: none"><li>• Developed a generalized biochemical process model BIOKEMOD-3P</li><li>• Simulated bioreactor landfill operation in a completely mixed condition</li><li>• The heat generation rate was related to biological reactions</li></ul>
Garg and Achari (2010)	<ul style="list-style-type: none"><li>• Developed a model to simulate gas, heat, and moisture transport through a landfill</li><li>• Heat generation was related to the methane production and consumption rates</li><li>• Gas generation and transport equations were coupled to a heat balance</li></ul>
Ng et al. (2015)	<ul style="list-style-type: none"><li>• Developed a model that incorporated water-gas-heat coupled reactive transport in unsaturated soil</li><li>• Included a proportional relationship between heat generation rate and methane oxidation rate</li><li>• Incorporated heat convection, heat conduction, and heat source from methane oxidation</li></ul>

---

## **Metal corrosion**

The two major types of metal corrosion are uniform corrosion and pitting corrosion. Uniform corrosion occurs in highly acidic or alkaline media (Vargel, 2004). While not studied under simulated landfill conditions, uniform corrosion could occur as a result of hydroxides released from co-disposed ash, or from carboxylic acids that accumulate during the initial phase of anaerobic waste decomposition. Pitting corrosion results in the formation of irregularly shaped cavities on the metal surface in media with a neutral pH (Vargel, 2004). The process of pitting corrosion can be divided into initiation and propagation stages. The presence of  $\text{Cl}^-$  ions initiates pitting corrosion since  $\text{Cl}^-$  ions can be adsorbed on the metal-oxide film and/or incorporated into the film (Szkłarska-Smiałowska, 1999). Normally, most pits will stop after a few days due to the re-passivation of metals when oxygen is present. However, re-passivation of metals may not occur in landfills due to the anaerobic conditions and high  $\text{Cl}^-$  concentrations that prevail. Therefore, the initiated pits in a landfill could continue to propagate.

Corrosion rates have been reported either as  $\text{mm}\cdot\text{yr}^{-1}$  or as the rate of  $\text{H}_2$  generation (Eqn. 3-16) (Vargel, 2004). The  $\text{H}_2$  generation rate was used to describe the efficiency of  $\text{H}_2$  generation from metal powder (Yavor et al., 2013). The surface area of metal powder can be 3 to 4 orders of magnitude higher than that of a metal-sheet in landfills. Smart et al. (2001) reported that the initial iron corrosion rate (the first 1000 hr) is one order of magnitude higher than the rate after 5000 hr ( $0.5 \mu\text{m}\cdot\text{yr}^{-1}$ ) under anaerobic conditions.

To prevent metal corrosion, metal beverage containers have a thin coating on the interior surface. The main types of coating for Al and steel cans are epoxy-based resins. The North American Metal Packaging Alliance estimated that 95% of food container coatings are epoxy type. It was assumed that Al containers have one coated and one uncoated side, while other metal

categories shown in Table 3-S6 do not have a coating on either side. Shabani-Nooshabadi et al. (2009) reported that the corrosion rate of the polyaniline-coated Al alloy 3004 (Al containers) was  $5.17 \times 10^{-4} \text{ mm} \cdot \text{yr}^{-1}$ . Ezuber et al. (2008) found that the corrosion rate of Al alloy AA1100 (Al foils) was  $0.0254 \text{ mm} \cdot \text{yr}^{-1}$  in seawater at 23 °C. The corrosion rate of bare Al was reported to be  $0.003 \text{ mm} \cdot \text{yr}^{-1}$  in the coastal waters (Eashwar et al., 1990). In this analysis, corrosion on the metals' coated and uncoated sides was considered to occur simultaneously.

## Modeling parameters

Calculation of the density of buried waste

$$\rho_s = \frac{\rho_{msw}\rho_{ash}}{\rho_{msw}x_{ash} + \rho_{ash}x_{msw}} \quad (3-S1)$$

where  $\rho_s$ ,  $\rho_{msw}$ , and  $\rho_{ash}$  are densities of buried waste (wet refuse plus ash), wet refuse, and ash, respectively and  $x_{msw}$  and  $x_{ash}$  are weight fractions of wet refuse and ash, respectively.

Calculation of the heat capacity of buried waste

$$C_{p,s} = x_{msw} \left[ (1 - \varphi) \sum_{i=1}^n C_{p,i} x_i + \varphi C_{p,H_2O} \right] + x_{ash} C_{p,ash} \quad (3-S2)$$

where  $C_{p,s}$ ,  $C_{p,i}$ , and  $C_{p,ash}$  are heat capacities of buried waste (wet refuse and ash), biodegradable component  $i$  in wet refuse, and ash, respectively and  $\varphi$  is the moisture content.

Calculation of the density of saturated water vapor ( $\rho_{v,H_2O}$ ):

$$\ln \left( \frac{\rho_{v,H_2O}}{\rho_c} \right) = m_1 \tau^{\frac{2}{6}} + m_2 \tau^{\frac{4}{6}} + m_3 \tau^{\frac{8}{6}} + m_4 \tau^{\frac{18}{6}} + m_5 \tau^{\frac{37}{6}} + m_6 \tau^{\frac{71}{6}} \quad (3-S3)$$

where  $m_1$  to  $m_6$  are dimensionless constants of the density function of water vapor (Table 3-S2),  $\tau$  is the normalized temperature (ratio is in °K), and  $\rho_c$  is the reference density of water vapor.

**Table 3-S2.** Constants of the density function (Eqn. 3-S3) of water vapor (Wagner and Pruß, 2002)

<b>Constant</b>	<b>Value</b>
$m_1$	-2.03150240
$m_2$	-2.68302940
$m_3$	-5.38626492
$m_4$	-17.2991605
$m_5$	-44.7586581
$m_6$	-63.9201063

**Table 3-S3.** Heat capacities of gases and water (approximate values at 20 °C and  $1.01 \times 10^5$  Pa)

<b>Gas component</b>	<b>Heat capacity (kJ/kg·°C)</b>
Water	4.18
O <sub>2</sub>	0.92
N <sub>2</sub>	1.04
CH <sub>4</sub>	2.22
CO <sub>2</sub>	0.82

**Table 3-S4.** Characteristics of MSW as discarded

		Weight (% <sup>a</sup> )	heat capacity (kJ/kg·°C)	Moisture (%)	$L_0$ (m <sup>3</sup> CH <sub>4</sub> /Mg waste) <sup>b</sup>	$k_m$ (yr <sup>-1</sup> ) <sup>c</sup>
Food	Total	21.5	1.72 <sup>d</sup>	79.0 <sup>e</sup>	458.5 <sup>f</sup>	0.096
	Carbohydrate <sup>g</sup>	22.4 <sup>g</sup>	1.72 <sup>d</sup>	79.0 <sup>e</sup>		0.096
	Lipids <sup>g</sup>	38.9 <sup>g</sup>	1.72 <sup>d</sup>	79.0 <sup>e</sup>		0.096
	Protein <sup>g</sup>	20.4 <sup>g</sup>	1.72 <sup>d</sup>	79.0 <sup>e</sup>		0.096
Wood	Total	8.1	1.36 <sup>d</sup>	10.3 <sup>h</sup>	17.8 <sup>i</sup>	0.03 <sup>j</sup>
Plastics	PET	2.3				
	HDPE	3.1				
	PVC	0.5				
	LDPE/LLDPE	4.3	1.80 <sup>k</sup>			
	PLA	0				
	PP	4.5				
	PS	1.4				
	other plastics	2.0				
	Glass	Total	5.1	0.66 <sup>d</sup>		
Metals	Ferrous	7.2	0.66 <sup>d</sup>			
	Aluminum	1.7	0.93 <sup>d</sup>			
	other nonferrous	0.4	0.93 <sup>d</sup>			
Yard trimmings	Total	8.3	1.36 <sup>d</sup>	60.0 <sup>l</sup>		
	Grass <sup>m</sup>	2.5			194.8 <sup>n</sup>	0.6 <sup>j</sup>
	Leaves <sup>m</sup>	3.3			65.3	0.114
	Branches <sup>m</sup>	2.5			59.4 <sup>o</sup>	0.03 <sup>j</sup>
Paper	Newsprint	1.6	1.34 <sup>d</sup>	6.0 <sup>l</sup>	74.3	0.022
	Old corrugated containers (OCC)	2.1	1.34 <sup>d</sup>	6.0 <sup>l</sup>	195.1	0.013
	Mixed paper	11.6	1.34 <sup>d</sup>	6.0 <sup>l</sup>	148.7	0.021
Textile	Total	7.9	1.3 <sup>d</sup>	10.0 <sup>l</sup>		

**Table 3-S4.** Characteristics of MSW as discarded (Continued)

	Cotton <sup>p</sup>	1.6		263.6 <sup>q</sup>	0.02 <sup>q</sup>
	Synthetic <sup>p</sup>	6.3			
Leather		2.2	1.59 <sup>k</sup>		
Other		4.4	0.85 <sup>k</sup>		
<b>Total</b>		100	1.32 <sup>r</sup>	19.7	

- a. Data were obtained from the U.S. EPA (2015). Tires were excluded as they are typically not buried in MSW landfills.
- b.  $L_0$ , the CH<sub>4</sub> generation potential, from Hodge et al., unless otherwise noted (Hodge et al., 2016).
- c. CH<sub>4</sub> generation rate constants were obtained from Hodge et al. (2016), unless otherwise noted.
- d. Heat capacities from Miller and Clesceri (2002).
- e. Weighted average based on the moisture contents of various food wastes (grocery, restaurant, university dining hall, hotel) reported in Lopez et al. (2016).
- f. Weighted average of carbohydrate (cellulose, starch, and hemicellulose), lipids, and protein.  $L_0$  of carbohydrate, lipids, and protein were calculated by multiplying the stoichiometric methane potential (Eqns. 3-7 to 3-9) by the fraction of the mass loss for each compound (Lopez et al., 2016). The stoichiometric yields of carbohydrates, lipid and protein were calculated to be 414.8, 1006.3 and 677.4 m<sup>3</sup> CH<sub>4</sub>/dry Mg, respectively.
- g. Values are the average content across several types of food waste reported in Lopez et al. (2016) and are reported as a percentage of food waste.
- h. Weighted average based on the moisture contents of residential and commercial wood waste in Wang et al. (2011).
- i.  $L_0$  of wood is the average of red oak (33.3), radiata pine (0.5), spruce (7.5), medium density fiberboard (4.6), plywood (6.3), particle board (5.6), oriented strand board-hardwood (84.5), and oriented strand board, softwood (0) from Wang et al. (2011).
- j.  $k$  of wood, grass, and branches were obtained from de la Cruz and Barlaz (2010).
- k. Heat capacities from Hanson et al. (2013).
- l. Moisture content from Staley and Barlaz. (2009).
- m. Weighted average based on relative contribution of grass (30.3%), leaves (40.1%), and brush (29.6%) (Oshins et al., 2000).
- n.  $L_0$  of grass from Levis and Barlaz (2014).
- o.  $L_0$  of branches from Wang and Barlaz (2016)
- p. It was assumed that textiles are composed of 20% of cotton and 80% of synthetic (weight basis).
- q. It was assumed that the  $L_0$  and  $k$  of cotton are equal to the value of office paper.
- r. The heat capacity of solid waste was calculated based as a weighted average.

**Table 3-S5.** Chemical constituents that undergo hydration and carbonation in municipal solid waste incinerator (MSWI) bottom ash samples<sup>a</sup>

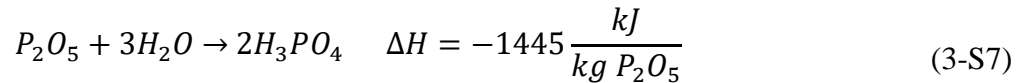
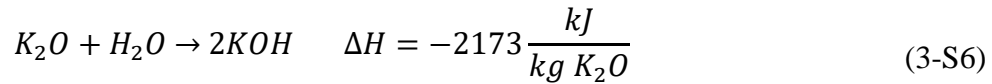
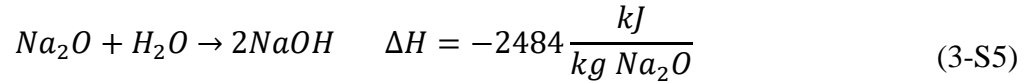
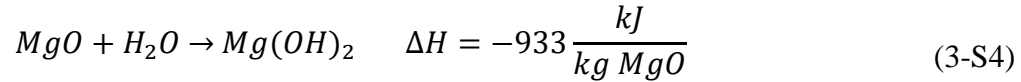
Constituents	Weight (%)	Hydrated at burial (%)
CaO	19.49	0
MgO	2.59	0
Na <sub>2</sub> O	4.52	0
K <sub>2</sub> O	1.19	0
P <sub>2</sub> O <sub>5</sub> <sup>b</sup>	1.65	0
inactive constituents <sup>c</sup>	70.58	0

a. Values are the average content across 5 MSWI samples reported in Rendek et al. (2007) and are reported as a percentage of bottom ash.

b. Undergoes hydration only.

c. Other constituents include SiO<sub>2</sub>, Al<sub>2</sub>O<sub>3</sub>, Fe<sub>2</sub>O<sub>3</sub>, TiO<sub>2</sub>, and MnO.

Hydration reactions of the oxides in ash



Carbonation reactions of the hydroxides

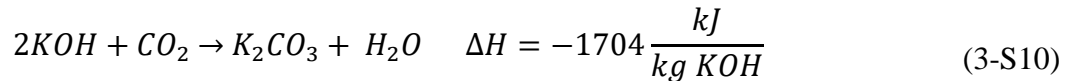
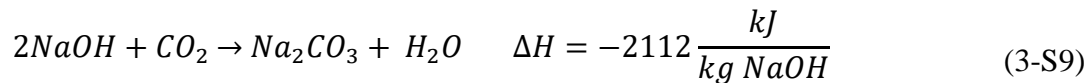
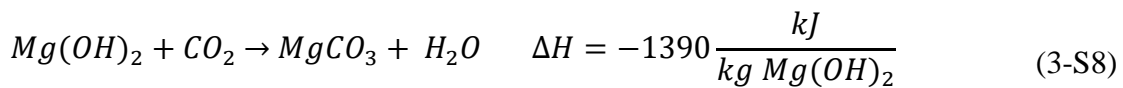


**Table 3-S6.** Average thicknesses of metals from containers and other sources

<b>Product Category</b>	<b>Percent of Metal (%)</b>	<b>Thickness (mm)</b>	<b>Coated Side</b>	<b>Alloy Type</b>
Al containers <sup>a</sup>	25 <sup>b</sup>	0.076 <sup>c</sup>	1	3004
Al foils and closures	15 <sup>b</sup>	0.016 <sup>d</sup>	0	1100
Other Al <sup>e</sup>	60 <sup>b</sup>	0.85 <sup>f</sup>	0	3004
Fe containers	5 <sup>g</sup>	0.32 <sup>h</sup>	1	Steel
Other Fe <sup>i</sup>	95 <sup>g</sup>	0.75 <sup>j</sup>	0	Steel

- a. Al containers include beer, soft drink and other cans.
- b. Weight percent of total Al discards from the U.S. EPA (2015).
- c. Data were obtained from Hosford and Duncan (1994).
- d. Data were obtained from U.S. Packaging & Wrapping LLC.
- e. Other Al includes durable/nondurable goods and other Al sources.
- f. The value is the average thickness of commercial embossed coated Al sheet for refrigerator inner panels.
- g. Weight percent of total Fe discards from the U.S. EPA (2015).
- h. The value is the average thickness of steel cans from ArcelorMittal.
- i. Other Fe includes durable goods and other Fe sources.
- j. The value is the average thickness of steel pre-coated sheets for home appliances.

**Table 3-S7.** Chemical composition of biodegradable waste components<sup>a</sup>

<b>Components</b>	<b>Carbohydrate<sup>b</sup> (%)</b>	<b>Lignin (%)</b>	<b>Protein (%)</b>	<b>Lipids (%)</b>
Food <sup>c</sup>	22.44		20.38	38.90
Wood <sup>d</sup>	57.46	28.33		
Yard trimmings				
Grass <sup>e</sup>	38.55	25.00		
Leaves <sup>e</sup>	25.80	43.80		
Branches <sup>e</sup>	53.80	32.60		
Paper				
Newsprint <sup>f</sup>	70.15	15.25		
OCC <sup>f</sup>	76.80	14.55		
Mixed paper <sup>g</sup>	73.76	10.89		
Textile				
Total				
Cotton <sup>h</sup>	90.70	2.70		
Synthetic				
<b>Total<sup>i</sup></b>	<b>25.37</b>	<b>7.04</b>	<b>4.37</b>	<b>8.35</b>

- a. Data given as % of dry weight except the total which is given as % wet weight for use in the model. Moisture contents are given in Table 3-S4.
- b. The carbohydrate content includes cellulose, hemicellulose, and starch.
- c. Weighted average based on the chemical compositions of various food wastes (grocery, restaurant, university dining hall, hotel) reported in Lopez et al. (2016).
- d. The weighted average values of wood were estimated based on the chemical compositions of residential and commercial wood waste in Wang et al. (2011).
- e. The carbohydrate content of grass is the average of the carbohydrate for grass and grass-2 in Eleazer et al. (1997). The same approach was also applied to calculate the carbohydrate and lignin contents of leaves and branches.
- f. The carbohydrate content of newsprint and old corrugated containers (OCC) was estimated based on the cellulose, hemicellulose, and lignin content of newsprint and CC in Wang et al. (2013).
- g. The carbohydrate and lignin content of mixed paper is the average of the values for newsprint, OCC, and copy paper (CP) in Wang et al. (2013).
- h. Data was obtained from Dorez et al. (2014).
- i. Calculated from the chemical content in this table and the waste composition (as discarded) given in Table 3-S4.

**Table 3-S8.** Biodegradable and reactive constituents in MSW considered in model

<b>Constituents</b>	<b>Content (wt. %)</b>
Carbohydrate <sup>a</sup>	25.4
Lignin	7.0
Protein	4.4
Lipids	8.3
Al <sup>b</sup>	1.7
Fe <sup>b</sup>	7.2
Other constituents <sup>c, d</sup>	46.0

- a. The carbohydrate content includes cellulose, hemicellulose, and starch.
- b. The Al and Fe contents were obtained from the U.S. EPA (2015) as described in Table 3-S4.
- c. Other constituents include plastics (18.0%), glass (5.1%), synthetic textiles (1.3%), and other materials.
- d. For some simulations, the waste was assumed to include combustion ash (base case -10%) and the composition of MSW was diluted accordingly. Ash composition is given in Table 3-S5.

## Nomenclature

**Table 3-S9.** Nomenclature

$A$	surface area, $\text{m}^2 \cdot \text{m}^{-3}$
$c$	concentration, $\text{kg} \cdot \text{m}^{-3}$
$C_p$	heat capacity, $\text{kJ} \cdot \text{kg}^{-1} \cdot ^\circ\text{C}^{-1}$
$f_{\text{CH}_4}$	inhibition function
$f_{\text{ini}}$	initiation function for pyrolysis
$\Delta H$	enthalpy, $\text{kJ} \cdot \text{kg}^{-1}$
$k$	reaction rate constant, $\text{yr}^{-1}$
$K_T$	a constant of the inhibition function, $^\circ\text{C}$
$L_0$	$\text{CH}_4$ generation potential, $\text{m}^3$ of $\text{CH}_4 \cdot \text{Mg}^{-1}$ waste
$L_{\text{eva}}$	latent heat of water, $\text{kJ} \cdot \text{kg}^{-1}$
$m_1$ to $m_6$	constants of density function of water vapor
$M_i$	waste mass placement in year $i$ , Mg
$Q$	flow rate, $\text{m}^3 \cdot \text{yr}^{-1}$
$Q_n$	$\text{CH}_4$ generation rate in year $n$ , $\text{m}^3 \cdot \text{yr}^{-1}$
$R$	reaction rate, $\text{kg} \cdot \text{m}^{-3} \cdot \text{yr}^{-1}$
$S$	heat source term, $\text{kg} \cdot \text{yr}^{-1}$
$t$	time, year
$T$	temperature, $^\circ\text{C}$
$T_{\text{ini}}$	initiation temperature, $^\circ\text{C}$
$V$	volume, $\text{m}^3$
$V_{\text{LEG}}$	the volume of landfill gas released from BOX1, $\text{m}^3$
$x$	weight fraction, dimensionless
<b>Greek letters</b>	
$\alpha$	corrosion rates, $\text{mm} \cdot \text{yr}^{-1}$
$\rho$	density, $\text{kg} \cdot \text{m}^{-3}$
$\rho_c$	reference density of water vapor, $\text{kg} \cdot \text{m}^{-3}$
$\tau$	normalized temperature
$\varphi$	moisture content
$\omega$	the volume ratio of BOX1 to BOX2
<b>Superscripts</b>	
$g$	gas phase
$l$	liquid phase
$in$	inlet
$am$	ambient
<b>Subscripts</b>	
$aer$	aerobic degradation process
$anaer$	anaerobic degradation process
$ash$	ash
$cel$	cellulose
$crb$	carbonation
$hyd$	hydration
$m$	$\text{CH}_4$
$msw$	municipal solid waste (wet)
$pyro$	pyrolysis
$s$	solid phase
$v$	vapor phase

## Supplemental results and discussion

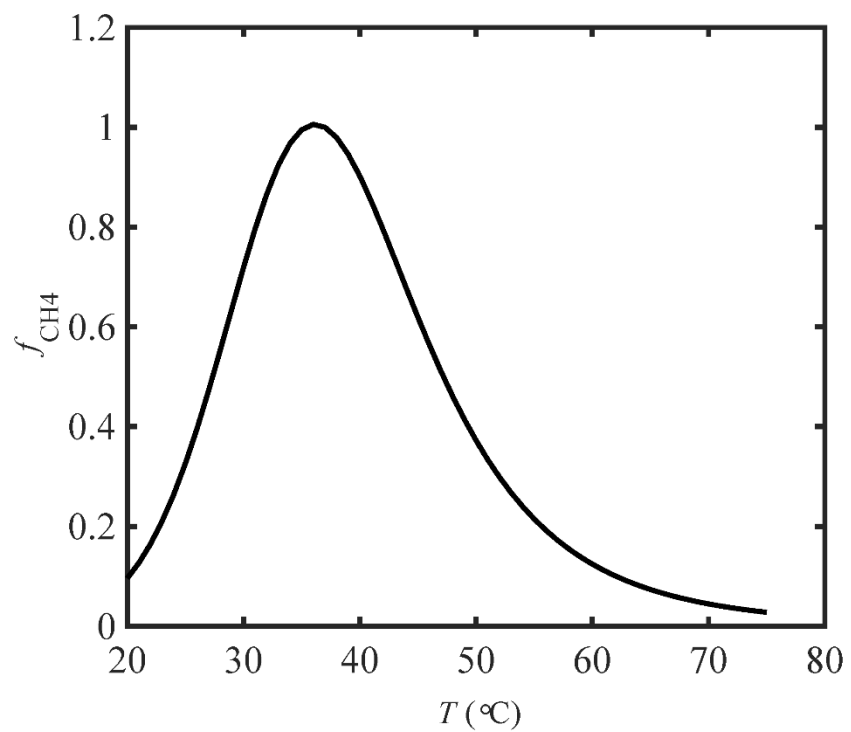


**Figure 3-S1.** Inhibition function described in Eqn. 3-11.

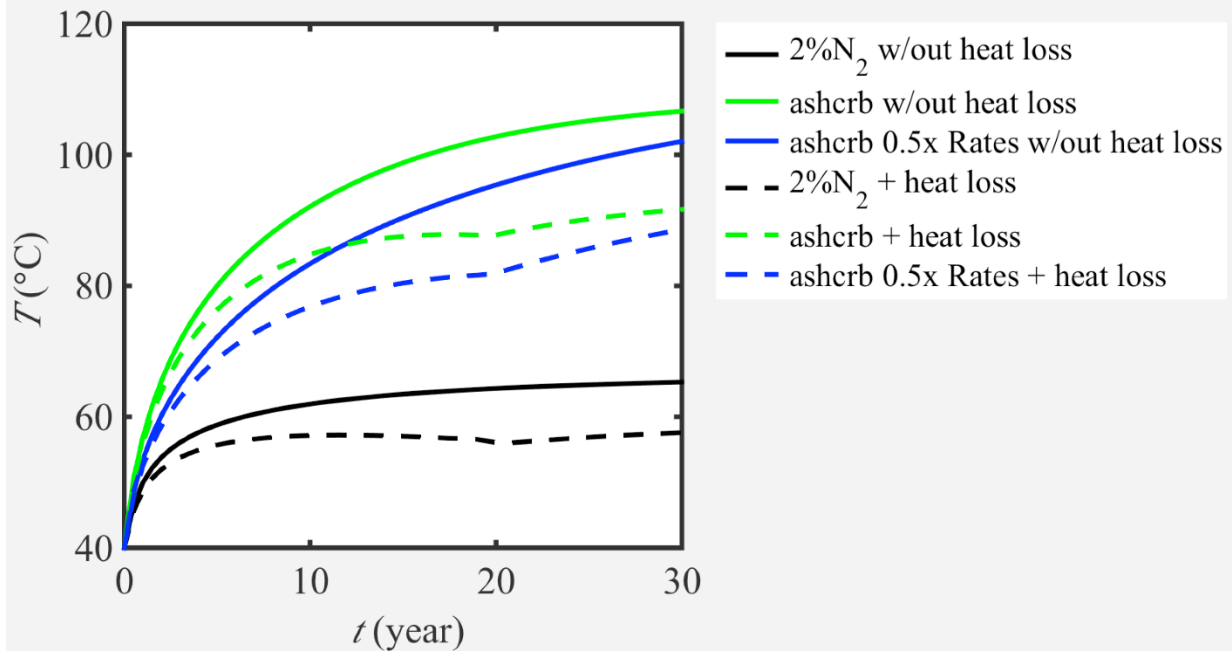


**Figure 3-S2.** Impact of ash carbonation on landfill temperature with varying carbonation rates. The solid and dashed black lines represent the base cases given in Figure 3-2. The blue and green lines represent the presence of 10% ash (Table 3-S5) and 90% MSW. The ashcrb simulation includes hydration and carbonation. For the ashcrb case, the ash hydration and carbonation rates are 0.5 and 0.1yr<sup>-1</sup>, respectively. These rates were decreased by 50% for the ashcrb 0.5x Rates case.

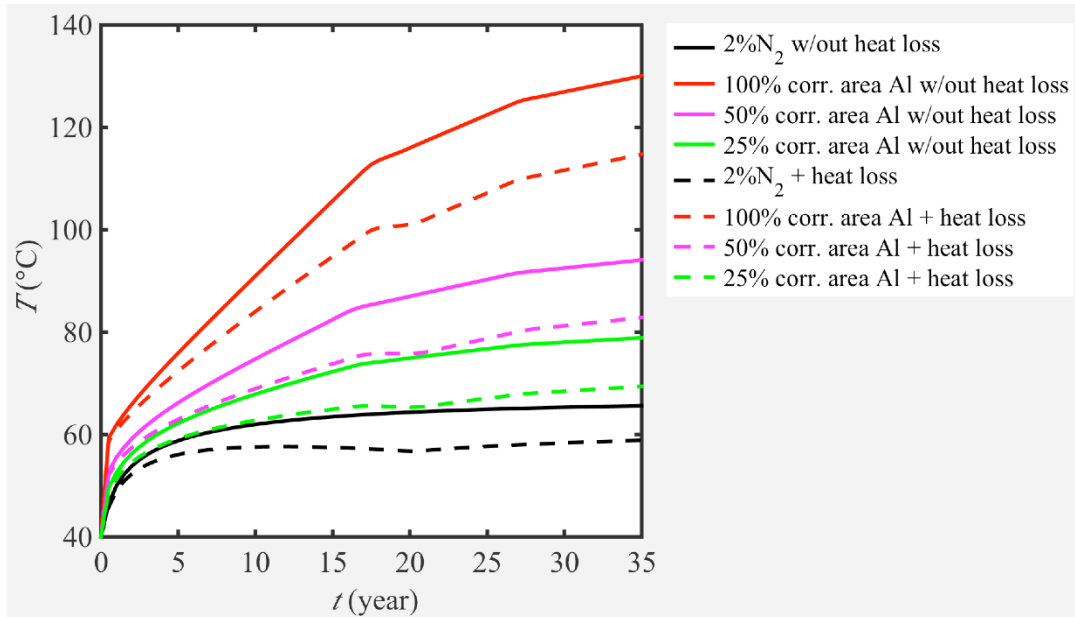


**Figure 3-S3.** Impact of Al corrosion on landfill temperature with temporally varying corrosion rates. The corrosion rate for the first 6 months was assumed to be ten times higher than the default rates given in Table 3-1. Thereafter, the default rates were used. The % represents the fraction of the total surface area available for corrosion. The solid and dashed black lines represent the base cases as given in Figure 3-2 and represent only biological reactions.

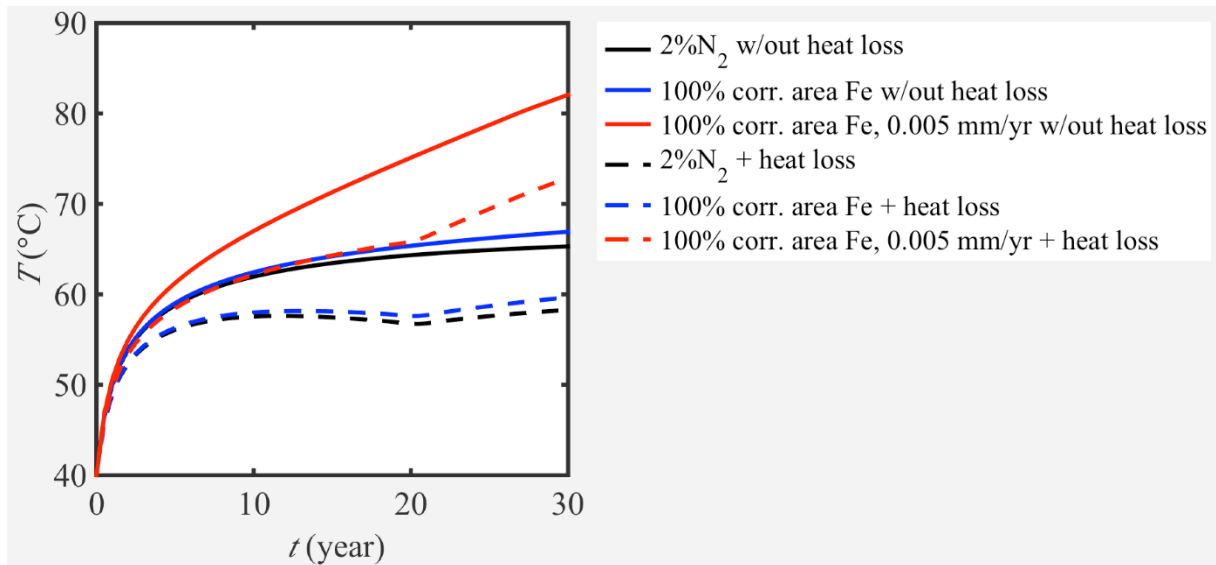


**Figure 3-S4.** Impact of Fe corrosion on landfill temperature with varying corrosion rates. The solid and dashed black lines represent the base cases as given in Figure 3-2 and represent only biological reactions. The Fe corrosion rate is 0.0005 mm/yr (Table 3-1) unless specified as 0.005 mm/yr. The % represents the fraction of the total surface area available for corrosion.

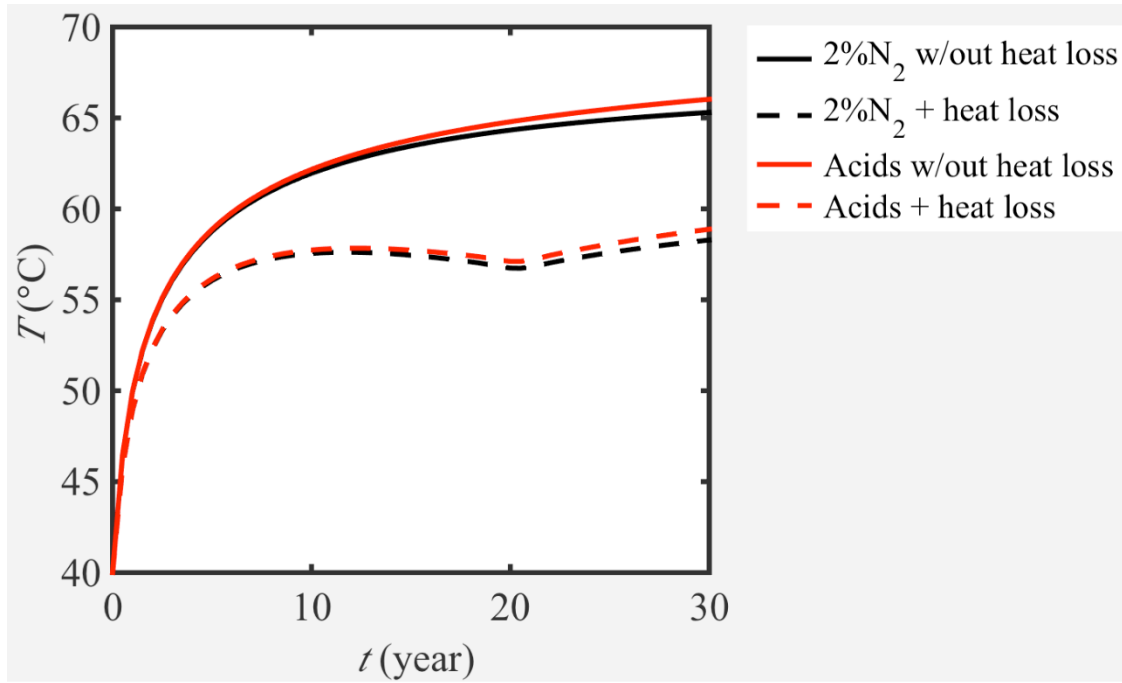


**Figure 3-S5.** Impact of acid-base neutralization reactions on landfill temperature. The solid and dashed black lines represent the base case given in Figure 3-2 and represents only biological reactions.

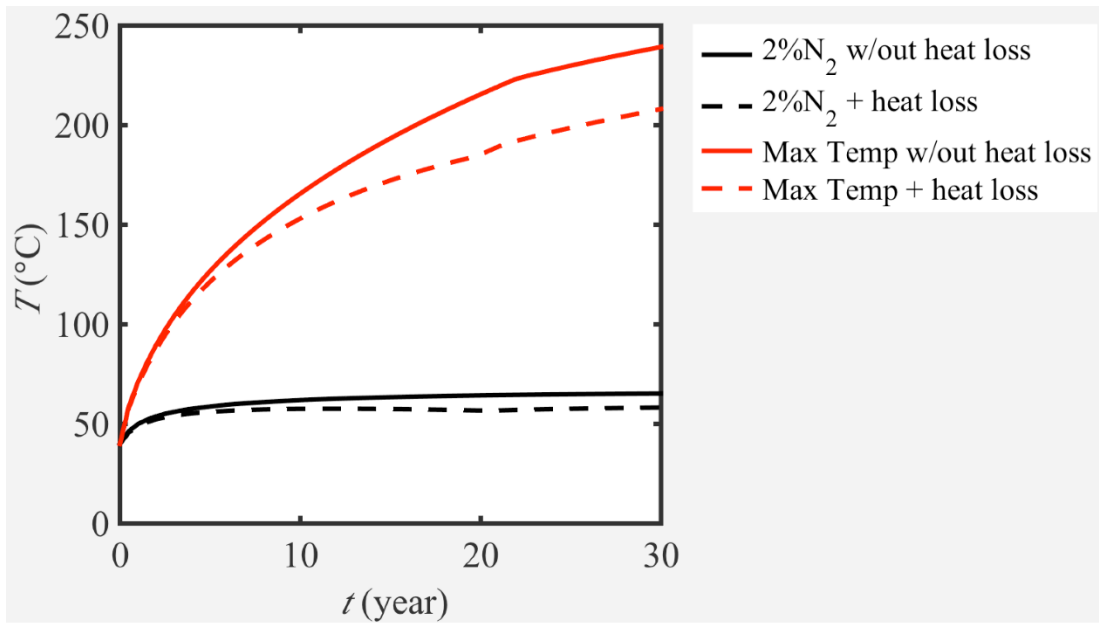


**Figure 3-S6.** Heat accumulation associated with MSW biodegradation, ash hydration and carbonation, Al and Fe corrosion, and acid-base neutralization reactions. The solid and dashed black lines represent the base case given in Figure 3-2. The red lines represent a case with 80% MSW, 20% ash, double the CH<sub>4</sub> generation rate, and the base case Al, Fe, and carboxylic acid contents.

### 3.9 References

- Ahmed, N., Wenzel, H. and Hansen, J.B., 2014. Characterization of Shredder Residues generated and deposited in Denmark. *Waste management*, 34(7), pp.1279-1288.
- Amend, J.P. and Shock, E.L., 2001. Energetics of overall metabolic reactions of thermophilic and hyperthermophilic Archaea and Bacteria. *FEMS microbiology reviews*, 25(2), pp.175-243.
- Antal, M.J. and Grønli, M., 2003. The art, science, and technology of charcoal production. *Industrial & Engineering Chemistry Research*, 42(8), pp.1619-1640.
- Calder, G.V. and Stark, T.D., 2010. Aluminum reactions and problems in municipal solid waste landfills. *Practice Periodical of Hazardous, Toxic, and Radioactive Waste Management*, 14(4), pp.258-265.
- Ciuta, S., Patuzzi, F., Baratieri, M. and Castaldi, M.J., 2014. Biomass energy behavior study during pyrolysis process by intraparticle gas sampling. *Journal of analytical and applied pyrolysis*, 108, pp.316-322.
- de la Cruz, F. B. D. la; Barlaz, M. A., 2010. Estimation of waste component-specific landfill decay rates using laboratory-scale decomposition data. *Environmental science & technology*, 44(12), pp.4722-4728.
- Dorez, G., Ferry, L., Sonnier, R., Taguet, A. and Lopez-Cuesta, J.M., 2014. Effect of cellulose, hemicellulose and lignin contents on pyrolysis and combustion of natural fibers. *Journal of Analytical and Applied Pyrolysis*, 107, pp.323-331.
- Eashwar, M., Subramanian, G. and Chandrasekaran, P., 1990. Marine fouling and corrosion studies in the coastal waters of Mandapam, India. *Bulletin of Electrochemistry*, 6(08), pp.699-702.
- Eleazer, W.E., Odle, W.S., Wang, Y.S. and Barlaz, M.A., 1997. Biodegradability of municipal solid waste components in laboratory-scale landfills. *Environmental Science & Technology*, 31(3), pp.911-917.
- El-Fadel, M., Findikakis, A.N. and Leckie, J.O., 1996. Estimating and enhancing methane yield from municipal solid waste. *Hazardous waste and hazardous materials*, 13(3), pp.309-331.
- El-Fadel, M., Findikakis, A.N. and Leckie, J.O., 1996b. Numerical modelling of generation and transport of gas and heat in sanitary landfills II. Model application. *Waste Management & Research*, 14(6), pp.537-551.
- El-Fadel, M., Findikakis, A.N. and Leckie, J.O., 1996. Numerical modelling of generation and transport of gas and heat in landfills I. Model formulation. *Waste management & research*, 14(5), pp.483-504.

- Ezuber, H., El-Houd, A. and El-Shawesh, F., 2008. A study on the corrosion behavior of aluminum alloys in seawater. *Materials & Design*, 29(4), pp.801-805.
- Fytanidis, D.K. and Voudrias, E.A., 2014. Numerical simulation of landfill aeration using computational fluid dynamics. *Waste management*, 34(4), pp.804-816.
- Garg, A. and Achari, G., 2010. A comprehensive numerical model simulating gas, heat, and moisture transport in sanitary landfills and methane oxidation in final covers. *Environmental modeling & assessment*, 15(5), pp.397-410.
- Gawande, N.A., Reinhart, D.R. and Yeh, G.T., 2010. Modeling microbiological and chemical processes in municipal solid waste bioreactor, part I: Development of a three-phase numerical model BIOKEMOD-3P. *Waste management*, 30(2), pp.202-210.
- Gholamifard, S., Duquennoi, C. and Eymard, R., 2007. A multiphase model of bioreactor landfill with heat and gas generation and transfer. In *Eurotherm Seminar (No. 81)*.
- Gholamifard, S., Eymard, R. and Duquennoi, C., 2008. Modeling anaerobic bioreactor landfills in methanogenic phase: Long term and short term behaviors. *Water research*, 42(20), pp.5061-5071.
- Grillo, R.J., 2014. Energy recycling–landfill waste heat generation and recovery. *Current Sustainable/Renewable Energy Reports*, 1(4), pp.150-156.
- Hanson, J. L.; Yesiller, N.; Kendall, L. A., 2008. Integrated temperature and gas analysis at a municipal solid waste landfill. In *Proceedings of the 16th International Conference on Soil Mechanics and Geotechnical Engineering*, pp.2265–2268.
- Hanson, J.L., Yesiller, N. and Oettle, N.K., 2008. Spatial Variability of Waste Temperatures in MSW Landfills. In *Global Waste Management Symposium Proceedings: Colorado, USA*.
- Hanson, J.L., Yeşiller, N. and Oettle, N.K., 2010. Spatial and temporal temperature distributions in municipal solid waste landfills. *Journal of Environmental Engineering*, 136(8), pp.804-814.
- Hanson, J.L., Yeşiller, N., Onnen, M.T., Liu, W.L., Oettle, N.K. and Marinos, J.A., 2013. Development of numerical model for predicting heat generation and temperatures in MSW landfills. *Waste management*, 33(10), pp.1993-2000.
- Hodge, K.L., Levis, J.W., DeCarolis, J.F. and Barlaz, M.A., 2016. Systematic evaluation of industrial, commercial, and institutional food waste management strategies in the United States. *Environmental science & technology*, 50(16), pp.8444-8452.
- Hosford, W.F. and Duncan, J.L., 1994. The aluminum beverage can. *Scientific American*, 271(3), pp.48-53.

- Jafari, N.H., Stark, T.D. and Thalhamer, T., 2017. Spatial and temporal characteristics of elevated temperatures in municipal solid waste landfills. *Waste management*, 59, pp.286-301.
- Klein, R., Nestle, N., Niessner, R. and Baumann, T., 2003. Numerical modelling of the generation and transport of heat in a bottom ash monofill. *Journal of hazardous materials*, 100(1-3), pp.147-162.
- Kwon, E.E. and Castaldi, M.J., 2012. Urban energy mining from municipal solid waste (MSW) via the enhanced thermo-chemical process by carbon dioxide (CO<sub>2</sub>) as a reaction medium. *Bioresource technology*, 125, pp.23-29.
- Levis, J. W.; Barlaz, M. A., 2004. Landfill Gas Monte Carlo Model Documentation and Results. Report to ICF for the U.S. EPA Waste Reduction Model (WARM); USEPA: Washington, D.C.; [http://www4.ncsu.edu/~jwlevis/Landfill\\_WARM-2014.pdf](http://www4.ncsu.edu/~jwlevis/Landfill_WARM-2014.pdf).
- Li, X., Bertos, M.F., Hills, C.D., Carey, P.J. and Simon, S., 2007. Accelerated carbonation of municipal solid waste incineration fly ashes. *Waste management*, 27(9), pp.1200-1206.
- Li, H., Sanchez, R., Qin, S.J., Kavak, H.I., Webster, I.A., Tsotsis, T.T. and Sahimi, M., 2011. Computer simulation of gas generation and transport in landfills. V: Use of artificial neural network and the genetic algorithm for short-and long-term forecasting and planning. *Chemical engineering science*, 66(12), pp.2646-2659.
- Liang, P., Wang, Z. and Bi, J., 2008. Simulation of coal pyrolysis by solid heat carrier in a moving-bed pyrolyzer. *Fuel*, 87(4-5), pp.435-442.
- Lopez, V.M., Florentino, B. and Barlaz, M.A., 2016. Chemical composition and methane potential of commercial food wastes. *Waste Management*, 56, pp.477-490.
- Luetlich, S.M. and Yafrate, N., 2016. Measuring Temperatures in an Elevated Temperature Landfill. In *Geo-Chicago 2016* (pp. 162-176).
- Miller, P. A.; Clesceri, N. L., 2002. *Waste Sites as Biological Reactors: Characterization and Modeling*; CRC Press.
- Milosavljevic, I., Oja, V. and Suuberg, E.M., 1996. Thermal effects in cellulose pyrolysis: relationship to char formation processes. *Industrial & Engineering Chemistry Research*, 35(3), pp.653-662.
- Mok, W.S.L. and Antal Jr, M.J., 1983. Effects of pressure on biomass pyrolysis. I. Cellulose pyrolysis products. *Thermochimica Acta*, 68(2-3), pp.155-164.
- Morales-Flórez, V., Santos, A., Romero-Hermida, I. and Esquivias, L., 2015. Hydration and carbonation reactions of calcium oxide by weathering: kinetics and changes in the nanostructure. *Chemical Engineering Journal*, 265, pp.194-200.

- Neusinger, R., Drach, V., Ebert, H.P. and Fricke, J., 2005. Computer simulations that illustrate the heat balance of landfills. *International journal of thermophysics*, 26(2), pp.519-530.
- Ng, C.W.W., Feng, S. and Liu, H.W., 2015. A fully coupled model for water–gas–heat reactive transport with methane oxidation in landfill covers. *Science of the Total Environment*, 508, pp.307-319.
- Nielsen, H.B., Mladenovska, Z., Westermann, P. and Ahring, B.K., 2004. Comparison of two-stage thermophilic (68 °C/55 °C) anaerobic digestion with one-stage thermophilic (55 °C) digestion of cattle manure. *Biotechnology and bioengineering*, 86(3), pp.291-300.
- Nozhevnikova, A.N., Kotsyurbenko, O.R. and Parshina, S.N., 1999. Anaerobic manure treatment under extreme temperature conditions. *Water Science and Technology*, 40(1), pp.215-221.
- Orfão, J.J., Antunes, F.J. and Figueiredo, J.L., 1999. Pyrolysis kinetics of lignocellulosic materials—three independent reactions model. *Fuel*, 78(3), pp.349-358.
- Oshins, C. and Block, D., 2000. Feedstock composition at composting sites. *Biocycle*, 41(9), pp.31-34.
- Rees, J.F., 1980. Optimisation of methane production and refuse decomposition in landfills by temperature control. *Journal of chemical technology and biotechnology*, 30(1), pp.458-465.
- Rendek, E., Ducom, G. and Germain, P., 2007. Assessment of MSWI bottom ash organic carbon behavior: A biophysicochemical approach. *Chemosphere*, 67(8), pp.1582-1587.
- Rothfuss, F., Bender, M. and Conrad, R., 1997. Survival and activity of bacteria in a deep, aged lake sediment (Lake Constance). *Microbial ecology*, 33(1), pp.69-77.
- Sanchez, R., Tsotsis, T.T. and Sahimi, M., 2010. Computer simulation of gas generation and transport in landfills. IV: Modeling of liquid–gas flow. *Chemical Engineering Science*, 65(3), pp.1212-1226.
- Shabani-Nooshabadi, M., Ghoreishi, S.M. and Behpour, M., 2009. Electropolymerized polyaniline coatings on aluminum alloy 3004 and their corrosion protection performance. *Electrochimica Acta*, 54(27), pp.6989-6995.
- Smart, N. R.; Blackwood, D. J.; Werme, L. The Anaerobic Corrosion of Carbon Steel and Cast Iron in Artificial Groundwaters, SKB Technical Report TR-01-22; Swedish Nuclear Fuel and Waste Management Co: Stockholm, 2001; pp 1-46.
- Smith, C.A., Compton, K.G. and Coley, F.H., 1973. Aerobic marine bacteria and the corrosion of carbon steel in sea-water. *Corrosion Science*, 13(9), pp.677-685.

- Sosnowski, P., Wieczorek, A. and Ledakowicz, S., 2003. Anaerobic co-digestion of sewage sludge and organic fraction of municipal solid wastes. *Advances in Environmental Research*, 7(3), pp.609-616.
- Speiser, C., Baumann, T. and Niessner, R., 2000. Morphological and chemical characterization of calcium-hydrate phases formed in alteration processes of deposited municipal solid waste incinerator bottom ash. *Environmental Science & Technology*, 34(23), pp.5030-5037.
- Staley, B.F. and Barlaz, M.A., 2009. Composition of municipal solid waste in the United States and implications for carbon sequestration and methane yield. *Journal of Environmental Engineering*, 135(10), pp.901-909.
- Szklarska-Smialowska, Z., 1999. Pitting corrosion of aluminum. *Corrosion science*, 41(9), pp.1743-1767.
- U. S. EPA, 1998. *Compilation of Air Pollutant Emission Factors, AP-42, Volume 1: Stationary Point and Area Sources, 5th ed., Supplement E, Chapter 2.4: Municipal Solid Waste Landfills*; U.S. Environmental Protection Agency: Washington, D.C.
- U.S. EPA, 2005. *Landfill Gas Emissions Model (LandGEM) Version 3.02 User's Guide*; U.S. Environmental Protection Agency: Washington, D.C.; <http://www.epa.gov/ttnca1/dir1/landgem-v302-guide.pdf>.
- U.S. EPA, 2015. *Municipal Solid Waste Generation, Recycling, and Disposal in the United States: Facts and Figures for 2013*; United States Environmental Protection Agency: Washington, DC.
- Vargel, C., 2004. *Corrosion of aluminium*. Elsevier.
- Wagner, W. and Pruß, A., 2002. The IAPWS formulation 1995 for the thermodynamic properties of ordinary water substance for general and scientific use. *Journal of physical and chemical reference data*, 31(2), pp.387-535.
- Wang, X., Padgett, J.M., de la Cruz, F.B. and Barlaz, M.A., 2011. Wood biodegradation in laboratory-scale landfills. *Environmental science & technology*, 45(16), pp.6864-6871.
- Wang, X., Padgett, J.M., Powell, J.S. and Barlaz, M.A., 2013. Decomposition of forest products buried in landfills. *Waste management*, 33(11), pp.2267-2276.
- Wang, X. and Barlaz, M.A., 2016. Decomposition and carbon storage of hardwood and softwood branches in laboratory-scale landfills. *Science of the Total Environment*, 557, pp.355-362.
- White, J., Robinson, J. and Ren, Q., 2004. Modelling the biochemical degradation of solid waste in landfills. *Waste Management*, 24(3), pp.227-240.

- Yavor, Y., Goroshin, S., Bergthorson, J.M., Frost, D.L., Stowe, R. and Ringuette, S., 2013. Enhanced hydrogen generation from aluminum–water reactions. *international journal of hydrogen energy*, 38(35), pp.14992-15002.
- Yoshida, H. T. N.; Hozumi, H. Theoretical Study on Heat Transport Phenomena in a Sanitary Landfill. In *Proceedings Sardinia 97, Sixth International Landfill Symposium, 1997*; pp 13–17.
- Zinder, S.H., Anguish, T. and Cardwell, S.C., 1984. Effects of temperature on methanogenesis in a thermophilic (58 °C) anaerobic digester. *Appl. Environ. Microbiol.*, 47(4), pp.808-813.

# **Chapter 4. Finite Element Modeling of Landfills to Inform Heat Generation, Transport and Accumulation**

## **4.1 Abstract**

In North America, temperatures nearing 100 °C have been reported in several municipal solid waste landfills. However, the temporal and spatial-dependent processes that result in excessive heat accumulation are still not well understood. The objective of this study was to develop a transient finite element three-dimensional model to describe the heterogeneity of landfills, to incorporate the impacts of boundary and initial conditions, and to consider spatially dependent heat transfer mechanisms to better understand heat generation, accumulation, and propagation. The model incorporates gas-liquid-heat reactive transfer with aerobic and anaerobic biological reactions, anaerobic metal corrosion, and ash hydration and carbonation. Increasing boundary temperature, biological reaction rates, and landfill height increases the maximum temperature in the central region of a landfill while the impact of thermal properties of MSW is negligible. Simulation results predict that placement of ash near the corner of a landfill reduces the size of the elevated temperature region relative to placement in the landfill center. Mixing heat-generating wastes (ash or AI) with MSW decreases maximum temperatures but results in elevated temperatures over a larger fraction of the landfill volume relative to segregated ash disposal.

## **4.2 Introduction**

There are reports of landfills permitted to accept municipal solid waste (MSW) and other non-hazardous wastes exhibiting subsurface temperatures in excess of 80 – 100 °C (Stark et al. 2011, Martin et al. 2012, Jafari et al. 2017, Benson 2017; Luettich, and Yafrate, 2016). This

temperature is well above values typically associated with MSW landfills, which are reported to range between 40 and 65 °C and generally are less than 55 °C (Hanson et al. 2010, Yesiller et al. 2015). Landfills exhibiting elevated temperatures over a large area are being referred to as elevated temperature landfills (ETLFs).

ETLFs are a relatively new phenomenon and have unique characteristics and challenges including substantial changes in the composition and quantity of landfill gas (LFG) and leachate, rapid waste subsidence, and in some cases, elevated liquid and gas pressures. These conditions, alone or in combination, may affect the waste containment system - engineered barriers (liners and covers), gas and leachate collection infrastructure, and the physical stability of the waste mass. While landfill owners typically increase their monitoring and management of landfills showing indicators of elevated temperatures, the underlying cause of heat production and accumulation that results in an ETLF is not clear. In some cases, the ETLF apparently resulted from the acceptance of a non-hazardous industrial waste (Calder and Stark, 2010). However, other landfills have accepted similar industrial wastes and are not experiencing widespread elevated temperatures, and other landfills that are experiencing elevated temperatures did not accept large quantities of heat generating waste. Research on the heat generation potential of various wastes that can be disposed in Subtitle D landfills is ongoing and it is apparent that both heat generation and accumulation (generation – loss) must be considered in diagnosing the occurrence of ETLFs.

Understanding the mechanisms that result in elevated temperatures is essential to predict, manage, and prevent ETLFs. In our previous work, a batch reactor model was developed to help elucidate the impact of biotic and abiotic reactions on heat generation in landfills accepting a wide range of wastes (Hao et al., 2017). The model predicted maximum temperatures associated with biological reactions of 62 to 69 °C for cases with and without heat loss, respectively. The inclusion

of ash hydration and carbonation, and Al corrosion (1.7% Al and 100% corroded area) reactions resulted in temperature increases of 14 and 26 °C, respectively, above temperatures predicted from biological reactions after 10 years. While the quantification of heat generation from chemical reactions is an important first step to understanding heat generation and accumulation, a batch reactor model cannot represent heat and mass transfer mechanisms in actual landfills that would ultimately predict spatial temperature profiles.

A number of models describe various aspects of landfills including temperature simulation, leachate recirculation, gas recovery, and heat generation. The emphasis of these models has been on describing the depth-wise temperature distribution in landfills by incorporating biodegradation reactions. The simulated maximum temperatures of the modeled MSW, bioreactor, and MSW incineration (MSWI) bottom ash landfills were 70, 55, and 100 °C, respectively (Yoshida et al., 1997; Gholamifard et al., 2008; Klein et al., 2003). The heat sources in the models were described by empirical functions such as a step-function, exponential growth and decay function, and bi-exponential decaying functions, but very few related the heat generating reaction to the stoichiometry of biotic and abiotic reactions (Klein et al., 2003; Hanson et al., 2008; Hanson et al., 2013). These empirical models have been successful in simulating temperatures at specific landfills, but they cannot be extended to predict temperatures in other landfills. In addition, the importance of waste placement strategies and scheduling, landfill depth and the disposal of a number of non-MSW wastes as it impacts heat generation, accumulation, and propagation has not been investigated.

The objective of this study was to develop a transient three-dimensional finite element model (FEM-3DM) that incorporates gas-liquid-heat reactive transfer in a landfill with biotic and abiotic reactions and spatially-dependent heat transfer processes (e.g. conduction and

condensation). The model incorporates waste age and both boundary and initial conditions. Modeled heat sources include aerobic and anaerobic biological reactions, anaerobic metal corrosion, and ash hydration and carbonation. As part of this research, we investigated the impacts of waste placement, landfill depth, waste heterogeneity and boundary conditions.

## **4.3 Modeling Approach**

### **4.3.1 Overview**

To represent the temperature distribution and evolution in landfills, a multi-physics transient FEM-3DM was developed by incorporating waste placement strategy, waste heterogeneity, initial and boundary conditions, fluid flow, and physical, chemical and biological heat sources and sinks.

The landfill is modeled as a square prism (Fig. 4-1). The height of the landfill is 80 m (unless otherwise noted) and its width and length are calculated based on daily waste disposal rate ( $R_{int}$  kg/day). The 80 m tall landfill is composed of 16 - 5 m high layers (Fig. 4-1). There are 9 cells in each layer for a total of 144 cells. Assuming a waste intake rate of 2500 tons/day ( $2.27 \times 10^6$  kg/day) and the time to fill up each cell ( $t_{cell}$ ) is 15 days, the volume of each cell is 38224 m<sup>3</sup> based on an assumed waste density ( $\rho_s$ ) of 1500 lb/yd<sup>3</sup> (890 kg/m<sup>3</sup>). Therefore, the length and width of each cell is 87.4 m and the length and width of the landfill is 262.2 m. The waste placement strategy is illustrated in Fig. 4-S1 of the Supporting Information (SI) where MSW is buried in a systematic pattern within each layer and from layer to layer until the landfill is full.

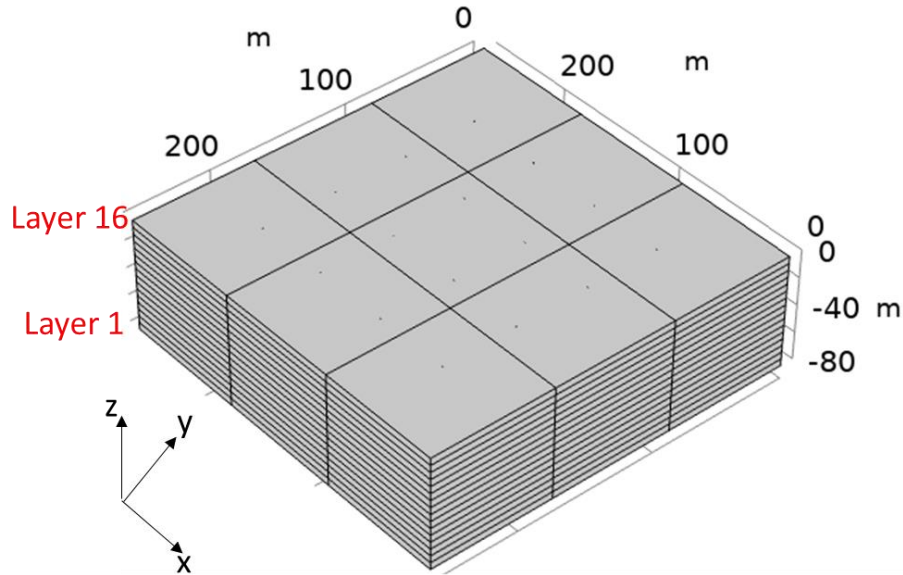


**Figure 4-1.** Geometry of the three-dimensional finite element model

The landfill is modeled as a three-phase (gas, liquid, and solid) system with the solid phase (MSW/other waste) modeled as a rigid porous medium with a constant porosity. The composition of MSW that is placed in each cell can vary and this variation will inform physical and thermal properties of each cell as well as the gas production rate. In this model, MSW composition is user-defined and the composition used previously was applied and restated in the SI (Hao et al., 2017). The gas phase is a four-component mixture ( $H_2O$ ,  $CO_2$ ,  $O_2$  and  $CH_4$ ) while the liquid phase includes infiltrated rainwater and the intrinsic moisture in waste at the time of placement. The perforated PVC gas wells under vacuum remove LFG at the gas generation rate as shown in Fig. S2e. Assuming a gas well density of 0.43 wells per ha (1 well per acre), there are 16 evenly distributed gas wells; each 15 cm in diameter and 60 m in length.

The heat generation terms include aerobic and anaerobic biodegradation, ash hydration and carbonation, and Al corrosion as described in Hao et al. (2017) and in the SI. The incorporated heat transfer mechanisms include conduction, evaporation, and condensation, and liquid and gas convection. The FEM-3DM allows water to evaporate and hot gas from one location to move to

a cooler location and condense with the release of energy. All phases have the same temperature at the thermal equilibrium state; thus, only one heat balance equation is required for the three-phase system. All parameters required to describe the physical characteristics of the landfill and the waste are presented in Table 4-S1.

### 4.3.2 Governing equations

#### *Gas balance*

The reactions and transport of CH<sub>4</sub> and CO<sub>2</sub> by diffusion and convection are calculated using Eqs. 4-1 to 4-3, and the vapor balance is shown in Eq. 4-4.

$$\varepsilon \frac{\partial c_{g,i}}{\partial t} + u_g \nabla c_{g,i} = \nabla(D_i \nabla c_{g,i}) + \sum_{i=CH_4, CO_2} R_{g,i} + \sum_{i=CH_4, CO_2} S_{g,i} \quad (4-1)$$

where  $\varepsilon$  is the porosity,  $c_{g,i}$  is the concentration of gas species  $i$ ,  $u_g$  is the gas phase velocity which is described by Darcy's Law (Eqs. 4-2 and 4-3),  $D_i$  is the diffusion coefficient of gas species  $i$ ,  $R_{g,i}$  is the source/sink term of reactions of gas species  $i$ , and  $S_{g,i}$  is the biotic generation rate of gas species  $i$ , which is estimated using a modified version of the US EPA's LandGem model that incorporates waste-specific methane production potentials and decay rates (US EPA, 2005; Hao et al., 2017).

The gas phase velocity is calculated based on Darcy's Law as shown in Eqs. 4-2 and 4-3.

$$\rho_g \nabla(u_g) = \sum_{i=CH_4, CO_2} M_i S_{g,i} \quad (4-2)$$

$$u_g = -\frac{\eta}{\mu_g} \nabla P \quad (4-3)$$

where  $\rho_g$  is the density of the gas phase,  $M_i$  is the molecular weight of gas species  $i$ ,  $\eta$  and  $\mu_g$  are the permeability of MSW and viscosity of the gas phase, respectively, and  $P$  is pressure.

#### *Liquid balance*

To simulate evaporation and condensation, a liquid (water) balance equation is coupled with the vapor balance equation as described in Eq. 4-4.

$$\varepsilon \frac{\partial c_{H_2O(g)}}{\partial t} + u_g \nabla c_{H_2O(g)} = \nabla (D_{H_2O(g)} \nabla c_{H_2O(g)}) + \varepsilon K_{evap} (a_{H_2O} c_{sat} - c_{H_2O(g)}) \quad (4-4)$$

where  $c_{H_2O(g)}$  is the concentration of water vapor,  $D_{H_2O(g)}$  is the diffusion coefficient of water vapor in the gas phase,  $K_{evap}$  is the evaporation rate,  $a_{H_2O}$  is the water activity, and  $c_{sat}$  is the vapor concentration under saturation conditions.

The model formulation assumes that there is no water accumulation and that infiltrated water is continuously removed by the leachate collection system. The liquid (water) balance equation is given by Eq. 4-5.

$$(1 - \varepsilon) \frac{\partial c_{H_2O(l)}}{\partial t} = \nabla (D_{H_2O(l)} \nabla c_{H_2O(l)}) - \varepsilon K_{evap} (a_{H_2O} c_{sat} - c_{H_2O(g)}) \quad (4-5)$$

where  $c_{H_2O(l)}$  and  $D_{H_2O(l)}$  are the concentration and diffusion coefficient of liquid water, respectively. The last term in Eqs. (4-4) and (4-5) calculates the amount of water that evaporates into the gas phase or condenses into the liquid phase (Halder et al., 2011). When the current vapor concentration,  $c_{H_2O(g)}$ , is less than the saturated vapor concentration at local temperature  $a_{H_2O} c_{sat}$ , evaporation occurs. Condensation occurs when  $a_{H_2O} c_{sat}$  is greater than  $c_{H_2O(g)}$ .

### *Solid balance*

The consumption of biodegradable waste and ash hydration/carbonation is described by first order reactions (Eq. 4-6) and the rate of Al corrosion is expressed in Eq. (3-18).

$$\frac{\partial c_{s,i}}{\partial t} = - \sum_{i=MSW, ash} R_{s,i} c_{s,i} \quad (4-6)$$

where  $c_{s,i}$  and  $R_{s,i}$  are the concentration and reaction rate of component  $i$ , respectively. The parameters used to describe the solid, liquid and gas phases are given in Table 4-S2, waste composition and characteristics are given in Tables 3-S4, 3-S7 and 3-S8, and ash and metal characteristics are given in Tables 3-S5 and 3-S6, respectively.

### *Heat balance*

The landfill system heat balance is given by Eq. 4-7. The first and second terms on the left side of Eq. 4-7 describe heat accumulation and convective heat loss, respectively. The first and second terms on the right side represent heat conduction and heat source/sink terms due to chemical reactions, and evaporation and condensation.

$$\begin{aligned} & [(1 - \varepsilon)\rho_s C_{ps} + \varepsilon\rho_f C_{pf}] \frac{\partial T}{\partial t} + (\rho_f C_{pf} u_f) \nabla T \\ & = \nabla \{ [(1 - \varepsilon)\kappa_s + \varepsilon\kappa_f] \nabla T \} + \sum_{i=bio, chem, condens.} Q_i \end{aligned} \quad (4-7)$$

where  $\rho_s$ ,  $C_{ps}$ , and  $\kappa_s$  are the density, heat capacity, and thermal conductivity of the solid phase,  $\rho_f$ ,  $C_{pf}$ , and  $\kappa_f$  are the density, heat capacity, and thermal conductivity of the fluid phase,  $T$  is

temperature, and  $Q_i$  includes the heat source/sink terms of evaporation and condensation, and biotic and abiotic reactions. The impact of gas transfer on temperature (convection and conduction) is negligible compared to the liquid and solid phases as  $\rho_l C_{pl}$  is four orders of magnitude greater than  $\rho_g C_{pg}$ .

*The source/sink terms of heat and mass balance equations*

The methods to calculate CH<sub>4</sub> generation and substrate biodegradation rates were adopted from Hao et al. (2017) and are summarized here. Methane generation is estimated using a modified version of the US EPA's LandGem model that incorporates the effects of temperature and waste composition Eq. 4-8.

$$S_{g,CH_4} = f_{CH_4}(T)k_{d,i}L_{0,i} \sum_{p=0}^n \sum_{q=0.0}^{0.9} \frac{M_{MSW}}{10} e^{-k_{d,i}t_{p,q}} \quad (4-8)$$

where  $S_{g,CH_4}$  is the CH<sub>4</sub> generation rate Eq. 4-1,  $f_{CH_4}(T)$  is defined in Eq. 4-S1 (Fig. 4-S3) and is designed to reduce methane generation at elevated (i.e., inhibitory) temperatures,  $k_{d,i}$  is the first-order decay rate constant of component  $i$ ,  $L_{0,i}$  is the CH<sub>4</sub> generation potential of biodegradable component  $i$ ,  $M_{MSW}$  is the waste mass placement in year  $p$ ,  $q$  is an intra-annual time increment used to calculate CH<sub>4</sub> generation, and  $t$  is time.

The CH<sub>4</sub> generation rate was used to estimate the substrate biodegradation rate using the stoichiometry of substrate conversion to CH<sub>4</sub>. For example, the decay rate of MSW component wood is given by Eq. 4-9,

$$R_{s,wood} = \frac{1 \text{ mol Cellulose}}{3 \text{ mol CH}_4 \times 22.4[\text{L/mol}]} M_{cel} f_{CH_4}(T) k_{d,wood} L_{0,wood} \quad (4-9)$$

where  $R_{s,wood}$  is the decay rate of wood,  $M_{cel}$  is the molecular weight of cellulose, and  $k_{d,wood}$  and  $L_{0,wood}$  are the first-order decay rate constant and CH<sub>4</sub> generation potential, respectively, of wood. Other biodegradable components include food, yard trimmings (grass, leaves, and branches), paper (newsprint, old corrugated containers, and mixed paper), and cotton.

The presence of N<sub>2</sub> in a landfill gas collection system suggests air intrusion, resulting in aerobic biodegradation. The available O<sub>2</sub> was estimated from the landfill gas modeled production rate and the user specified N<sub>2</sub> concentration (default concentration: 4%). Since aerobic reactions are much faster than anaerobic reactions, O<sub>2</sub> was assumed to be consumed instantaneously. Eq. 4-10 displays the biotic heat generation rate ( $Q_{bio}$ ), consisting of anaerobic and aerobic biodegradation in the first and second terms, respectively.

$$Q_{bio} = \sum_{i=cellulose, protein, lipid} \delta_i S_{g,i} + \frac{21}{78} \rho_{O_2} S_{g,N_2} \quad (4-10)$$

where  $\delta_i$  is the stoichiometric factor of biodegradable substrate  $i$ ,  $\rho_{O_2}$  is the density of O<sub>2</sub>, and  $S_{g,N_2}$  is the N<sub>2</sub> flow rate.

The heat gain/loss due to condensation and evaporation (phase change,  $Q_{PC}$ ) is estimated using Eq. 4-11.

$$Q_{PC} = -\Delta H_{vap} K_{evap} (a_{H_2O} c_{sat} - c_{H_2O(g)}) \quad (4-11)$$

where  $\Delta H_{vap}$  is the enthalpy of phase change of water.

During the waste burial period, the landfill working surface is exposed to the atmosphere. The exposure leads to an additional heat loss mechanism due to gas convection (Eq. 4-12).

$$Q_{conv_{air}} = \begin{cases} -\frac{A_{cell}}{V_{cell}} h_{air} (T - T_{atm}) & \text{cells exposed to the atmosphere} \\ 0 & \text{other cells} \end{cases} \quad (4-12)$$

where  $Q_{conv_{air}}$  is the heat loss rate due to air convection,  $A_{cell}$  and  $V_{cell}$  are the surface area and volume of the cell exposed to the atmosphere,  $h_{air}$  is the convective heat transfer coefficient of air, and  $T_{atm}$  is the atmospheric temperature (default of 20 °C).

### 4.3.3 Boundary and initial conditions

The domain and boundaries that applied in the model are illustrated in Fig. 4-S2. Fig. 4-S2a displays the domain of the landfill, which is used in the initial and source/sink terms of heat and mass transfer processes. Figs. 4-S2b to 4-S2d are the specific boundaries for heat balance equations and are also insulated boundaries for mass balance equations. Fig. 4-S2e displays the surface of the gas wells which is used for the boundary conditions of heat and mass transfer related to gas wells.

#### *Initial conditions*

For Darcy's equation, the initial pressure is defined as atmospheric pressure. A uniform initial temperature (20 °C) and uniform gas, liquid and solid initial concentrations are assumed throughout the landfill domain (Fig. 4-S2a) and the expressions are described by Eqs. 4-13 to 4-15.

$$c_{g,i}(x, y, z, 0) = 0 \quad (4-13)$$

$$c_l(x, y, z, 0) = \frac{\omega \rho_w}{M_w} \quad (4-14)$$

$$c_{s,i}(x, y, z, 0) = c_{s,i,0} \quad (4-15)$$

where  $c_l$  is the water concentration,  $\omega$  is the moisture content in the waste,  $\rho_w$  and  $M_w$  are the density and molecular weight of water, respectively, and  $c_{s,i,0}$  is the initial concentration of biodegradable substrate component  $i$ .

*Boundary conditions for the mass balance equations*

The landfill surface boundaries (Figs. 4-S2b to 4-S2d) are no-flux boundaries for the gas, liquid and solid phases as described by Eqs. 4-16 to 4-18. For the gas balance equation (Eq. 4-1), LFG can only be transported out from the gas well surface boundary (Fig. 4-S2e) as shown in Eq. 4-19.

$$-\mathbf{n} \cdot (-D_{g,i} \nabla c_{g,i}) = 0 \quad (4-16)$$

$$-\mathbf{n} \cdot (-D_l \nabla c_l) = 0 \quad (4-17)$$

$$-\mathbf{n} \cdot (-D_{s,i} \nabla c_{s,i}) = 0 \quad (4-18)$$

$$-\mathbf{n} \cdot (-D_{g,i} \nabla c_{g,i}) = k_{c,i}(c_{ext,g,i} - c_{g,i}) \quad (4-19)$$

In Eqs. 4-16 to 4-19,  $\mathbf{n}$  is the normal vector,  $k_{c,i}$  is the mass transfer coefficient for convection which is equal to the LFG removal velocity defined in Eq. 4-20, and  $c_{ext,g,i}$  is the concentration of gas species  $i$  as it leaves the landfill. Since the LFG removal rate is equal to the LFG generation rate, the LFG removal velocity is estimated from Eq. 4-20.

$$u_{GW} = -22.4[L/mol] \frac{V_{LF}}{A_{GW}} \sum_{i=CH_4, CO_2, H_2} S_{g,i} \quad (4-20)$$

where  $u_{GW}$  is the LFG removal velocity,  $V_{LF}$  is the landfill volume, and  $A_{GW}$  is the total surface area of gas wells.

For the Darcy's equation (Eqs. 4-2 and 4-3), an outlet boundary condition is applied to the gas well surface boundary (Fig. 4-S2e) and the expression is given in (Eq. 4-21). An atmospheric pressure boundary condition is applied on the top boundary (Fig. 4-S2b).

$$-\mathbf{n} \cdot \mathbf{u}_g = -u_{GW} \quad (4-21)$$

The negative velocity on the right side of Eq. 4-21 denotes that the LFG flows out of the landfill domain.

#### *Boundary conditions for the heat balance equation*

The top boundary of the landfill (Fig. 4-S2b) is exposed to the atmosphere with a constant temperature (20 °C). Assuming the landfill domain is beneath the earth surface, a convective heat flux boundary condition (Eq. 4-22) is applied to the side and bottom boundaries (Figs. 4-S2c and 4-S2d). The side and bottom boundaries are defined by a soil temperature that is 15 °C (default) 5 m outside of the landfill domain.

$$-\mathbf{n} \cdot [(1 - \varepsilon)\kappa_s + \varepsilon\kappa_l]\nabla T = h_{soil}(T_{soil} - T) \quad (4-22)$$

where  $h_{soil}$  is the heat transfer coefficient defined in Eq. 4-23, and  $T_{soil}$  is the soil temperature 5 m from the side and bottom boundaries (default of 15 °C).

The heat transfer coefficient of the soil layer ( $h_{soil}$ ) is estimated using Eq. 4-23

$$h_{soil} = \frac{\kappa_{soil}}{l_{soil}} \quad (4-23)$$

where  $\kappa_{soil}$  is the thermal conductivity of soil and  $l_{soil}$  is the thickness of the soil layer.

An outflow boundary condition is used to describe the removal of heat from the gas well surface (Fig. 4-S2e), given by Eq. 4-24. The boundary condition suggests that the only heat transfer occurring across the gas well surface boundary is by convection.

$$-\mathbf{n} \cdot [(1 - \varepsilon)\kappa_s + \varepsilon\kappa_l]\nabla T = 0 \quad (4-24)$$

#### 4.3.4 Mesh/solvers utilized in the model

The governing partial differential equations (PDEs) for mass and heat transfer were discretized and solved by the nonlinear solvers provided in COMSOL Multiphysics™ 5.4 software package. Non-uniform tetrahedral-triangle mesh elements with different mesh sizes were applied, with greater mesh densities near the gas wells to capture the thin mass and heat boundary layers close to edges (Fig. 4-S4). The finer mesh can compute gradients in state variables being tracked by the model. Model simulations were performed to represent a 30-year period (1-year intervals) by a time-dependent solver with the BDF (Backward Differentiation Formula) method (Curtiss and Hirschfelder, 1952). The discretized linear systems were solved by direct methods MUMPS (MULTifrontal Massively Parallel Sparse direct solver) (Amestoy et al., 2000) and GMRES

(Generalized Minimum RESidual) iterative methods (Saad and Schultz, 1986). Each simulation required four days on a Dell workstation with 128 GB RAM and an Intel Xeon Gold 5122 CPU.

#### **4.4 Results and Discussion**

Heat generation and accumulation for the “base case” with biological reactions only are described first (Figs. 4-2, 4-3, and 4-S5), followed by sensitivity analyses for the evaluation of the impacts of boundary conditions (Fig. 4-4), landfill height (Fig. 4-5), biodegradation rates (Fig. 4-6), and the thermal conductivity of MSW (Fig. 4-S6). Next, heat accumulation and propagation for scenarios in which ash buried in the center and corner of a landfill are compared (Figs. 4-7 and 4-8, 4-S7 to 4-S11, and 4-S13), followed by simulations with evenly distributed ash-MSW or AI-MSW mixtures (Figs. 4-9 and 4-S12). Finally, model simulations and published field temperature data are compared in Fig. 4-10.

##### **Base case: MSW only**

Temperatures from 3 to 30 years are presented in Fig. 4-2 for a case in which a landfill receives MSW only. The MSW undergoes aerobic biodegradation based on the presence of 4% N<sub>2</sub> in the LFG as well as anaerobic biodegradation. The landfill is about half full in Year 3 and completely full at the end of Year 6. Results show that the temperature at the top of the landfill is always cooler than the center and bottom boundary. The maximum temperature increases over time in response to the biological reactions and reduced heat loss as it fills. A temperature gradient forms from the center to the top of the landfill, indicating heat loss due to conduction. The maximum temperature in Year 15 is ~50 °C (Fig. 4-2c), which is within the reported temperature range of actual landfills (Hanson et al., 2010). The center-to-top temperature gradient increases with increasing center temperatures. The center-to-side and center-to-bottom temperature gradients are lower due to the convective heat transfer from the top surface to the environment.

By Year 30 (Fig. 4-2d), the maximum temperature has increased to  $\sim 55\text{ }^{\circ}\text{C}$  at a depth of 50 m. Biological heat production is reduced based on temperature inhibition above  $50\text{ }^{\circ}\text{C}$  (Fig. 4-S3) so the anaerobic biodegradation rate decreases with time (Eq. 4-8).

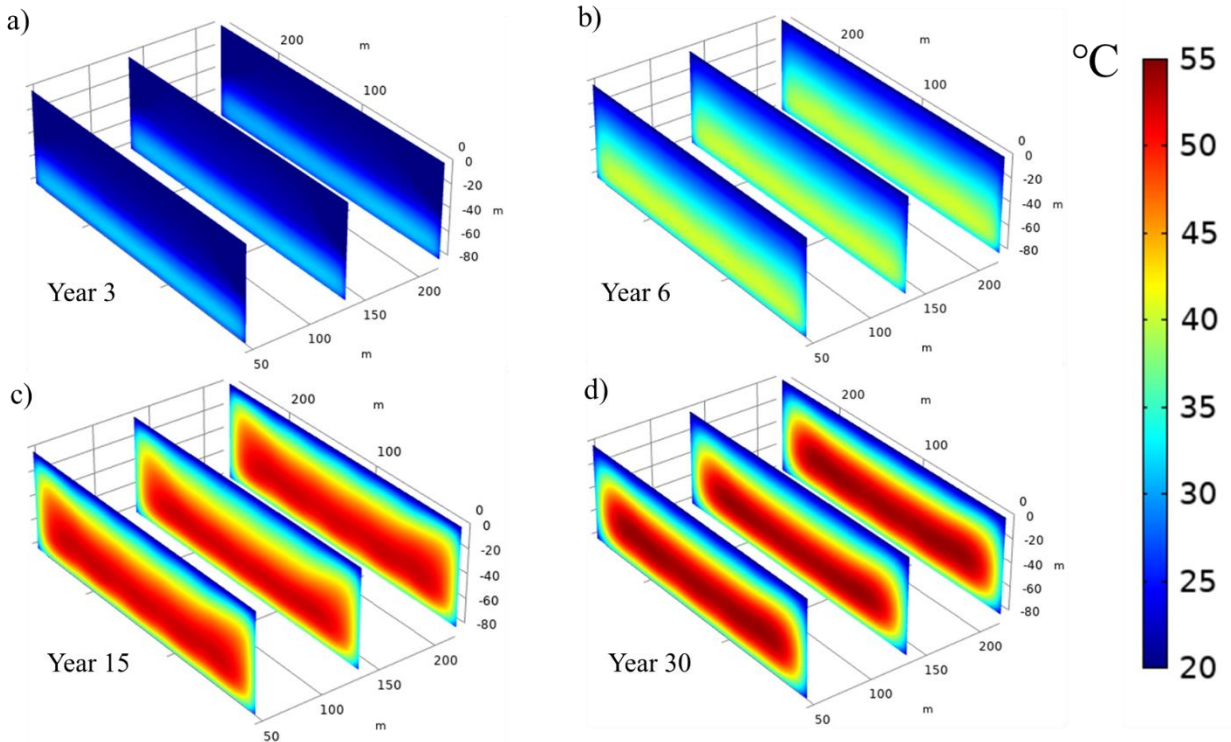


**Figure 4-2.** Temperature contours for a landfill receiving MSW only

Simulated center and edge temperature profiles for the MSW only case are shown in Fig. 4-3. In Year 6, temperatures near the landfill bottom are greater than temperatures at shallow depths as the waste was buried from bottom to top. It should be noted that the temperature decreases from 70 to 80 m due to the impacts of conductive heat transfer at the bottom boundary. From Years 6 to 20, the maximum temperature increases from  $35$  to  $40\text{ }^{\circ}\text{C}$ , indicating that the biotic heat generation rate is greater than the heat loss rate. In addition, a convex temperature profile forms and the maximum temperature occurs at a depth of 50 m. A similar profile has been observed in a number of field studies (Yoshida et al., 1997; Hanson et al., 2010; Yeşiller et al.,

2015; Jafari et al., 2017), suggesting heat accumulation in the center of landfills and conductive/convective heat loss from the top and bottom boundaries. The temperature increase is sustained from Years 6 to 20, followed by a decrease due to the asymptotic decay rate assumed for substrate consumption and gas production. The maximum temperatures in the center of the landfill are 15 °C (Year 20) higher than temperatures on the edge due to the impact of conductive heat transfer at the side boundaries (Fig. 4-3 and 4-S2d). In actual landfills, some fraction of the landfill sides will be above the surface and therefore have increased heat loss and reduced temperatures. Moreover, the temperature profiles in Years 30 and 20 are close (Fig. 4-3b), indicating that heat generation and loss are balanced in the center of the landfill over this time period. Fig. 4-3 illustrates the extent to which the heat loss rate in the center of the landfill is lower than the rate at the edge.

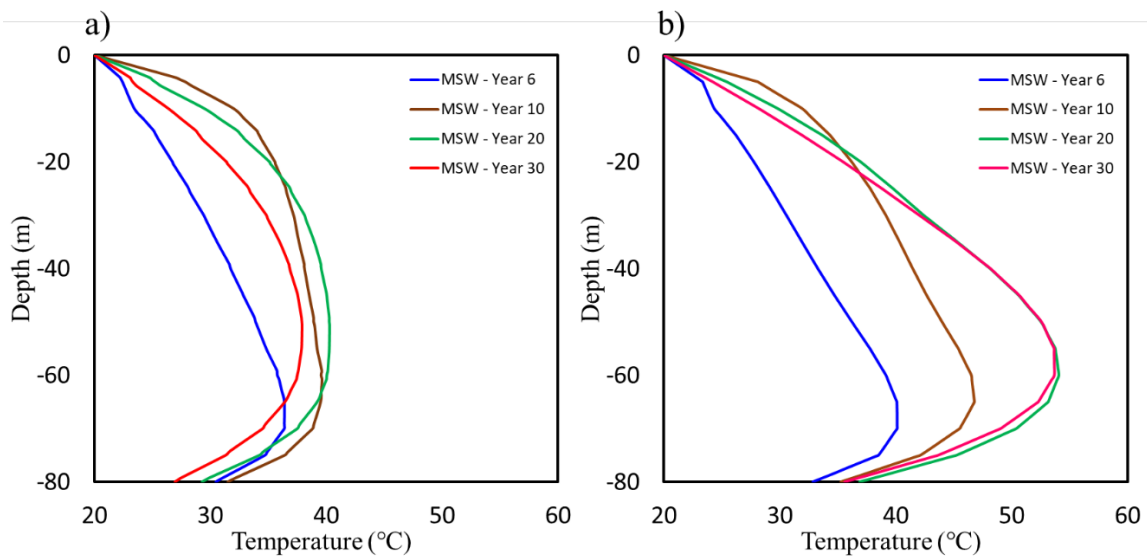


**Figure 4-3.** Temperature profiles for MSW only in the central cross section (a. vertical profiles 5 m from the landfill edge; b. vertical profiles in the center)

Transient temperature profiles for 8 locations at the landfill’s center and 5 m from the edge are illustrated in Fig. 4-S5. The temperature begins to increase after Year 1, and the maximum

temperature in each location occurs between Years 7 to 20. In Figs. 4-S5a and 4-S5b, the locations closer to the center of the landfill have longer periods of temperature increase as heat loss increases from the center out. In Fig. 4-S5a, the maximum temperatures of the center, edge, bottom corner, and top corner are 40, 35, 33, and 27 °C, respectively. The model simulations quantify how the heat loss rate in the top corner is the highest where the impact of the boundary is the most significant.

### **Sensitivity of boundary conditions**

Simulation results shown in Figs. 4-3 and 4-S5 indicate that boundary conditions play an important role in heat accumulation and transport. The impact of boundary conditions is presented in Fig. 4-4 in which the top boundary temperature was increased from 20 to 30 °C as might occur in southern regions of the U.S. in the summer. Fig. 4-4a shows that the increase of the top boundary temperature increases the temperatures for 2 to 10 °C at shallow regions (depth from 0 to 50 m) due to reduced conductive heat transfer.

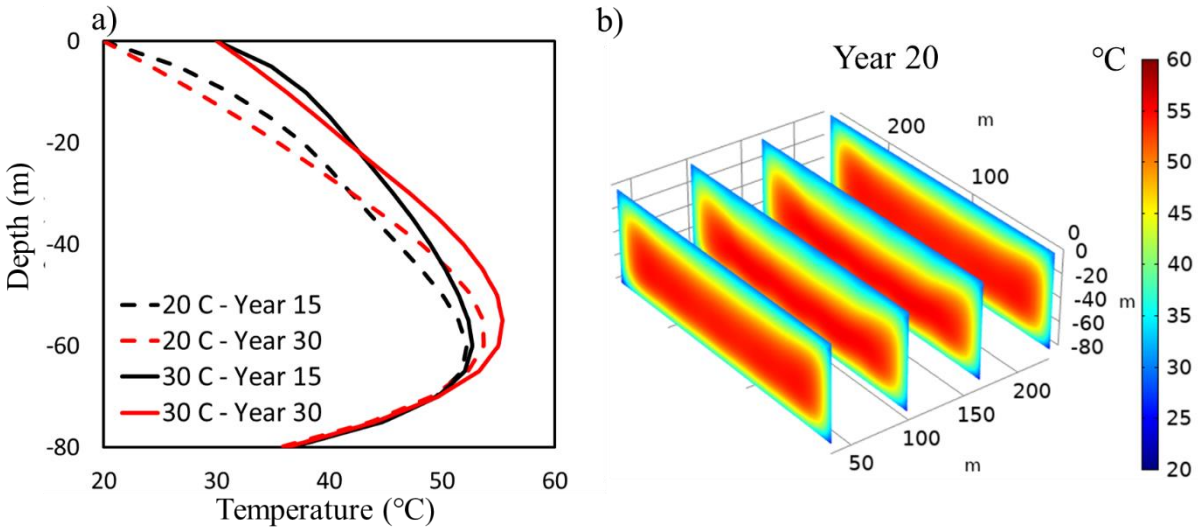


**Figure 4-4.** Temperature profiles and contours for MSW only with 20 and 30 °C at the top boundary  
(a. vertical profiles in the center at 20 and 30 °C; b. temperature contours in Year 20 with a 30 °C boundary)

### Sensitivity of landfill height

The impact of landfill height is illustrated by comparing the normalized temperature profiles, temperature evolution, and volume fraction of regions with temperatures above 40 °C for 40 and 80 m high landfills (Fig. 4-5). The 40 and 80 m landfills are full in 3 and 6 years, respectively. For the 40 m landfill (Fig. 4-5a), the maximum temperature in Year 15 is ~10 °C higher than in Year 6, indicating the impact of heat accumulation associated from biotic reactions in uninhibited temperature ranges (< 47 °C) (Fig. 4-S3). From Years 15 to 30, the maximum temperature in the 40 m landfill decreases from 47 °C to 41 °C, which indicates that heat loss is exceeding heat generation as described with respect to Fig. 4-2. For the 80 m landfill, the maximum temperature increases 13 °C from Years 6 to 15 and an additional 2 °C from Years 15 to 30, demonstrating how the impact of conductive heat transfer is reduced with increasing landfill height. The convex shape of the temperature-depth relationship is predicted for both landfills. As the 80 m landfill is only full at the end of Year 6, the deeper maximum temperature for the 80 m

landfill at Year 6 is likely because the landfill was not full until Year 6, hence there was a steeper temperature gradient from the center of the landfill to the surface. In addition, the 80 m landfill has more waste with a wider range of age compared to the shallow landfill, resulting in a shift in elevation of the maximum temperature location with time. However, for the 40 m landfill, the maximum temperature region was located near the vertical center (0.6) from Years 6 to 30.

The volume fraction of the waste that exceeds 40 °C is presented in Fig. 4-5b. As expected, a larger fraction of the waste exceeds 40 °C in the deeper landfill. The higher rate of heat loss in the 40 m landfill is explained by the greater temperature gradient. As the temperature exceeds 47 °C, the rate of heat generation is reduced due to inhibition of anaerobic biodegradation, which contributes to the decreasing waste mass above 40 °C in the 80 m landfill after Year 15. Moreover, inhibition of biotic reactions occurs in the deep landfill at elevated temperatures, leading to 1) slower consumption of the biodegradable substrates and 2) a slight decreasing volume fraction from Years 15 to 30 (Fig. 4-5b). The shallow landfill does not reach the inhibition temperature (> 47 °C) and the volume fraction (Fig. 4-5b) rapidly decreases from 0.5 to 0.2, resulting from less waste disposal and greater impact of heat conduction than the deep landfill.

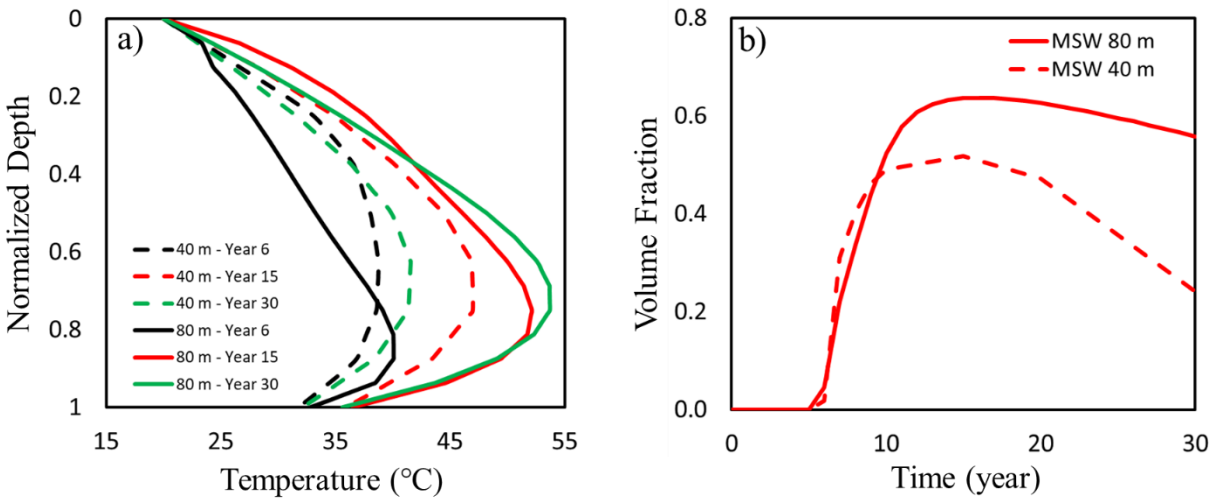


**Figure 4-5.** Temperature profiles and evolution of volume fraction for 40 m and 80 m high landfills  
 (a. normalized vertical temperature profiles in the center of the landfill; b. evolution of volume fraction with temperature above 40 °C)

#### **Sensitivity of biodegradation rate and thermal conductivity of MSW**

To investigate the impact of biodegradation rate on heat accumulation, a simulation was conducted with the methane decay rate constant doubled (Fig. 4-6). In Years 6, 15 and 30, the maximum temperatures increased 8, 4, and 2 °C, respectively, when the decay rates are doubled. The slight temperature decrease from Years 15 to 30 is attributed to the inhibition of biodegradation. Fig. 4-6b shows that the maximum temperatures are ~5 °C higher and reached faster than the base case as more heat is generated at increased decay rates.

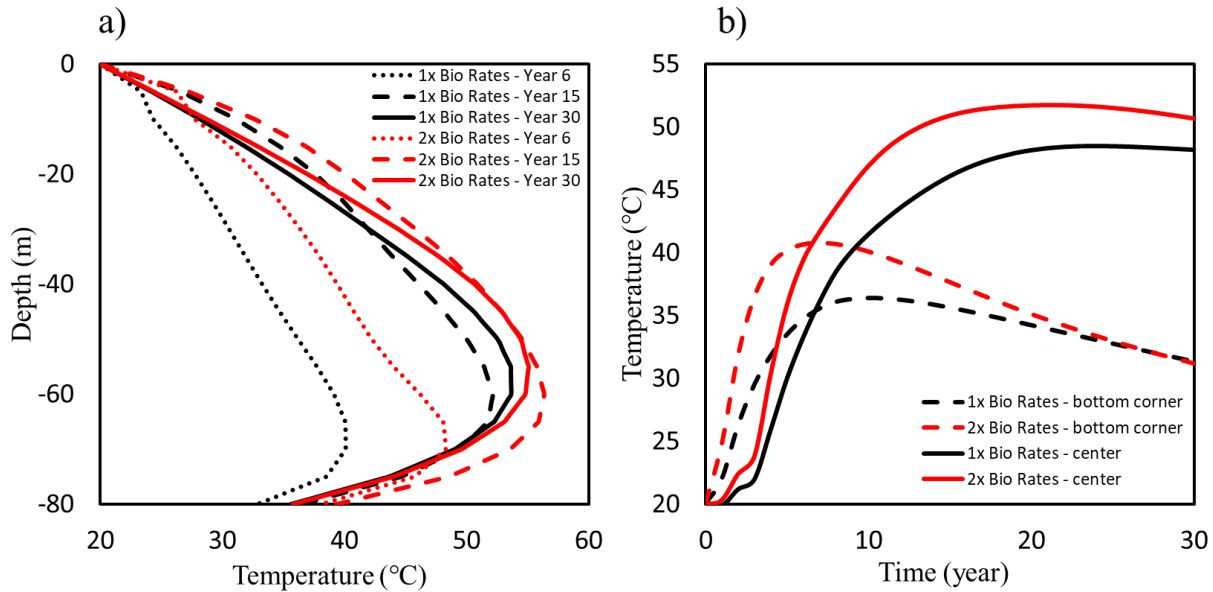


**Figure 4-6.** Temperature profiles and evolution for MSW only with doubled decay rates (a. vertical profiles in the center; b. temperature evolution at the geometric center of the landfill)

Sensitivity to the thermal conductivity of MSW was also examined by doubling the default value to  $1.2 \text{ W} \cdot \text{m}^{-1} \cdot \text{K}^{-1}$ . Fig. 4-S6 illustrates a slight temperature decrease ( $< 2 \text{ }^\circ\text{C}$ ) relative to the base case, indicating that the impact of thermal conductivity is relatively small. This is important given that the thermal conductivity of the waste will change with waste composition.

### Impact of ash and metal corrosion

In addition to MSW, landfills may receive non-hazardous industrial wastes including Al-containing waste and ash from both coal and MSW combustion. Figs. 4-7a and 4-S7a illustrate scenarios in which columns of pure ash are buried in the center and corner of a landfill, respectively. In both scenarios, ash was buried in Layers 2 to 15 and the first ash-containing cells are Cells 14 (ash-in-center) and 10 (ash-in-corner) in Layer 2 (Fig. 4-S1b). The mass of ash disposed did not fill a complete column so the ash column is surrounded by MSW. The overall volume ratio of ash to MSW in each ash-containing cell is 1:3.

For the ash-in-center scenario, the temperature contours in the diagonal cross sections (Fig. 4-7) illustrate that the heat accumulation attributable to ash hydration/carbonation results in more heat accumulation than the MSW only case (Fig. 4-7 vs Fig. 4-2). The simulation results in Fig. 4-8a show that the maximum temperature in the center of the ash column exceeds 100 °C in Year 2 and further increases to 180 °C in Year 6 when ash disposal stops. The similar temperature profiles for Years 6 to 30 indicate that the heat generation rate (ash hydration and carbonation) is approximately equal to the heat loss rate in which heat conduction is dominant due to the extreme temperature gradient to the top and bottom boundaries. In addition, the maximum temperature in the ash column occurs at 10 m above the bottom boundary, suggesting that the conductive heat transfer rate from the hottest zone to the bottom boundary is lower than the heat transfer rate to the top boundary. Heat propagation from the ash column to the adjacent MSW is displayed in Fig. 4-7 and 4-8b. In Year 2, the impacted regions due to ash hydration/carbonation are confined to the location of the ash column. After Year 6, the maximum temperature in the ash column decreases while temperatures in the adjacent MSW increase, illustrating the role of heat transfer or propagation from reactive waste to the adjacent MSW.

For the ash-in-corner scenario, Fig. 4-S7 illustrates an expanding elevated temperature region (> 200 °C). The maximum temperature for the ash-in-corner scenario is 10 to 20 °C higher than the ash-in-center scenario, indicating a lower heat loss rate due to the restricted evaporation/condensation as water vapor cannot transfer out of the landfill walls (Fig. 4-S8).

Heat propagation for the MSW only, ash-in-center, and ash-in-corner scenarios are illustrated using isothermal contours for Years 6, 15, and 30 (Fig. 4-S9). There are no temperature regions above 65 °C for the MSW only case while expanding temperature regions (> 80 °C) exist in the ash-in-center and ash-in-corner scenarios. Comparing the contours shown in Figs. 4-S9h

and S9i, the heat loss of ash-in-center scenario in the xy-plane is isotropic while heat transfer is highly impacted by side boundaries for the ash-in-corner scenario. To illustrate the impact of the disposal location of the pure ash column, the volume fractions of regions with elevated temperatures ( $> 65\text{ }^{\circ}\text{C}$  and  $> 80\text{ }^{\circ}\text{C}$ ) for the ash-in-center and ash-in-corner scenarios are displayed in Fig. 4-S10. For the ash containing cases, the higher volume fraction for the ash-in-center scenario indicates larger elevated-temperature affected regions. In contrast, the lower volume fractions for the ash-in-corner scenario denotes less elevated-temperature affected regions with greater maximum temperatures. While minimizing the temperature impacts of ash is an appropriate objective, ash placement must also consider temperature impacts on a geomembrane such that placement in a true corner adjacent to a liner would not be appropriate. In reality, the difference in affected volume fraction between the center and corner disposal scenarios is small enough that operational considerations may dictate ash placement.

Figs. 4-8 and 4-S11 illustrate the temperature contours and profiles for the ash-in-center scenario assuming that ash hydration occurs prior to disposal (Eqs. 3-12, and 3-S4 to 3-S7) and only carbonation (Eqs. 3-13, and 3-S8 to 3-S10) occurs after burial. Simulation results in Figs. 8c and 8d indicate that pre-hydration of ash can reduce the maximum temperature by  $\sim 40\text{ }^{\circ}\text{C}$  (Fig. 4-8c) and decrease the volume of regions with elevated temperatures (Fig. 4-8d).

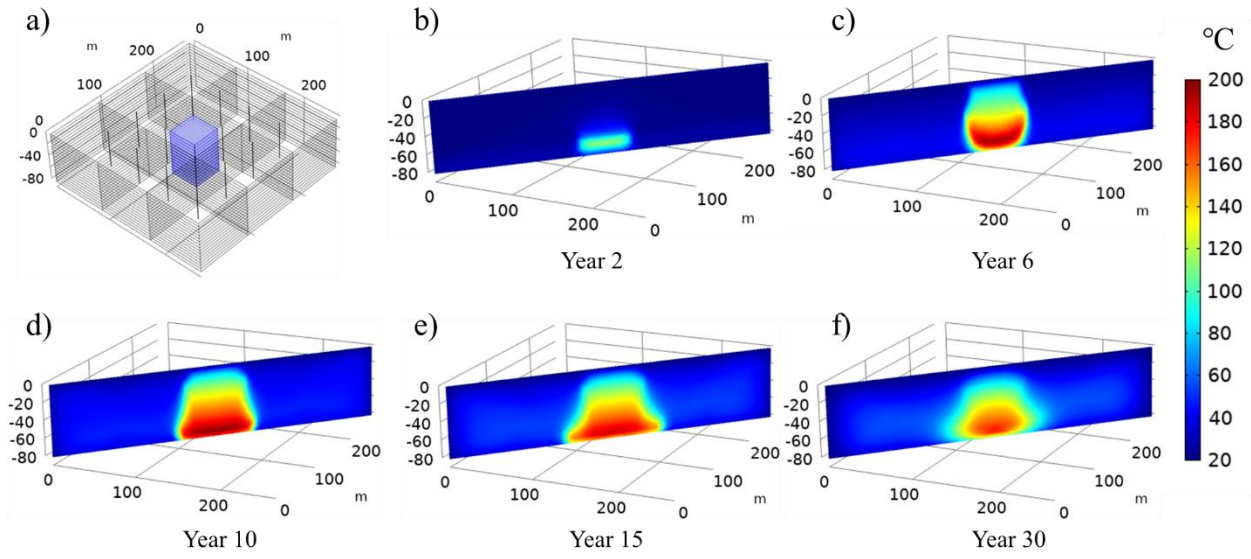


**Figure 4-7.** Temperature contours for the landfill with an ash column in the center (the disposal scenario is illustrated in part a)

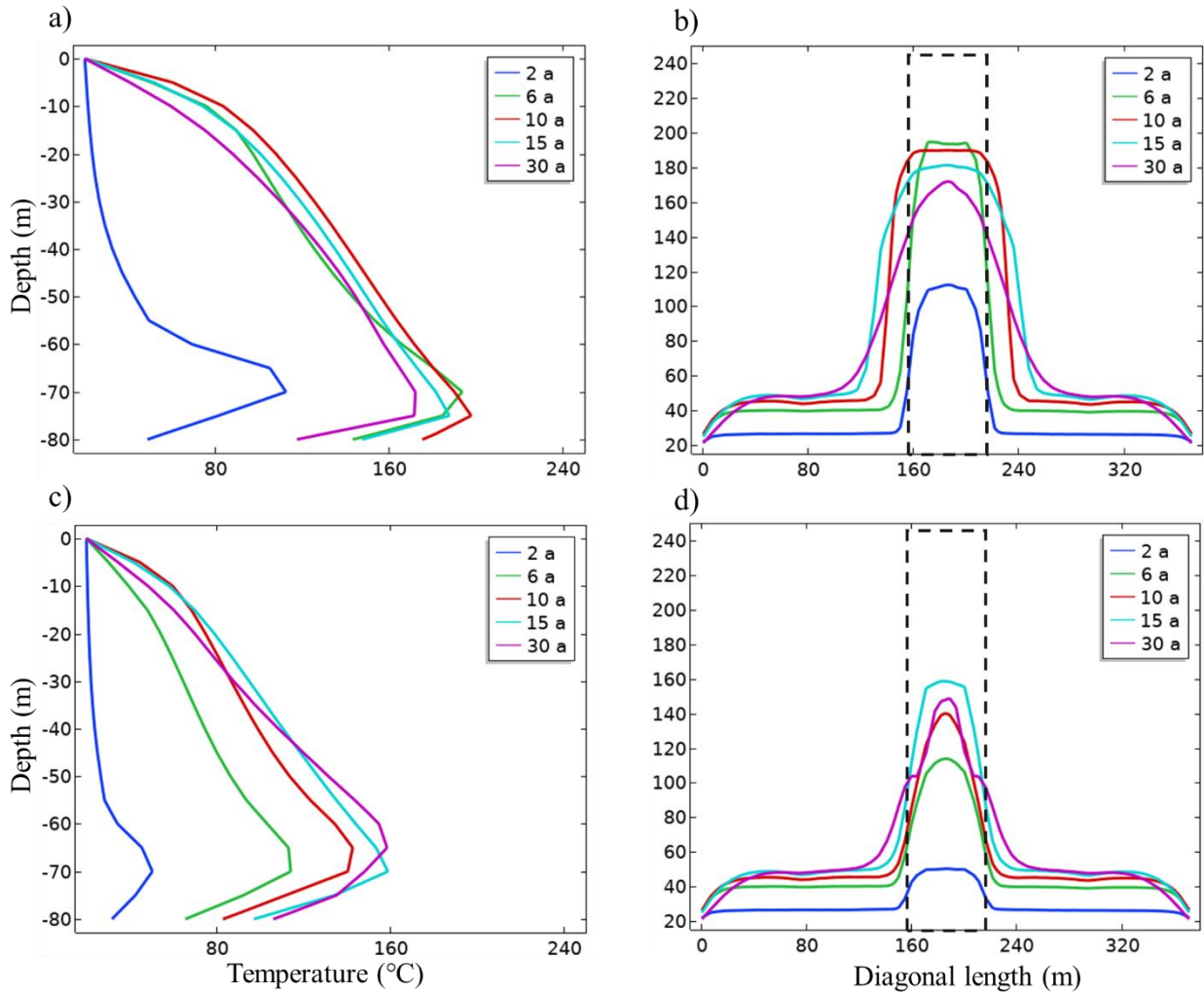


**Figure 4-8.** Temperature profiles for a landfill with an ash column (dashed line) in the center (a and b: hydration and carbonation; c and d: carbonation only) (a. and c. vertical profiles in the center of the landfill; b. and d. horizontal profiles at 70 m in the diagonal cross section)

In contrast to the ash disposal strategy described above, ash may also be mixed with MSW. Fig. 4-9 illustrates the temperature profiles of an ash-MSW mixture with 10% and 20% ash. The temperature profiles are much cooler than when ash is segregated. At 10% and 20% ash, the maximum temperature never exceeds 80 and 120 °C, respectively. However, at 20% ash, 64% of the total MSW volume exceeds 80 °C in Year 20. This affected volume is considerably higher

than the segregated ash scenarios and indicates the need to carefully evaluate ash disposal quantities.

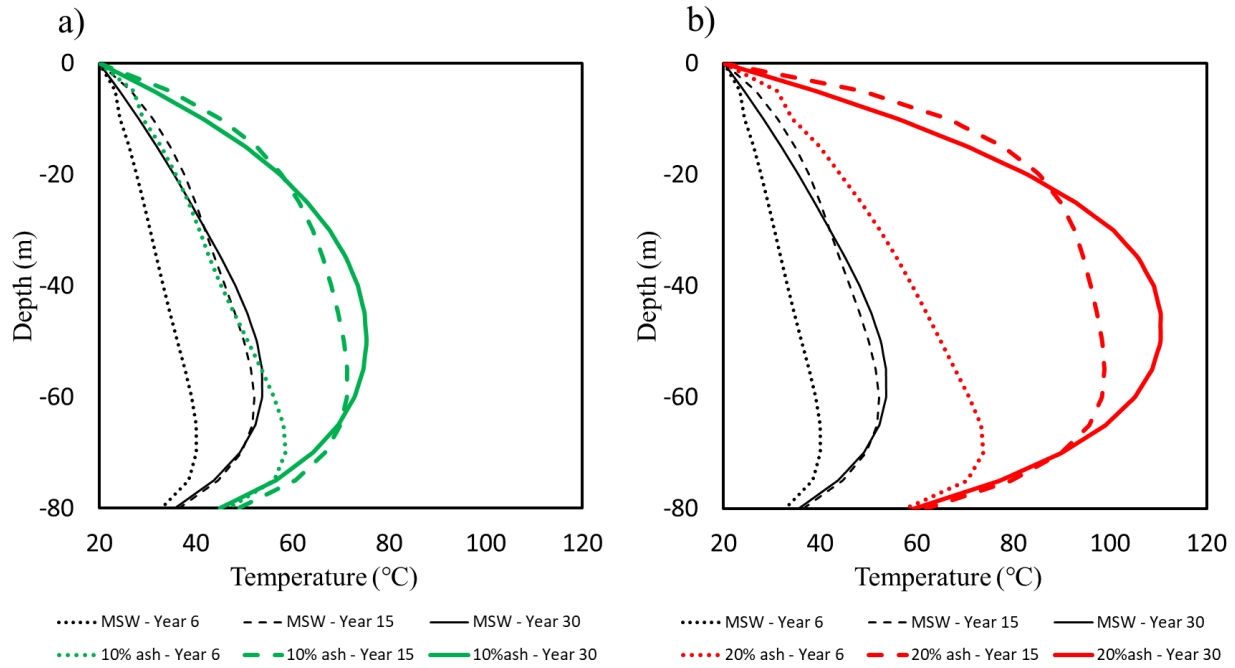


**Figure 4-9.** Temperature profiles for ash-MSW mixture with 10 % (a) and 20% (b) ash

Metals are an additional reactive waste that may be mixed with MSW. The temperature contours in MSW landfills with 1.7% and 3.4% Al are illustrated in Fig. 4-S12. The disposal of Al-MSW mixtures leads to maximum temperature of 100 and 140 °C for 1.7 and 3.4% Al, respectively. Given the potential importance of both ash and Al as heat sources, research is needed to evaluate rate constants and the extent of reaction appropriate to landfills.

## Simulation summary

The impacts of waste composition and disposal strategies are quantified using the cumulative normalized landfill volume (CNLV) with temperatures greater than 65 and 80 °C (Table 4-1). To understand Table 4-1, Fig. 4-S13 shows the CNLV in the temperature range from 20 to 200 °C for MSW only and ash-in-center cases in Year 20. The CNLVs > 65 and > 80 °C are 0 for MSW only. For ash, the CNLVs < 65 and < 80 °C are 0.89 and 0.92, respectively; therefore, the CNLVs > 65 and > 80 °C are 0.11 and 0.08 (Fig. 4-S13, Table 4-1).

In Table 4-1, the CNLV of the ash-in-center scenario is slightly greater than that of the ash-in-corner scenario, indicating that the corner scenario has a smaller elevated temperature region. The decrease in CNLV from the hydration and carbonation to carbonation only scenarios suggests that pre-hydrating ash (prior to disposal) is one approach to reduce the energy in the ash. For the cases with reactive waste evenly distributed in landfills, the CNLV > 65 °C is significantly greater than ash-in-center and ash-in-corner scenarios. When the concentration of reactive waste is relatively low (10% ash and 1.7% Al), the CNLVs > 80 °C are close to 0. However, when these waste disposal quantities are doubled, there is a marked increase in CNLV.

**Table 4-1.** Cumulative normalized landfill volume (CNLV) with temperatures greater than 65 °C and 80 °C in Year 20

Case	CNLV > 65 °C	CNLV > 80 °C
<b>MSW only</b>	0	0
<b>ash-in-center</b>	0.11	0.08
<b>ash-in-corner</b>	0.08	0.07
<b>ash-in-center (carbonation only)</b>	0.05	0.03
<b>10% ash</b>	0.49	0
<b>20% ash</b>	0.81	0.64
<b>1.7% Al</b>	0.60	0.04
<b>3.4% Al</b>	0.86	0.71

## **4.5 Comparison of Model Simulations to Field Data**

Model simulations were compared to field temperature data published by Hanson et al. (2010) by comparing the temperature profiles for the 40 m depth simulation to published data (Fig. 4-10). Hanson et al. (2010) investigated the long-term spatial and temporal variations of temperatures at landfills in different climatic regions including Alaska, British Columbia, Michigan, and New Mexico. Hanson et al.'s data are compared to our Year 10 simulation, allowing that the simulated landfill required 3 years to fill. In Fig. 4-10, our simulation temperature profile at the doubled biological decay rate is closer to the profiles of the Michigan landfill than the base case. Michigan is likely most typical of an eastern US landfill in terms of rainfall, leading to a potentially higher biological degradation rate than the default. Of course, a proper comparison between our model and field data would require extensive site-specific information. Nonetheless, model simulations and the field data are comparable and both illustrate maximum temperatures deep in the landfill.

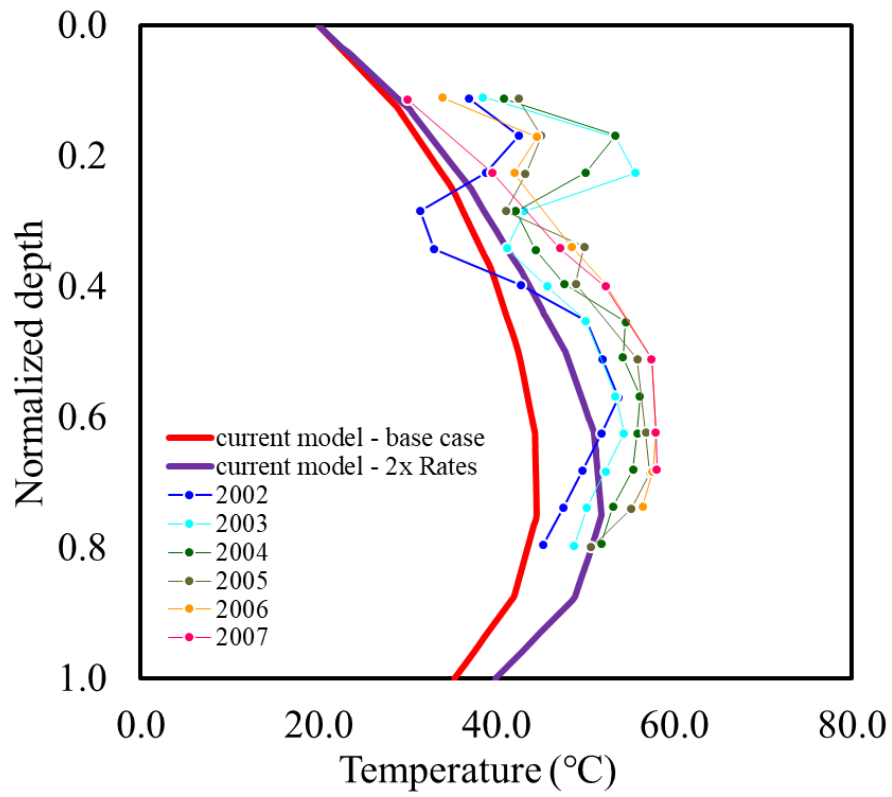


**Figure 4-10.** Normalized temperature profiles for simulation results and field data (Hanson et al. 2010)

## 4.6 Summary and Implications

A transient finite element 3D model was developed to describe spatially dependent heat transfer mechanisms in landfills. Model simulations showed that more heat accumulates in a deeper landfill, resulting in a higher peak temperature with a greater normalized volume above 40 °C. While an increased landfill footprint would reduce the height for the same waste disposal rate, this approach would increase cost and is also likely to result in more leachate requiring treatment. The model was useful in exploring the impact of three disposal scenarios involving ash; segregation in the center, segregation in a corner, and mixing with the MSW. The impacted waste volume associated with the corner and center scenarios are sufficiently close that operational considerations may dictate ash placement. Simulations do show that the disposal of 10 to 20% ash distributed in MSW can result in 49 to 81% of the waste mass exceeding 65 °C, which suggests that a segregation strategy has merit. By hydrating the waste prior to burial, about 40% of the total energy can be eliminated prior to burial and reduce the maximum temperature by ~40 °C. Whether the ash is hydrated by the waste generator or at a landfill will be a function of multiple site-specific considerations. Similarly, the presence of Al had a marked impact of waste temperatures. For both ash hydration/carbonation and Al corrosion, reaction rate constants were adopted from the literature for systems other than landfills. In ongoing research, we are measuring rate constants for these reactions under landfill-relevant conditions.

## Notation List

*The following symbols are used in this paper:*

$a$  = water activity;  
 $A$  = surface area;  
 $c$  = concentration;  
 $C_p$  = heat capacity;  
 $D$  = diffusion coefficient;  
 $f_{CH_4}$  = inhibition function;  
 $h_{air}$  = convective coefficient of air;  
 $h_{soil}$  = heat transfer coefficient of soil;  
 $\Delta H$  = enthalpy;  
 $k$  = reaction rate constant;  
 $k_d$  = decay rate constant of biodegradable component;  
 $l_{soil}$  = thickness of the soil layer below the bottom of landfill;  
 $L_0$  =  $CH_4$  generation potential;  
 $M$  = molecular weight;  
 $P$  = pressure;  
 $Q$  = heat generation rate;  
 $Q_{conv\_air}$  = heat loss rate of air convection;  
 $Q_{PC}$  = heat gain/loss rate due to phase change;  
 $R$  = reaction rate;  
 $R_{int}$  = waste intake rate;  
 $S$  = generation rate;  
 $t$  = time;  
 $t_{cell}$  = time to fill up each cell;  
 $T$  = temperature;  
 $u$  = velocity;  
 $V$  = volume;  
 $\alpha$  = corrosion rates;  
 $\delta$  = conversion parameter of biodegradable substrate;  
 $\varepsilon$  = porosity;  
 $\eta$  = permeability;  
 $\kappa$  = thermal conductivity;  
 $\mu$  = viscosity;  
 $\rho$  = density; and  
 $\omega$  = moisture content, dimensionless.

## 4.7 Supplemental Data

### Waste placement strategy

The waste placement strategy, as illustrated in Fig. 4-S1, describes the waste burial sequence in the landfill layers and cells. In Fig. 4-S1a and 4-S1b, two placement strategies are incorporated for even and odd layers, respectively. The burial sequences are marked as Cell 1 to Cell 9 in odd layers and as Cell 10 to Cell 18 in even layers. Assuming waste disposal starts at one of the corner cells (Cell 1) in the bottom layer (Layer 1, unless otherwise noted) shown in Fig. 4-S1a, the time to fill up Cell 1 is 15 days based on the waste intake rate. Starting from Day 16, waste is buried in Cell 2, which is next to Cell 1. Then, at Day 31, Cell 3 is used for waste disposal and it is next to both Cells 1 and 2. Following the sequence from Cell 4 to Cell 9 in Fig. 4-S1a, the time to fill up Layer 1 is 135 days (0.37 years). The scheme of waste disposal strategy of Layer 1 is also illustrated in Fig. 4-S1c. After completing waste disposal in Layer 1, waste is buried in Cell 10, Layer 2, which is on top of Cell 9, Layer 1. The burial sequence from Cell 10 to Cell 18 in Layer 2 is similar to Layer 1 as illustrated in Fig. 4-S1b. Applying the two placement strategies to all layers, the total time to fill the landfill is  $15 \times 144 = 2160$  days (5.9 years).

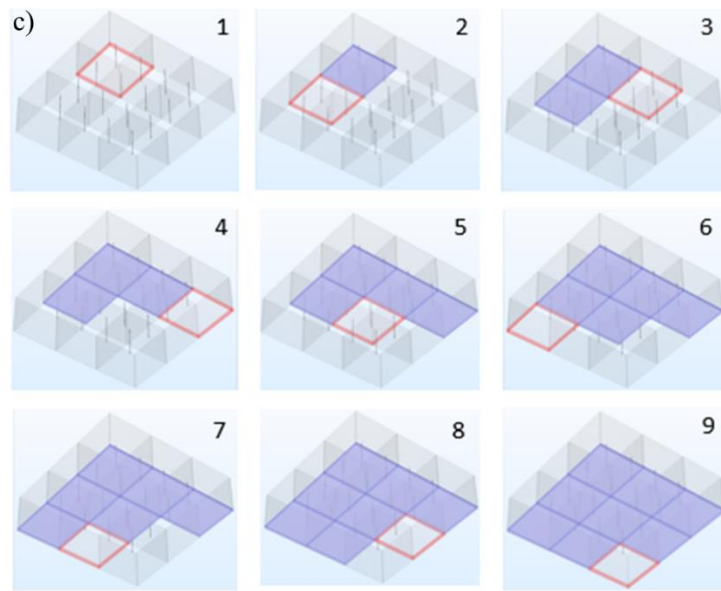
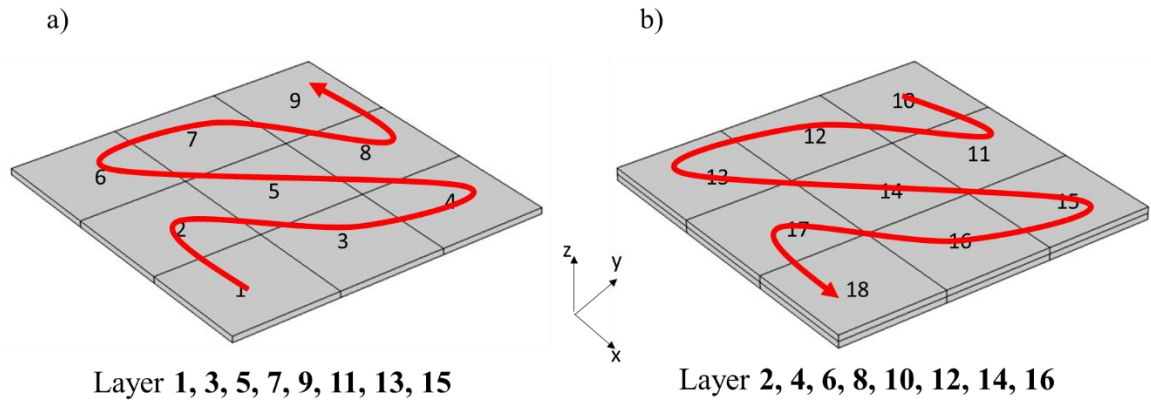


**Figure 4-S1.** Scheme of the waste disposal strategy

## Heat sources

### *Aerobic Biodegradation*

Aerobic cellulose oxidation is shown in Eq. 3-S5. Since aerobic reactions are much faster than anaerobic reactions, O<sub>2</sub> was assumed to be consumed instantaneously after entering the landfill.

### *Anaerobic Biodegradation*

Three biodegradable components of MSW (carbohydrates, protein, lipids) were considered as substrates for CH<sub>4</sub> generation. The stoichiometry and energetics for each substrate are presented in Eqs. 3-S7 to 3-S9, with carbohydrates (cellulose, hemicellulose, and starch) represented as cellulose.

To account for the influence of temperature on CH<sub>4</sub> generation, an inhibition function,  $f_{CH_4}(T)$ , was developed based on the normalized experimental CH<sub>4</sub> potential of waste samples obtained from an actual landfill (unpublished data). The fitted inhibition function and the normalized experimental data are shown in Eq. 4-S1 and Fig. 4-S3.

$$f_{CH_4}(T) = \begin{cases} 1 & T < 37^\circ\text{C} \\ \frac{1}{\left\{ e^{\left[ -\left( \frac{36.4-47.5}{5.7} \right)^2 \right]} + 1 \right\}} \left\{ e^{\left[ -\left( \frac{T-47.5}{5.7} \right)^2 \right]} + e^{\left[ -\left( \frac{T-36.4}{5.62} \right)^2 \right]} \right\} & 37^\circ\text{C} \leq T \leq 47.5^\circ\text{C} \\ e^{\left[ -\left( \frac{T-47.5}{12} \right)^2 \right]} & T > 47.5^\circ\text{C} \end{cases} \quad (4-S1)$$

### *Ash hydration and carbonation*

Ash disposed in landfills typically contains several oxides/hydroxides (e.g., Speiser et al. 2000; Rendek et al. 2007). The hydration of oxides is shown in Eqs. 3-12, and 3-S4 to 3-S7. Ultimately, the generated hydroxides are converted to carbonates by reacting with CO<sub>2</sub>, as described by Eqs. 3-13, and 3-S8 to 3-S10 (Li et al. 2007)

Both water and CO<sub>2</sub> were assumed to be present in excess. The rates of ash hydration and carbonation were assumed to follow first-order reaction models (Eqs. 3-18 and 3-19).

### *Anaerobic metal corrosion*

Landfills receive Al in elemental form from both MSW and special wastes that may include Al processing waste and auto shredder residue (Calder and Stark 2010; Ahmed et al. 2014). Al has been reported to undergo corrosion reaction (Eq. 3-16). The reaction rate for anaerobic Al corrosion is described by Eq. 3-18.

**Table 4-S1.** Default model parameters used to describe landfill characteristics

<b>Parameter</b>	<b>Unit</b>	<b>Value</b>	<b>Comments and citations</b>
Waste intake rate ( $R_{int}$ )	$\text{kg}\cdot\text{yr}^{-1}$	$8.28\times 10^8$	Yearly waste mass for medium sized landfill (2500 US tons per day)
Infiltration rate	$\text{m}^3\cdot\text{m}^{-2}\cdot\text{yr}^{-1}$	0.137	Value used in industry for landfills in regions receiving $\sim 100$ cm rain $\cdot\text{yr}^{-1}$
Initial temperature	$^{\circ}\text{C}$	20	Assumed in consideration of some self-heating associated with initial aerobic decomposition
Ambient temperature	$^{\circ}\text{C}$	20	Assumed environmental temperature
Waste density	$\text{kg}\cdot\text{m}^{-3}$	890	Approximate industry average
Ash density	$\text{kg}\cdot\text{m}^{-3}$	1281	Approximate industry average
Waste heat capacity	$\text{kJ}\cdot\text{kg}^{-1}\cdot^{\circ}\text{C}^{-1}$	1.32	Estimated as the sum of the heat capacity of individual components multiplied by their fractions. Default waste composition data given in Tables 3-S4, 3-S7, and 3-S8 and heat capacities given in Table 3-S4 (Yoshida et al. 1997).
Ash heat capacity	$\text{kJ}\cdot\text{kg}^{-1}\cdot^{\circ}\text{C}^{-1}$	0.8	Liang et al. (2008)
CH <sub>4</sub> generation rate constant ( $k_d$ )	$\text{yr}^{-1}$	component specific	Data for $k_d$ given in Table 3-S4.
CH <sub>4</sub> Production potential ( $L_0$ )	$\text{m}^3 \text{ CH}_4\cdot\text{Mg}^{-1}$ waste	component specific	Data for $L_0$ given in Table 3-S4.
N <sub>2</sub>	%	4	Used to quantify air intrusion
Corrosion rate of Al (alloy 3004)	$\text{mm}\cdot\text{yr}^{-1}$	0.003	Eashwar et al. (1990)
Corrosion rate of Al (alloy 1100)	$\text{mm}\cdot\text{yr}^{-1}$	$2.54\times 10^{-4}$	Ezuber et al. (2008)
Corrosion rate of coated Al (alloy 3004)	$\text{mm}\cdot\text{yr}^{-1}$	$5.17\times 10^{-4}$	Shabani-Nooshabadi et al. (2009)
Rate of ash hydration	$\text{yr}^{-1}$	0.5	Assumption
Rate of ash carbonation	$\text{yr}^{-1}$	0.1	Assumed rate is 20% of hydration rate based on literature from other environments (Morales-Flórez et al. 2015)

**Table 4-S2.** Physical parameters of MSW, leachate, and landfill gas (adopted from Hao et al., 2017; Tian and Benson, unpublished data, 2019)

	MSW	leachate	landfill gas
Heat capacity ( $\text{kJ}\cdot\text{kg}^{-1}\cdot^{\circ}\text{C}^{-1}$ )	1.32	4.18	1.54
Density ( $\text{kg}\cdot\text{m}^{-3}$ )	890	1000	1.13
Thermal conductivity ( $\text{W}\cdot\text{m}^{-1}\cdot\text{K}^{-1}$ )	0.6	0.6	0.025
Diffusion coefficient ( $\text{m}^2\cdot\text{s}^{-1}$ )	-	$4\times 10^{-9}$	$3\times 10^{-6}$
Viscosity ( $\text{Pa}\cdot\text{s}$ )	-	$8.9\times 10^{-4}$	$1.4\times 10^{-5}$

## Supplemental results and discussion

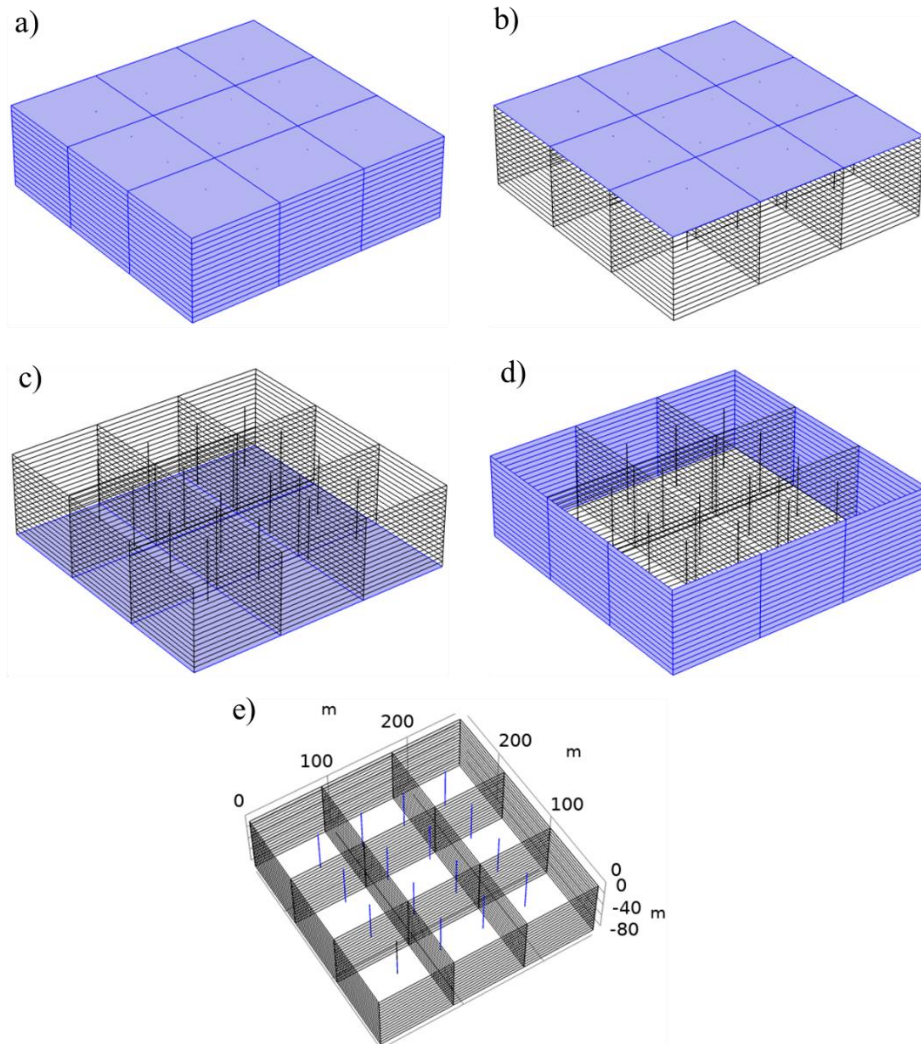


**Figure 4-S2.** Domain and boundaries applied in the model  
(a. domain for the entire landfill; b. top boundary; c. bottom boundary; d. side boundaries; e. gas wells)

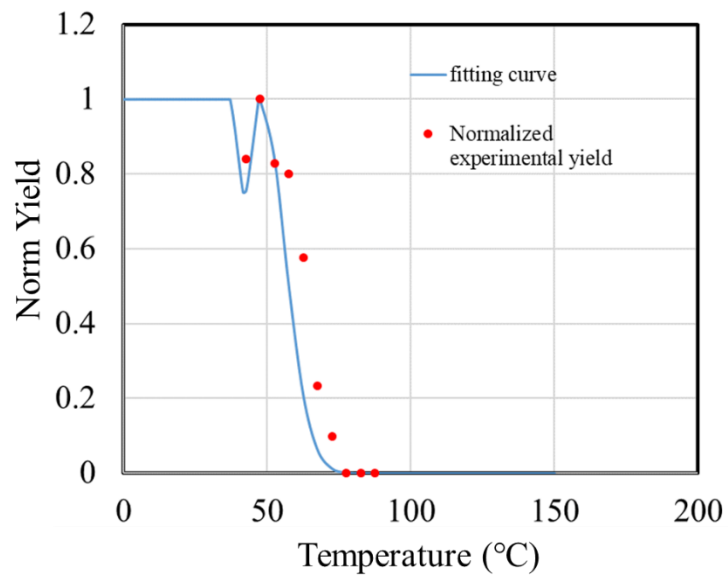


**Figure 4-S3.** Inhibition function and normalized experimental CH<sub>4</sub> potential described in Eq. 4-S1

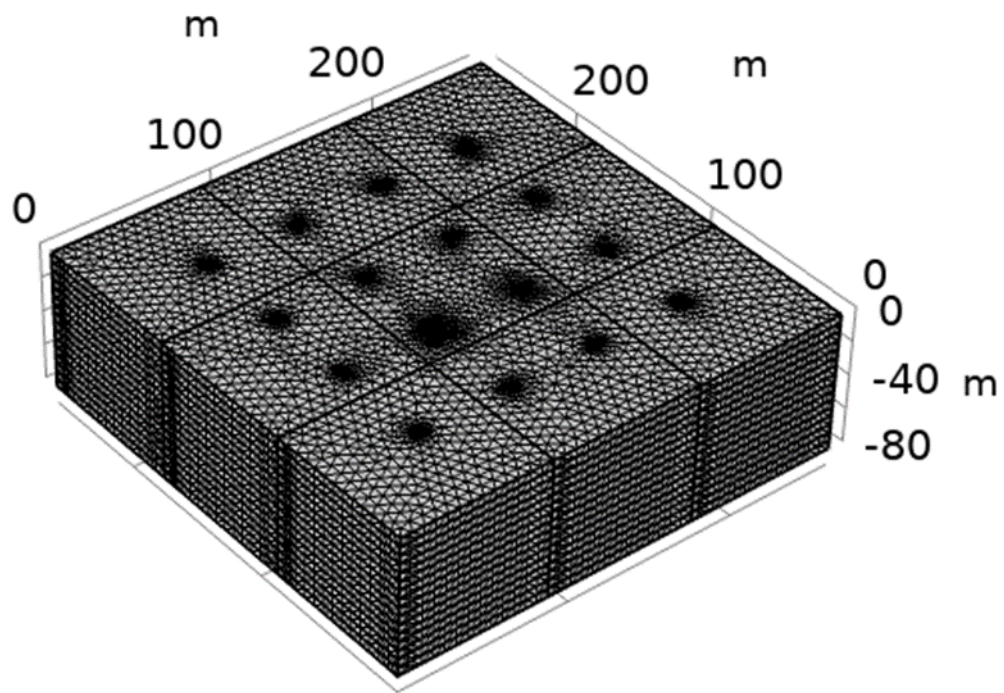


**Figure 4-S4.** Discretization of the landfill domain

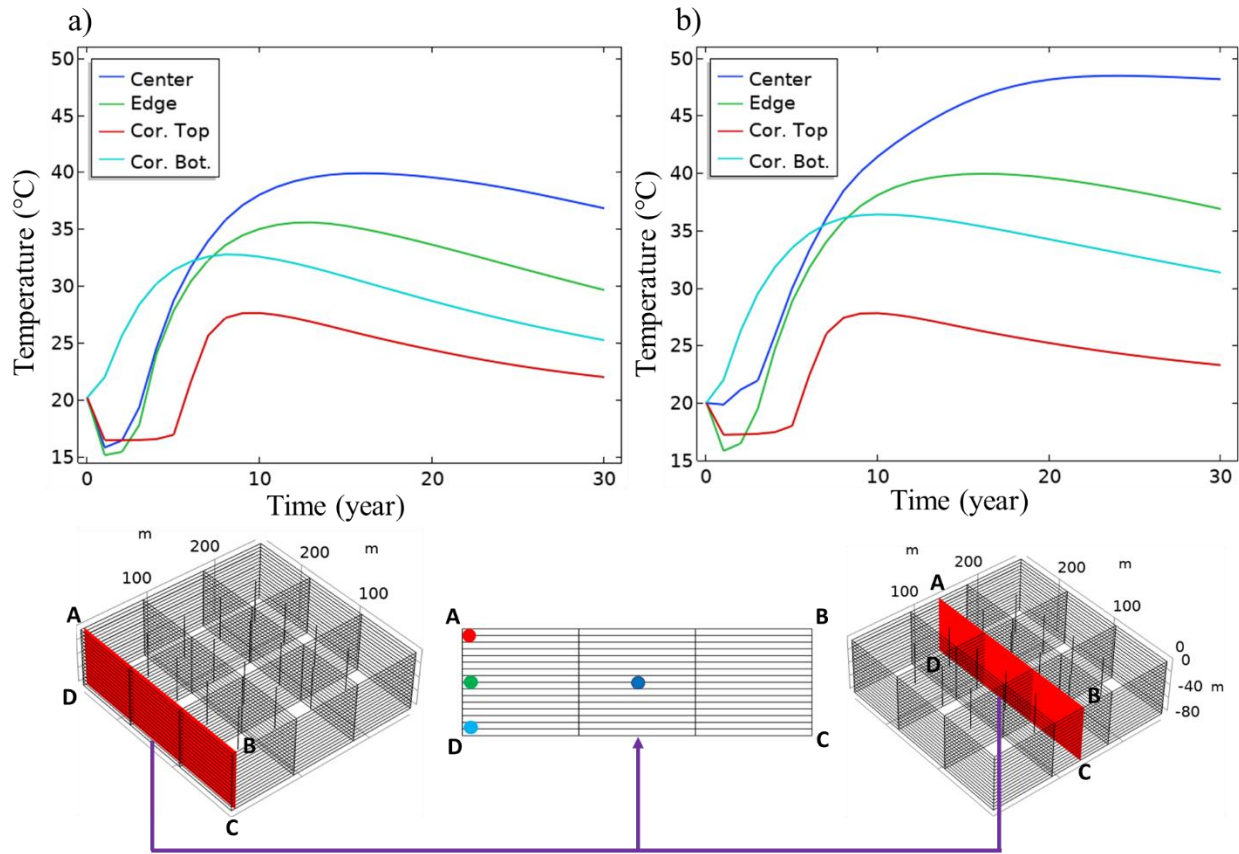


**Figure 4-S5.** Cross section for temperature evolution for the 80 m MSW only case (a. 5 m from the edge; b. in the center)

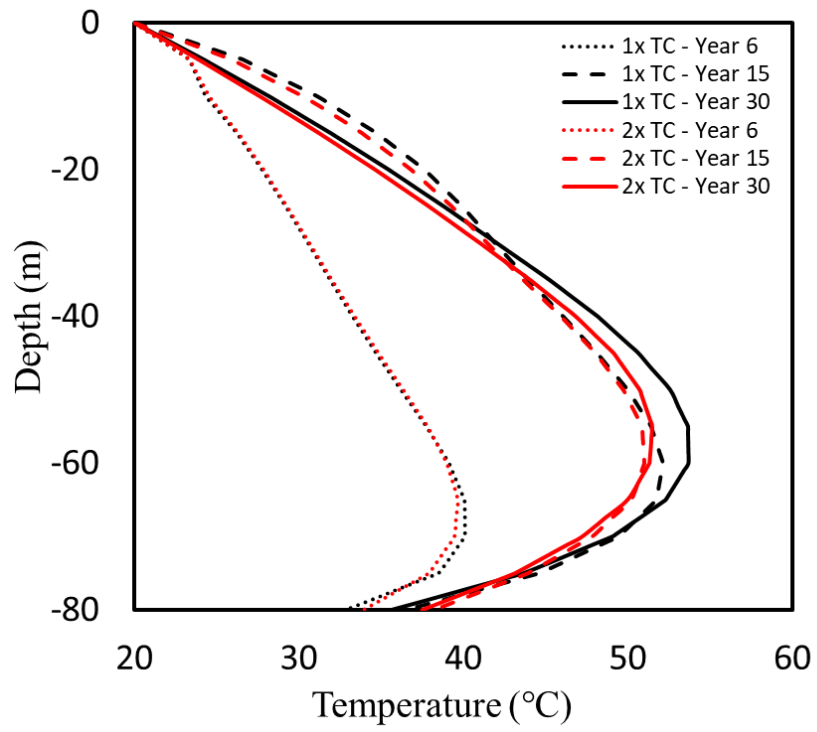


**Figure 4-S6.** Temperature profiles for MSW only with doubled MSW thermal conductivity

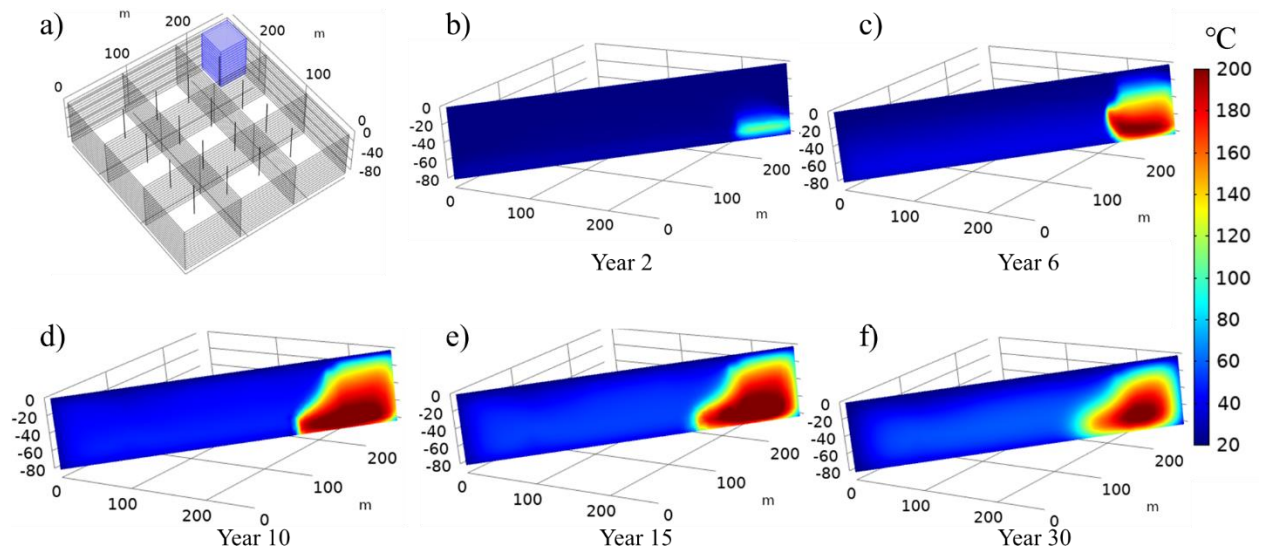


**Figure 4-S7.** Temperature contours for a landfill with an ash column in the corner (the disposal scenario is illustrated in part a)

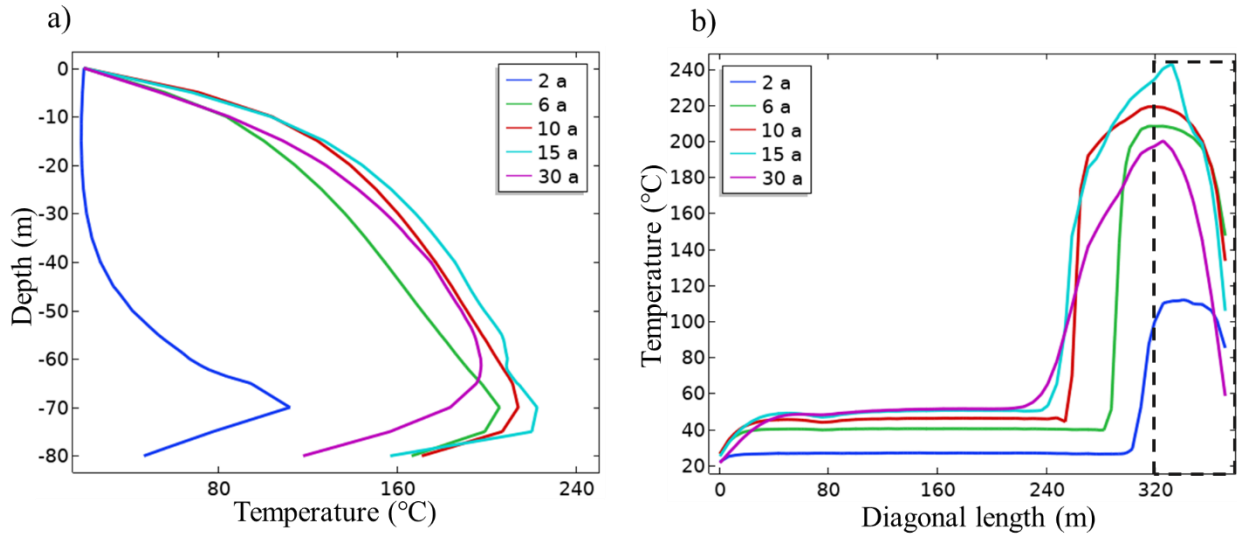


**Figure 4-S8.** Temperature profiles for a landfill with an ash column (dashed line) in the corner  
 (a. vertical profiles in the center of the ash column; b. horizontal profiles at 70 m in the diagonal cross section)

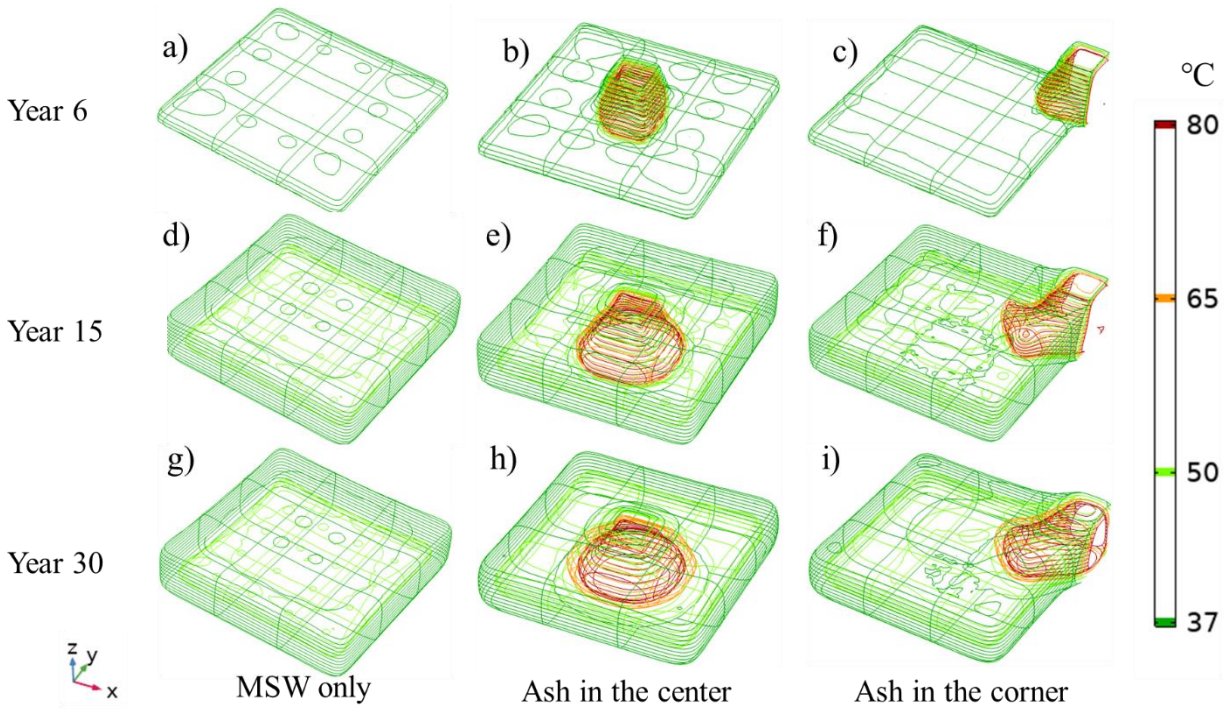


**Figure 4-S9.** Isothermal contours for MSW only, ash column in the center, and ash column in the corner

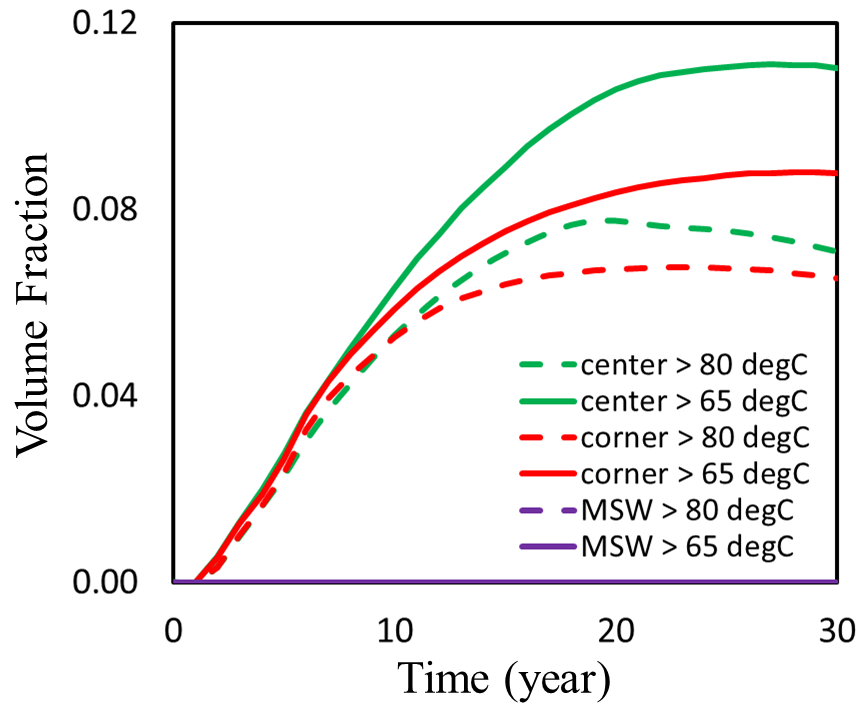


**Figure4-S10.** Volume fraction of regions with elevated temperatures for the MSW only, ash-in-center, and ash-in-corner cases

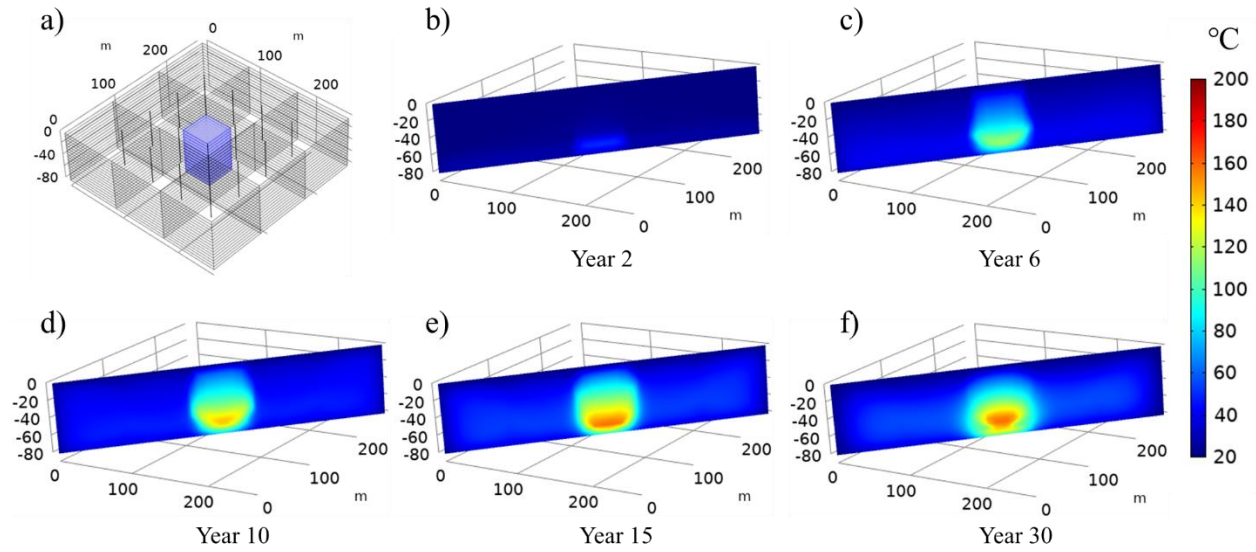


**Figure 4-S11.** Temperature contours for a landfill with an ash column in the center with carbonation only (the disposal scenario is illustrated in part a)

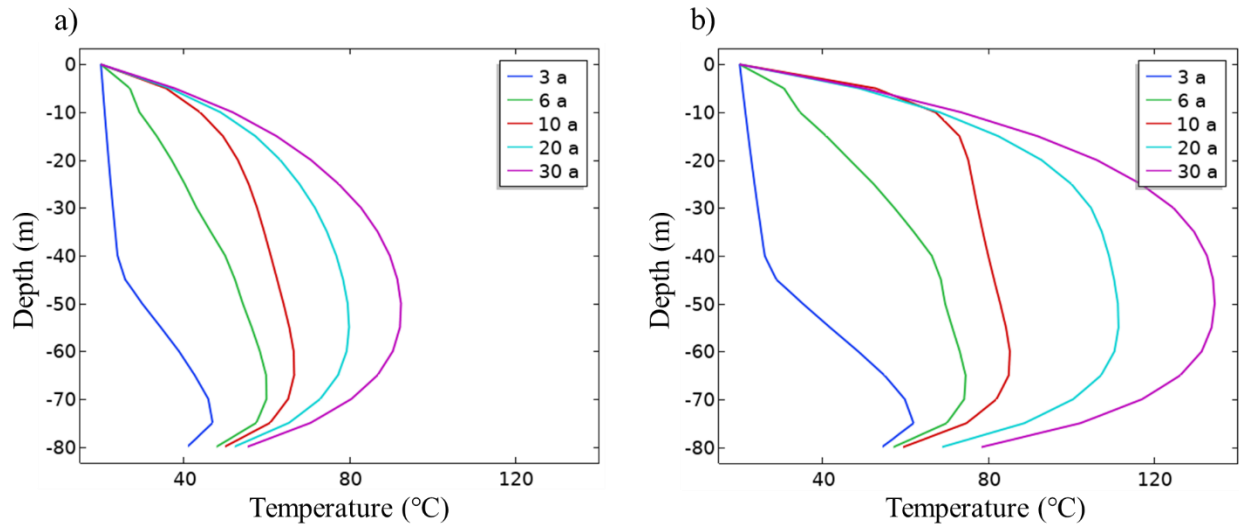


**Figure 4-S12.** Temperature profiles for Al-MSW mixture with 1.7 % (a) and 3.4% (b) Al

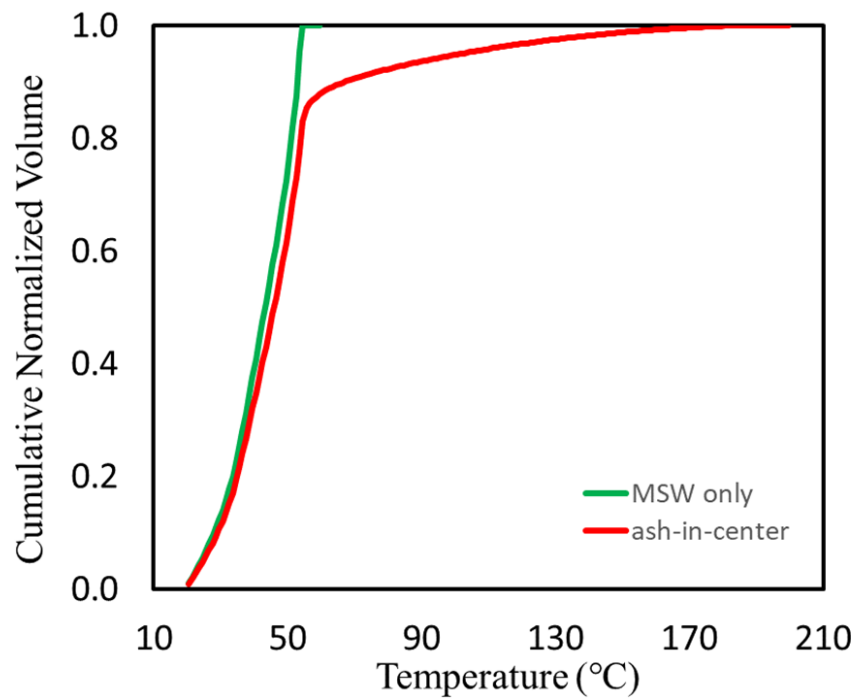


**Figure 4-S13.** Cumulative normalized volumes with varying temperatures for MSW only and ash-in-center cases in Year 20

## 4.8 References

- Ahmed, N., Wenzel, H. and Hansen, J.B., 2014. Characterization of Shredder Residues generated and deposited in Denmark. *Waste management*, 34(7), pp.1279-1288.
- Amestoy, P.R., Duff, I.S. and L'Excellent, J.Y., 2000. Multifrontal parallel distributed symmetric and unsymmetric solvers. *Computer methods in applied mechanics and engineering*, 184(2-4), pp.501-520.
- Benson, C.H., 2017. Characteristics of gas and leachate at an elevated temperature landfill. In *Geotechnical Frontiers 2017* (pp. 313-322).
- Calder, G.V. and Stark, T.D., 2010. Aluminum reactions and problems in municipal solid waste landfills. *Practice Periodical of Hazardous, Toxic, and Radioactive Waste Management*, 14(4), pp.258-265.
- de la Cruz, F. B. D. la; Barlaz, M. A., 2010. Estimation of waste component-specific landfill decay rates using laboratory-scale decomposition data. *Environmental science & technology*, 44(12), pp.4722-4728.
- Curtiss, C.F. and Hirschfelder, J.O., 1952. Integration of stiff equations. *Proceedings of the National Academy of Sciences of the United States of America*, 38(3), p.235-243.
- Dorez, G., Ferry, L., Sonnier, R., Taguet, A. and Lopez-Cuesta, J.M., 2014. Effect of cellulose, hemicellulose and lignin contents on pyrolysis and combustion of natural fibers. *Journal of Analytical and Applied Pyrolysis*, 107, pp.323-331.
- Eashwar, M., Subramanian, G. and Chandrasekaran, P., 1990. Marine fouling and corrosion studies in the coastal waters of Mandapam, India. *Bulletin of Electrochemistry*, 6(08), pp.699-702.
- Eleazer, W.E., Odle, W.S., Wang, Y.S. and Barlaz, M.A., 1997. Biodegradability of municipal solid waste components in laboratory-scale landfills. *Environmental Science & Technology*, 31(3), pp.911-917.
- Ezuber, H., El-Houd, A. and El-Shawesh, F., 2008. A study on the corrosion behavior of aluminum alloys in seawater. *Materials & Design*, 29(4), pp.801-805.
- Gholamifard, S., Eymard, R. and Duquennoi, C., 2008. Modeling anaerobic bioreactor landfills in methanogenic phase: Long term and short term behaviors. *Water research*, 42(20), pp.5061-5071.
- Halder, A., Dhall, A. and Datta, A.K., 2011. Modeling transport in porous media with phase change: applications to food processing. *Journal of Heat Transfer*, 133(3), p.031010.

- Hanson, J.L., Liu, W.L. and Yesiller, N., 2008. Analytical and numerical methodology for modeling temperatures in landfills. In *GeoCongress 2008: Geotechnics of Waste Management and Remediation* (pp. 24-31).
- Hanson, J.L., Yeşiller, N. and Oettle, N.K., 2010. Spatial and temporal temperature distributions in municipal solid waste landfills. *Journal of Environmental Engineering*, 136(8), pp.804-814.
- Hanson, J.L., Yeşiller, N., Onnen, M.T., Liu, W.L., Oettle, N.K. and Marinos, J.A., 2013. Development of numerical model for predicting heat generation and temperatures in MSW landfills. *Waste management*, 33(10), pp.1993-2000.
- Hao, Z., Sun, M., Ducoste, J.J., Benson, C.H., Luettich, S., Castaldi, M.J. and Barlaz, M.A., 2017. Heat generation and accumulation in municipal solid waste landfills. *Environmental science & technology*, 51(21), pp.12434-12442.
- Hodge, K.L., Levis, J.W., DeCarolis, J.F. and Barlaz, M.A., 2016. Systematic evaluation of industrial, commercial, and institutional food waste management strategies in the United States. *Environmental science & technology*, 50(16), pp.8444-8452.
- Hubert, J., Liu, X.F. and Collin, F., 2016. Numerical modeling of the long term behavior of Municipal Solid Waste in a bioreactor landfill. *Computers and Geotechnics*, 72, pp.152-170.
- Jafari, N.H., Stark, T.D. and Thalhamer, T., 2017. Spatial and temporal characteristics of elevated temperatures in municipal solid waste landfills. *Waste management*, 59, pp.286-301.
- Klein, R., Nestle, N., Niessner, R. and Baumann, T., 2003. Numerical modelling of the generation and transport of heat in a bottom ash monofill. *Journal of hazardous materials*, 100(1-3), pp.147-162.
- Levis, J. W.; Barlaz, M. A., 2014. Landfill Gas Monte Carlo Model Documentation and Results. Report to ICF for the U.S. EPA Waste Reduction Model (WARM); USEPA: Washington, D.C.; [http://www4.ncsu.edu/~jwlevis/Landfill\\_WARM-2014.pdf](http://www4.ncsu.edu/~jwlevis/Landfill_WARM-2014.pdf).
- Li, X., Bertos, M.F., Hills, C.D., Carey, P.J. and Simon, S., 2007. Accelerated carbonation of municipal solid waste incineration fly ashes. *Waste management*, 27(9), pp.1200-1206.
- Liang, P., Wang, Z. and Bi, J., 2008. Simulation of coal pyrolysis by solid heat carrier in a moving-bed pyrolyzer. *Fuel*, 87(4-5), pp.435-442.
- Lopez, V.M., Florentino, B. and Barlaz, M.A., 2016. Chemical composition and methane potential of commercial food wastes. *Waste Management*, 56, pp.477-490.
- Luettich, S.M. and Yafrate, N., 2016. Measuring Temperatures in an Elevated Temperature Landfill. In *Geo-Chicago 2016* (pp. 162-176).

- Martin, J.W., Stark, T.D., Thalhamer, T., Gerbasi-Graf, G.T. and Gortner, R.E., 2012. Detection of aluminum waste reactions and waste fires. *Journal of Hazardous, Toxic, and Radioactive Waste*, 17(3), pp.164-174.
- Miller, P. A.; Clesceri, N. L., 2002. *Waste Sites as Biological Reactors: Characterization and Modeling*; CRC Press.
- Morales-Flórez, V., Santos, A., Romero-Hermida, I. and Esquivias, L., 2015. Hydration and carbonation reactions of calcium oxide by weathering: kinetics and changes in the nanostructure. *Chemical Engineering Journal*, 265, pp.194-200.
- Nastev, M., Therrien, R., Lefebvre, R. and Gelinas, P., 2001. Gas production and migration in landfills and geological materials. *Journal of contaminant hydrology*, 52(1-4), pp.187-211.
- Neusinger, R., Drach, V., Ebert, H.P. and Fricke, J., 2005. Computer simulations that illustrate the heat balance of landfills. *International journal of thermophysics*, 26(2), pp.519-530.
- Oshins, C. and Block, D., 2000. Feedstock composition at composting sites. *Biocycle*, 41(9), pp.31-34.
- Rendek, E., Ducom, G. and Germain, P., 2007. Assessment of MSWI bottom ash organic carbon behavior: A biophysicochemical approach. *Chemosphere*, 67(8), pp.1582-1587.
- Saad, Y. and Schultz, M.H., 1986. GMRES: A generalized minimal residual algorithm for solving nonsymmetric linear systems. *SIAM Journal on scientific and statistical computing*, 7(3), pp.856-869.
- Shabani-Nooshabadi, M., Ghoreishi, S.M. and Behpour, M., 2009. Electropolymerized polyaniline coatings on aluminum alloy 3004 and their corrosion protection performance. *Electrochimica Acta*, 54(27), pp.6989-6995.
- Speiser, C., Baumann, T. and Niessner, R., 2000. Morphological and chemical characterization of calcium-hydrate phases formed in alteration processes of deposited municipal solid waste incinerator bottom ash. *Environmental Science & Technology*, 34(23), pp.5030-5037.
- Staley, B.F. and Barlaz, M.A., 2009. Composition of municipal solid waste in the United States and implications for carbon sequestration and methane yield. *Journal of Environmental Engineering*, 135(10), pp.901-909.
- Stark, T.D., Martin, J.W., Gerbasi, G.T., Thalhamer, T. and Gortner, R.E., 2011. Aluminum waste reaction indicators in a municipal solid waste landfill. *Journal of Geotechnical and Geoenvironmental Engineering*, 138(3), pp.252-261.
- U.S. EPA, 2005. *Landfill Gas Emissions Model (LandGEM) Version 3.02 User's Guide*; U.S. Environmental Protection Agency: Washington, D.C.; <http://www.epa.gov/ttnecatc1/dir1/landgem-v302-guide.pdf>.

- U.S. EPA, 2015. Municipal Solid Waste Generation, Recycling, and Disposal in the United States: Facts and Figures for 2013; United States Environmental Protection Agency: Washington, DC.
- Wang, X., Padgett, J.M., de la Cruz, F.B. and Barlaz, M.A., 2011. Wood biodegradation in laboratory-scale landfills. *Environmental science & technology*, 45(16), pp.6864-6871.
- Wang, X., Padgett, J.M., Powell, J.S. and Barlaz, M.A., 2013. Decomposition of forest products buried in landfills. *Waste management*, 33(11), pp.2267-2276.
- Wang, X. and Barlaz, M.A., 2016. Decomposition and carbon storage of hardwood and softwood branches in laboratory-scale landfills. *Science of the Total Environment*, 557, pp.355-362.
- Yeşiller, N., Hanson, J.L. and Yee, E.H., 2015. Waste heat generation: A comprehensive review. *Waste Management*, 42, pp.166-179.
- Yoshida, H., Tanaka, N. and Hozumi, H., 1997, October. Theoretical study on heat transport phenomena in a sanitary landfill. In *Proc., 6th Int. Landfill Symp (Vol. 1, pp. 110-119)*.

## Chapter 5. Conclusions and Recommendations

### Conclusions

This dissertation describes a batch reactor model and a finite element 3D model to describe heat generation, accumulation, and propagation from biotic and abiotic reactions that occur in MSW landfills. The major conclusions of this work are as follows.

- The batch reactor model was developed to identify an appropriate mathematical approach for the representation of heat generation sources including aerobic and anaerobic biological reactions, anaerobic metal corrosion, acid-base reactions, ash hydration and carbonation, and pyrolysis. While neither metal corrosion nor ash hydration and carbonation in municipal solid waste (MSW) landfills is fully understood, the results showed that these reactions have the potential to significantly increase landfill temperature. In the batch reactor model, the landfill temperature and reactant concentrations do not vary spatially within the landfill which represents an important limitation in representing landfills.
- The transient three-dimensional finite element model (FEM-3DM) was developed to describe spatially dependent heat transfer mechanisms in landfills. The FEM-3DM was useful in exploring the impact of three disposal scenarios involving ash; segregation of ash in the center of the landfill, segregation in a corner, and mixed with the MSW. The simulation results for the 80 m landfill receiving MSW only showed a convex temperature profile in the landfill body and the maximum temperature occurs at a depth of 50 m. Model simulations showed that more heat accumulates in a deeper landfill. The maximum temperatures and the volume fraction with temperature above 40 °C of the 80 and 40 m landfills are 54 and 47 °C, and 0.64 and 0.47 in year 15, respectively.

- The impacted waste volume associated with the ash disposal in corner and center scenarios are close for both maximum temperatures and cumulative normalized landfill volume (CNLV) with elevated temperatures. Thus, other considerations will likely influence waste placement. By hydrating the waste prior to burial, about 40% of the total energy could be eliminated prior to burial, this results in a reduction of the maximum temperature by ~40 °C in the FEM-3DM. Simulations predicted that the disposal of 10 to 20% ash can result in 49 to 81% of the waste mass, respectively, that exceeds 65 °C. This landfilling strategy suggests that a segregation burial approach has merit so to minimize the volume of MSW that experiences an elevated temperature (65 °C). When the concentration of reactive waste is relatively low (10% ash and 1.7% Al), the CNLV above 65 °C are 0.49 and 0.60, respectively, while above 80 °C, their CNLV are close to 0. However, when these waste disposal rates quantities are doubled, there is a marked increase in CNLV.
- Model simulations and published field data are comparable and both illustrate maximum temperatures deep in the landfill.

### **Implications and Recommendations**

This work has contributed to an improved understanding of heat generation, accumulation, and propagation in MSW landfills. Landfill owners and operators can use the developed models to (1) predict temperatures within landfills; (2) understand causes and mechanisms of elevated temperature landfills; and (3) quantify the impacts of boundary conditions, waste properties, landfill operational conditions such as geometry of landfills and acceptance and placement of special waste. Detailed implications and recommendations are as follows:

- In addition to MSW, many landfills receive non-hazardous industrial wastes including ash from both coal and MSW combustion, ash used to solidify liquid wastes, auto shredder

residue (ASR) that contains Al and Fe, and perhaps other Al-containing wastes. These wastes represent a source of revenue. The model results showed the importance of ash hydration/carbonation and metal corrosion to waste temperature. However, in the proposed models, the parameter values associated with these reactions were adopted from literature on systems other than landfills. Methods to measure the heat production potential of such wastes under landfill-relevant conditions are required. Appropriate methods are under development and will be used to parameterize the developed models to evaluate the quantity of a given waste that can be disposed without the accumulation of unacceptable heat. The batch reactor model could be used as a first estimate due to its simplicity.

- Constant reaction rates are used for metal corrosion and ash hydration/carbonation in the batch reactor and 3D finite element models. However, metal corrosion is temperature-dependent, and reaction rate constants can be described by the Arrhenius equation. In future work, a function should be added so that these reactions rates increase with increasing temperature.
- The 3D finite element model predicts temperature at each discrete point in the landfill domain. There are ~800,000 discrete points for a typical case (80 m landfill with MSW only), and model run times of 3 – 4 days were typical. However, simulation results showed that temperatures in a considerable number of discrete points are close, indicating that the behavior of heat transfer in those points is similar. The points with similar mass and heat transfer behavior can be grouped as one characteristic point without losing important information. Therefore, to eliminate computational complexity and reduce computational time, it might be possible to simplify the 3D finite element model by considering heat generation and transfer at several characteristic discrete points. It is recommended to

explore the development of a compartmental batch reactor model (CBRM) by discretizing a landfill domain into several characteristic compartments and reduce simulation time from days to minutes. A revised batch reactor model will be used to describe heat and mass transfer in each compartment.

- Exothermic pyrolysis of refuse, which is hypothesized to be initiated due to a local accumulation of heat, was modeled empirically and predicted a sharp temperature increase based on an assumed initiation temperature of 120 °C. However, the simulation results must be considered illustrative until a better understanding of landfill pyrolysis is developed.
- It would be desirable to conduct additional research to compare model predictions to measured landfill temperatures and revise the model as appropriate. In future research, field data from MSW landfills will be used to compare to temperatures predicted from model simulations. The finite element model will be parameterized using site-specific values/conditions such as landfill geometry, waste disposal schedule and strategy, and waste properties.